Winter 2023

Distribution and Mixotrophy of Cryptophyte Phytoplankton in the Northern Gulf of Alaska

Megan O'Hara

Western Washington University, megantohara3@gmail.com

Distribution and Mixotrophy of Cryptophyte Phytoplankton in the Northern Gulf of Alaska

By

Megan O'Hara

Accepted in Partial Completion
of the Requirements for the Degree
Master of Environmental Science

ADVISORY COMMITTEE

Dr. Suzanne Strom, Chair

Dr. Brooke Love

Dr. Brady Olson

Dr. Gwenn Hennon

Graduate School

David L. Patrick, Dean

Master's Thesis

In presenting this thesis in partial fulfillment of the requirements for a master's degree at Western Washington University, I grant to Western Washington University the non-exclusive royalty-free right to archive, reproduce, distribute, and display the thesis in any and all forms, including electronic format, via any digital library mechanisms maintained by WWU.

I represent and warrant this is my original work and does not infringe or violate any rights of others. I warrant that I have obtained written permissions from the owner of any third party copyrighted material included in these files.

I acknowledge that I retain ownership rights to the copyright of this work, including but not limited to the right to use all or part of this work in future works, such as articles or books.

Library users are granted permission for individual, research, and non-commercial reproduction of this work for educational purposes only. Any further digital posting of this document requires specific permission from the author.

Any copying or publication of this thesis for commercial purposes, or for financial gain, is not allowed without my written permission.

Megan O'Hara

01/10/2023

Distribution and Mixotrophy of Cryptophyte Phytoplankton in the Northern Gulf of Alaska

A Thesis
Presented to
The Faculty of
Western Washington University

In Partial Fulfillment
Of the Requirements for the Degree
Master of Science

by
Megan O'Hara
January 2023

Abstract

The Northern Gulf of Alaska (NGA) is a productive subarctic marine ecosystem that supports high abundances of plankton, fishes, seabirds, and mammals. Research has shown that this high productivity is primarily controlled by seasonal and spatial heterogeneity in the lower trophic level food web. Marine cryptophytes are a crucial, yet understudied, phytoplankton group in the NGA. Cryptophytes have the capacity for mixotrophy (acquiring energy through photosynthesis and feeding) which can improve trophic transfer efficiency, increase cellular growth rates, and improve retention of nutrients in the water column. Field samples collected in spring, summer, and fall 2021 surveyed the contribution of marine cryptophytes to the phytoplankton community in the NGA and assessed how natural variability in environmental factors influenced their distribution and mixotrophic capabilities. Our study demonstrated high spatial and temporal variability in cryptophyte biomass and community composition across the NGA. Cryptophytes were found in highest abundances in summer and fall, with smaller cells (3-10 μm) dominating the cryptophyte community composition during the summer in nearshore waters and larger cells (10-25 μm) playing an important role offshore in the fall. This variability, along with a capacity to live in a wide range of environmental conditions in the NGA, suggests that cryptophytes are versatile protists. Analysis of small cell-dominated phytoplankton communities generated carbon biomass estimates up to 600 μgC/L and carbon to chlorophyll ratios up to 300. These values were higher than previously expected for a small cell community in the NGA and indicated high carbon transfer potential from small cells despite low chlorophyll concentrations in some seasons. Cryptophytes and other nanoeukaryotes consistently made up ~75 % of the total phytoplankton community biomass in summer and fall in the NGA. This research suggests that cryptophytes are a critical component of the lower trophic level food web in the NGA in summer and fall. Despite their diverse environmental range in 2021, time series analyses of four summers (2018-2021) of cryptophyte data showed lower abundance, biomass, and average cell size during 2019, an anomalously warm year in the NGA. Finally, we found empirical evidence for in situ mixotrophy and the mechanisms that regulate cryptophyte mixotrophy in the NGA. Cryptophyte mixotrophy was highest in larger cells (> 10 μm) in summer and fall and had a strong positive relationship with prey (*Synechococcus* spp.) concentration, a moderate positive relationship with phosphate, and a weak negative relationship with ammonium. Findings from this research improved our understanding of the basic biology and ecology of this important group of primary producers and will provide novel information to integrate estimates of cryptophyte biomass and mixotrophy into our ecosystem food web model.

Acknowledgements

I would like to share sincere gratitude to my thesis advisor, Dr. Suzanne Strom for her

mentorship, support, and advice. I could not have done it without her guidance and patience.

Special thanks to Kelley Bright and Kerri Fredrickson for their help in developing methods,

problem solving in the lab, answering questions, and teaching me how to be a sea-going

oceanographer. Another special thank you to the fellow NGA-LTER graduate students that

provided a positive and welcoming community during long weeks at sea. I would also like to

thank the captains and crews of the R/V Sikuliaq and the M/V Tiglax for their hard work and

facilitation of my dreams to become an oceanographer. Thank you to my committee members

Dr. Brooke Love, Dr. Brady Olson, and Dr. Gwenn Hennon for their feedback and

encouragement in both my research and career pursuits. Dr. Brian Bingham's teaching and

guidance of statistics were truly instrumental to my graduate education. Finally, I would like to

thank my friends and family near and far for their support. To my cohort Heidi, Katie, Meghan,

Nicole, and Sara I would not have made it to the end without you; I am thankful to have found a

solid support system here at WWU. This research was funded by the National Science

Foundation (grant #1656070), North Pacific Research Board (grant #2018), and Western

Washington University (College of the Environment Flora Summer Stipend, Small Grant, and

Dean's Fund for Sustainability).

Table of Contents

List of Figures

List of Tables

Introduction

The Northern Gulf of Alaska (NGA) is a productive subarctic marine ecosystem that supports high abundances of plankton, fishes, seabirds, and mammals. Research has shown that this high productivity is influenced by seasonal and spatial heterogeneity in the lower trophic level food web. Short- and long-term climatological patterns generate highly variable phytoplankton stocks in the NGA. In addition to this natural variability, the NGA is experiencing anthropogenic warming (Walsh et al. 2018). During summer and fall in the NGA small cell-dominated phytoplankton communities, including marine cryptophytes, dominate. Cryptophytes are a crucial, yet understudied, phytoplankton group in the NGA. This project utilized environmental samples from the NGA to survey the contribution of marine cryptophytes to the phytoplankton community and to assess how natural variability in environmental factors influence the distribution and mixotrophic capabilities of cryptophytes.

Study Site Characterization

The NGA has been intensively studied via a long-term monitoring program for over two decades and is now a study site in the National Science Foundation-funded Long-Term Ecological Research (LTER) network. The study region is comprised of a wide continental shelf, a narrow slope, deep-sea offshore waters, and Prince William Sound (Waite and Mueter 2013). The continental shelf connects the offshore region to a glacially carved coastal mountain range. Complex geological history has formed the shelf bathymetry into shallow banks that connect to deep gullies (Waite and Mueter 2013). Strong seasonal variability in day length, water temperature, micro- and macronutrient availability, freshwater input, precipitation, and storm

intensity influence the biological productivity of the NGA (Wilson and Overland 1986). Additionally, transport mechanisms supporting onshore flow of macronutrients enhance production on the shelf while mechanisms exporting iron-rich waters from nearshore can episodically enhance production in offshore regions (Wu et al. 2009). Since cross-shelf primary productivity gradients mirror gradients in bioavailable iron, it is hypothesized that iron is a major factor in the ecosystem productivity of the NGA (Strom et al. 2006). Spatial and temporal variability in climatological patterns and physical features in the NGA influence phytoplankton community composition, biomass, cell size, nutrient utilization, growth rate, and degree of micro- and macronutrient limitation (Strom et al. 2006; Waite and Mueter 2013).

What are Marine Cryptophytes?

Cryptophytes are flagellated protists within the 2.5–50 µm size range found in fresh, estuarine, and marine waters (Altenburger et al. 2020; Yoo et al. 2017). The diversity of cryptophytes across all ecosystems encompasses approximately 220 species, many unnamed, spanning three phylogenetic orders and 40 genera (Stoecker and Lavrentyev 2018; Yang et al. 2020). Unique taxonomic features of cryptophytes include a periplast cell wall structure, exhibiting taxon-specific scale patterns beneath the plasma membrane, and a nucleomorph, or reduced red algae nucleus that is residual from a previous evolutionary endosymbiotic event (Clay et al. 1999; Kugrens and Lee 1987; Kugrens and Lee 1988; Novarino 2012; Novarino and Lucas 1993). Cryptophytes also contain chlorophyll-c2 and the carotenoid accessory pigments alloxanthin and alpha-carotene (Heidenreich and Richardson 2020).

Cryptophytes are cosmopolitan protists capable of surviving in a wide range of environmental conditions within the euphotic zone (Clay et al. 1999). Physiological studies

2

indicate that cryptophytes have high photosynthetic efficiencies and can acclimate to varying

spectral irradiance (Heidenreich and Richardson 2020; Roberts and Laybourn-Parry 1999).

Cryptophytes use chlorophyll-a as their major light harvesting pigment, supplemented by

phycoerythrin. Phycoerythrin allows differentiation of cryptophytes from other phytoplankton

under epifluorescence microscopy by its orange, autofluorescent glow under blue light

illumination (Heidenreich and Richardson 2020). There is much debate over their preferred

environmental conditions, but cryptophytes have been detected from the coast to the open

ocean in temperate, polar, and tropical waters (Heidenreich and Richardson 2020; Yoo et al.

2017). The consensus is that cryptophytes commonly inhabit stratified and shallow upper mixed

layers of the water column (Mendes et al. 2013; Mendes et al. 2018). Stratified, micro- and

macronutrient-limited surface layers are prevalent in the summer and early fall in the NGA,

likely favoring small-celled phytoplankton groups such as cryptophytes (Gerringa et al. 2000).

Several studies demonstrate cryptophyte preference for lower salinity waters while others

suggest an affinity for colder waters (Mendes et al. 2013; Moline et al. 2004; Schofield et al.

2017). The weight of evidence with respect to environmental conditions is not sufficient to

determine an ecological niche for marine cryptophytes. Niche versatility, species diversity, and

the use of mixotrophy to supplement nutritional needs could explain cryptophyte's expansive

environmental range (Leeuwe et al. 2020).

Cryptophyte Mixotrophy

Mixotrophic phytoflagellates, like cryptophytes, are protists that inherently contain

chloroplasts but can also feed (Stoecker et al. 2017). The diversity of algal lineages involved in

phytoflagellate mixotrophy suggests that this is a highly effective adaptation (Flynn and Mitra

2009). In nutrient limited environments, such as the NGA during summer and fall, mixotrophic

phytoflagellates that can obtain nitrogen, phosphorus, or iron from feeding generally have a

competitive advantage over pure autotrophs (Mitra et al. 2014) and can reach faster growth

rates as mixotrophs than when employing photosynthesis or feeding alone (Adolf et al. 2006;

Burkholder et al. 2008; Jeong et al. 2010).

Prior research indicates that cryptophytes in the NGA have the capacity for mixotrophy,

the acquisition of energy and nutrients through both photosynthesis and heterotrophy (Busse

2021). Mixotrophy can improve primary production and trophic transfer efficiency, increase

cellular growth rates, and improve retention of nutrients within the water column (Mitra et al.

2016; Stoecker and Lavrentyev 2018; Wassmann and Reigstad 2011; Leeuwe et al. 2020). There

is a general lack of field research focused on cryptophyte mixotrophy. A recent study hints that

mixotrophy in cryptophytes serves more as a strategy for fixed carbon acquisition than for

macronutrient acquisition in the NGA (Busse 2021). Further research into the impact of

environmental variables on the regulation of cryptophyte mixotrophy is needed.

Cryptophyte Contribution to Phytoplankton Communities

Due to their small size and mixotrophic capacity cryptophytes play diverse roles in marine

food webs. Not only do they potentially exert grazing control on marine bacteria populations,

but they also provide an avenue for carbon transfer out of the microbial loop (Mitra et al.

2014). Mixotrophic cryptophytes fulfill a vital linkage between marine bacteria prey and

heterotrophic predators. Cryptophyte chloroplasts, particularly from cells of the *Teleaulux,*

Plagioselmis, and *Geminingera* genera, are commonly retained by mixotrophic ciliates and

dinoflagellates that use kleptochloroplastidy as their nutritional strategy (Hansen et al. 2013;

Stoecker and Lavrentyev 2018; Yoo et al. 2017). These mixotrophic ciliates and dinoflagellates can be key components of the NGA ecosystem during the summer and fall (Strom et al. 2007). Additionally, cryptophytes are nutritious prey due to their soft outer body wall, absence of toxins, and high concentrations of long-chain essential fatty acid (LCEFA) (Brett and Müller-Navarra 1997; Galloway and Winder 2015). When transferred to higher trophic levels these LCEFA help structure marine food webs by promoting high growth and reproduction rates in zooplankton and fish (Galloway and Winder 2015; Litzow et al. 2006; Sterner and Schulz 1998).

Cryptophytes in Future Climate-Changed Oceans

The complex relationships of the marine food web are shifting amidst a changing climate (Walsh et al. 2018). Global climate change is influencing storm intensity, wind patterns, precipitation rates, glacial melt, light intensity, water temperature, and strength of water column stratification throughout the oceans (Beamer et al. 2017; Walsh et al. 2018; Wassmann and Reigstad 2011). These changes are predicted to favor smaller and less specialized phytoplankton, such as mixotrophic phytoflagellates (Mendes et al. 2018; Wassmann and Reigstad 2011). Smaller phytoplankton, like cryptophytes, that are efficient at dissolved nutrient utilization are favored to outcompete larger organisms in future climate change-impacted oceans (Henson et al. 2021). Similarly, high species diversity, occupation of diverse environmental niches, and plasticity in nutritional strategy via mixotrophy offers cryptophytes a competitive advantage over less versatile phytoplankton in adapting to changing environments (Lindemann et al. 2016; Rammel 2021; Stoecker and Lavrentyev 2018). Shifts in phytoplankton community composition will impact trophic transfer efficiency, micro- and macronutrient availability, and biogeochemical cycling processes in the NGA.

Study Objectives

This study aims to understand (1) seasonal, cross-shelf, and interannual variability in cryptophyte biomass; (2) cryptophyte contribution to the composition and total biomass of small cell-dominated phytoplankton communities in the NGA; and (3) whether cryptophytes in the NGA are mixotrophic and under which conditions. We hypothesized that cryptophyte biomass would comprise a greater proportion of the total phytoplankton community in warmer, more stratified waters. We also hypothesized that the average cryptophyte cell size would be smaller and that rates of mixotrophy would be higher in offshore HNLC waters compared to nearshore and shelf environments. Lastly, we hypothesized that cryptophytes in high micro- and macronutrient nutrient environments would be purely autotrophic and that photosynthetically active radiation (PAR) would be negatively correlated to cryptophyte mixotrophy. Sampling at various spatial and temporal scales aided our understanding of the seasonal transition and interannual variability of phytoplankton communities in the NGA. A combination of epifluorescence microscopy and flow cytometry methods yielded data on small cell-dominated phytoplankton communities including the cyanobacteria *Synechococcus* spp. and photosynthetic eukaryotes, including cryptophytes, picoeukaryotes, and nanoeukaryotes. Findings will improve our understanding of the basic biology and ecology of this important group of primary producers, allow us to estimate the contribution of cryptophytes to the lower trophic level food web during various seasons in the NGA, and provide novel information to integrate mixotrophy by phytoflagellates into our ecosystem food web model.

Materials and Methods

Study Site Characterization

This study occurred in the Northern Gulf of Alaska as part of the NGA-LTER program primarily in 2021 but included a limited number of field samples from 2018-2020. Field samples were collected during the spring (04/23/21 – 05/04/21) and summer (06/27/21 – 07/09/21) cruises aboard the R/V Sikuliaq, and the fall cruise (09/13/21 – 09/25/21) aboard the M/V Tiglax. Additional microscopy samples from 2018 – 2020 that were collected and processed using methods from Strom et al. (2016) allowed interannual comparison of cryptophytes in the NGA. Numerous stations within four distinct regions were sampled during each cruise in 2021 including the Kodiak Line (KOD, sampled in spring and summer only), the Seward Line (GAK), the Middleton Line (MID), and Prince William Sound (PWS) (Figure 1). The KOD transect is the most oceanic and is ~ 130 km from the GAK transect. The GAK transect extends furthest offshore while the MID transect has the highest freshwater input, primarily from the Copper River. The GAK and MID transects are ~75 km apart.

In situ temperature and salinity values were collected from CTD sensors. Photosynthetically active radiation (PAR) data were collected continuously throughout each cruise using a LiCor 1400 2-π deck-board sensor mounted on the exterior of the vessel. Inorganic nutrient samples were collected from CTD Niskin bottles, pre-filtered (0.8 µm), stored at -80 °C, and analyzed for nitrogen (nitrite and nitrate), ammonium, phosphate, and silicate by the Aguilar-Islas laboratory at the University of Alaska, Fairbanks. Corresponding size fractionated chlorophyll and phaeopigment (<20 µm and >20 µm) samples were collected for each depth sampled.

Cryptophyte Quantification and Assessment of Mixotrophy

Epifluorescence microscopy slides were made to quantify the abundance, distribution, and mixotrophy of marine cryptophytes in the NGA. Seawater samples were collected from Niskin bottles using a standard CTD rosette at select stations at 10 m depth in spring and at the surface, 10 m, and near the sub-surface chlorophyll maximum (12 m – 30 m) in summer and fall 2021. These stations and depths were selected to provide high resolution spatial data both across the study site and within the euphotic zone. Additional sampling depths were added in summer and fall due to increased variability in the mixed-layer depth during these seasons. Samples were prescreened from CTD Niskin bottles through Nitex mesh (100 µm) attached to silicone tubing and collected into 60 ml narrow mouth polycarbonate bottles prefilled with 3 mL 10 % glutaraldehyde (final concentration 0.5 % v/v) and 250 µL DAPI stain (final concentration 0.4 µg/mL). Methods were modified to include 500 µL DAPI stain for summer and fall samples due to weak staining of spring samples (DAPI final concentration range for all samples was 0.4 – 0.8 µg/mL). Preserved samples were stored upright in a shipboard refrigerator for 12-24 h to allow cells to fix and stain. Microscope slides were prepared by filtering known volumes (40 mL – 60 mL) through a 1.2 µm pore size (25 mm) mixed cellulose ester membrane backing filter layered beneath a 0.8 µm pore size (25 mm) Nuclepore track-etch membrane filter. Filters were slide-mounted using immersion oil and stored upright in a slide box at -80 °C except during transport on dry ice to Shannon Point Marine Center (SPMC) in Anacortes, WA. All samples were processed within 6 months of slide preparation using epifluorescence microscopy. Methods for preservation and microscopy are from Strom et al. (2016).

Samples were analyzed using epifluorescence microscopy to determine the spatial and temporal distribution of cryptophytes and to assess the prevalence of ambient feeding (mixotrophy) on *Synechococcus* spp. prey by cryptophytes. Cryptophytes were easily identified by their unique pigment phycoerythrin which autofluoresces orange under blue light illumination. Cells between 3 µm and 25 µm, sphere or tear shaped, and glowing orange and green were classified as cryptophytes (Figure 2). Cryptophyte size class was measured using a microscope stage micrometer (3-5 µm, 5-10 µm, 10-15 µm, 15-20 µm and 20-25 µm) and shape category ('tear-shaped' or 'sphere-shaped') was recorded for each cell. The 20-25 µm size class was added to summer and fall methods; this size class was not observed in spring samples. Small cells (3-10 µm) were counted in grids under oil immersion (1000x), with 25 total grids counted for each sample. After wiping off the immersion oil, a minimum of 250 cells, or four transects if cryptophyte density was sparse, were counted under 400x magnification to enumerate cells 10-25 µm. Cell abundance (cells/mL) was computed using the total cells counted in each size class and shape category, the total area of grids or transects counted (mm^2), the total slide area (mm^2), and volume filtered (mL) after a correction for preservatives. Some samples had zero cryptophyte cells, particularly in spring.

A mixotrophy event was classified as a cryptophyte cell containing a round, yellow *Synechococcus* spp. cell ~1 µm in size (Figure 3). Mixotrophy was only recorded if prey cell(s) were completely inside of the cryptophyte cell. Additional information on mixotrophic ingestion was recorded including the size and shape of the predator, and the number of *Synechococcus* spp. cells ingested. Mixotrophy was quantified as the fraction of active mixotrophic cryptophyte cells out of total cells counted for each size class and shape.

9

Cell biovolume (BV) was computed separately for 'tear-shaped' and 'sphere-shaped' cryptophytes. The estimated cell diameter of sphere-shaped cells was assumed to be the median of the size range in that size class, for example the estimated diameter of cells 3-5 μm was 4 μm. The biovolume of a sphere-shaped cryptophyte was then computed using the estimated cell diameter for each size class: $BV_{sphere} = \frac{4}{3} * pi * \left(\frac{est.diameter}{2}\right)^3$. Similarly, the estimated cell length for tear-shaped cells was also assumed to be the median of the size range in that size class. Since tear shaped cells do not have a consistent diameter, the estimated cell width was assumed to be 70 % that of the estimated length based on cell measurements made by the Strom lab using a microscope stage micrometer. Tear-shaped cryptophyte biovolume was then computed using an estimate for cell width and length for each size class: $BV_{tear} = \frac{4}{3} * pi * \left(\frac{est.length}{2}\right) * \left(\frac{est.width}{2}\right)^2$. The carbon to volume relationship for photosynthetic nanoflagellates determined by Verity et al. (1992) was used to estimate cryptophyte biomass for each size class and shape: $Biomass = 10^{(-0.363 + 0.863 * (\log{(BV)})}$. Carbon biomass per cell (pg C/cell) was then multiplied by the cell abundance (cells/mL) to obtain carbon biomass (ng C/L) estimates for each size and shape category. The distinct cryptophyte shape categories were combined due to unreliability of distinction in some samples, so the actual data presented does not include differentiation by shape in the abundance, biovolume, or biomass estimates for each cryptophyte size class.

Cryptophyte Interannual Comparison

Interannual comparison of cryptophyte mean 10 m cell abundance (cells/mL), biomass (ngC/L), and cell size (μm) used epifluorescence microscopy data collected in summer on the

GAK transect from 2018 – 2021. The GAK transect was divided into 'shelf' and 'offshore' segments for each year. Sample size for 10 m GAK summer samples varied among years (2018 shelf n = 3, 2018 offshore n = 1; 2019 shelf n = 4, 2019 offshore n = 2; 2020 shelf n = 5, 2020 offshore n = 3; 2021 shelf n = 9, 2021 offshore n = 6).

Flow Cytometry

Flow cytometry (FC) samples were collected to estimate the community composition and biomass contribution of cryptophytes to small cell-dominated phytoplankton communities in the NGA. Seawater samples for FC were collected into 30 mL polycarbonate bottles from Niskin bottles on a standard CTD rosette at surface, 10 m, and subsurface chlorophyll maximum depths from select stations on the GAK and MID transects in summer and fall 2021. The polycarbonate bottles were inverted to ensure uniform distribution of particles, then a 1.5 mL subsample was transferred into a 2 mL cryovial under a fume hood. Samples were immediately fixed with 94 µL of pre-filtered (0.2 µm) 8 % paraformaldehyde (final concentration 0.5 % v/v, aqueous solution, EM grade). After the fixed samples incubated in the dark at room temp for 10 min the cryovials were flash frozen in liquid nitrogen for at least 5 min. FC samples were stored onboard at -80 °C until transported in a liquid nitrogen shipper back to SPMC. At SPMC samples were stored in darkness at -80 °C until analysis. All FC samples were processed within 10 months of fixation on a Luminex Guava EasyCyte HT flow cytometer.

Calibration beads were run on the flow cytometer at the beginning and end of each day to confirm laser and flow rate consistency. Analytical replicates (n = 4) of 150 µL of each field sample separated by two wells of ultrapure water to avoid sample carryover were processed in a 96-well plate. A count saturation threshold of 3 x 10^5 cells/mL was determined for the Guava

flow cytometer, so data from all samples were evaluated to verify that the total cell abundance did not surpass this threshold.

To obtain fluorescence signal and abundance data, analysis methods were developed by testing a combination of laboratory phytoplankton cultures of known size and fluorescence properties and field samples collected for methods development purposes. To separate the fluorescence signal of each phytoplankton group and phytoplankton from other particles, gates were manually assigned on scatter plots (cytograms) based on unique combinations of fluorescence intensity, forward scatter, and side scatter of each event counted (O'Neill et al. 2013). Cytogram statistical gates were determined for *Synechococcus* spp., picoeukaryotes, nanoeukaryotes, and cryptophytes. Picoeukaryotes and nanoeukaryotes were defined based on their high red fluorescence (high chlorophyll-a content) and low to moderate yellow fluorescence (Figure 4a). Since picoeukaryotes are smaller than nanoeukaryotes we expected their red fluorescence signal to scale down accordingly (Figure 4a).

Synechococcus spp. and cryptophytes were distinguished from other events based on high yellow fluorescence from their accessory pigment phycoerythrin (Figure 4a) (Olson et al. 1990). Although cryptophytes are nanoeukaryotes, we differentiated them from other photosynthetic nanoeukaryote events based on yellow fluorescence to focus our analysis on the cryptophyte contribution to small cell phytoplankton community biomass in the NGA. *Synechococcus* spp. were separated from cryptophytes based on forward scatter, a proxy for size (Figure 4b). Separating cryptophytes from *Synechococcus* spp. was challenging since *Synechococcus* spp*.* were abundant and formed a distinct cluster while cryptophytes were scarcer (Figure 4b). Additionally, cryptophytes had a wide range of cell sizes and associated

12

fluorescence signals (Sosik et al. 2003). Due to the challenges in accurately differentiating

cryptophyte and *Synechococcus* spp., FC data were compared to a subsample of

epifluorescence microscopy cell counts. A 0.81x correction factor was applied to all

Synechococcus spp. data since cell concentration estimates from FC were consistently higher

than those from microscopy. Cryptophyte microscopy cell counts were drastically different than

FC measured abundance. All cryptophyte data used in these analyses were from

epifluorescence microscopy to compensate for this discrepancy. Microscopy comparison for

picoeukaryotes and nanoeukaryotes was not necessary because these populations consistently

formed tight groups on the FC cytograms. An additional challenge to interpreting cytograms

was distinguishing the events of live cells from those of decaying particles or debris (Olusoji et

al. 2021).

Carbon biomass estimates for each phytoplankton group were obtained by multiplying

cell abundance values generated by the flow cytometer and taxa-specific biomass conversion

factors. We used 200 fg C/cell as the biomass conversion factor for *Synechococcus* spp. (Radi

2009; Strom et al. 2016). Cell biomass for picoeukaryotes, nanoeukaryotes, and cryptophytes

was determined using the Verity et al. (1992) carbon to volume relationship for photosynthetic

flagellates as defined above. The average picoeukaryote cell was assumed to be 2 μm and

sphere shaped, equating to 1,490 fg C/cell. Our nanoeukaryote biomass conversion factor was

12,580 fg C/cell. This nanoeukaryotic biomass conversion factor was computed using the

average C content of nanoeukaryote cells as estimated from epifluorescence microscopy

measurements of cell size, converted to BV using appropriate shape assumptions. Carbon-to-BV

conversion was from Verity et al. (1992). Samples used for these nanoeukaryote estimates were

collected from 10 m depth during 2018 and 2020 on the GAK and MID transects. We did not include 2019 data since it was an anomalously warm year and we wanted to capture average cell size under typical NGA conditions. Cryptophyte biomass for 2021 was determined using epifluorescence microscopy methods as described above.

The total small cell phytoplankton community carbon biomass was calculated by adding the carbon biomass of *Synechococcus* spp., picoeukaryotes, nanoeukaryotes, and cryptophytes for each sample. Carbon to chlorophyll ratios (C:chl) were then derived using the total small cell community carbon biomass at 10 m to chlorophyll-a in cells <20 μm at 10 m for each station on the GAK and MID transects in summer and fall 2021.

Statistical Analyses

All statistical analyses and figures were generated using *R: A Language and Environment for Statistical Computing* (R Core Team, 2022). Data analysis focused on 10 m samples unless clearly specified since that was the largest sample size and allowed both spatial and temporal comparison of cryptophytes without the confounding influence of unequal sampling of other depths.

NMDS analyses were performed to summarize cryptophyte and small cell-dominated phytoplankton community assemblages. The ordination space on each NMDS biplot presents similar samples close together and dissimilar samples further apart. A sample, or dot, represents an entire 10 m cryptophyte community or an entire 10 m small cell-dominated phytoplankton community at a unique location and time. A Bray-Curtis dissimilarity measure was used because it accounts for both relative abundance and presence/absence in the data. Auto-transformations for a Wisconsin double standardization and a sqrt transformation were

performed; low stress and convergent solutions were found with two NMDS dimensions (RStudio, package 'vegan').

Correlative relationships among cryptophyte biomass and environmental variables were assessed with Spearman correlation analysis (RStudio, package 'corrplot'). A false discovery rate adjustment 'FDR' adjustment to accommodate for false positive p-value results was performed due to the large number of variables assessed in this analysis. Corrected p-values were reported (RStudio, package 'psych'). The same Spearman correlation analysis methods were used for FC data.

Multiple linear regression models assessed relationships between cryptophyte biomass in summer and fall 2021 and numerous environmental variables including salinity, phosphate, nitrogen (nitrite + nitrate), ammonium, and cumulative PAR received 48 hours prior to sample collection (RStudio, package 'stats'). Variables for linear model analysis were chosen based on prior knowledge of the NGA and basic physiological requirements of cryptophytes. Limitations on the number of 10 m observations (n = 128) encouraged us to use all depths sampled (0 m – 30 m) and confined our analysis to a maximum of 6 predictive variables. All cryptophyte biomass data were log transformed to meet assumptions of residual variance and normality. Each linear model passed a variance inflation factor (VIF) test (VIF < 5) to confirm that no predictors were collinear (RStudio, package 'car').

Relationships among cryptophyte mixotrophy and hypothesized environmental predictors of flagellate mixotrophy were analyzed with Poisson regression generalized linear models (RStudio, package 'MASS'). Poisson regression was used because the mixotrophy dataset contained a high proportion of 0 outcomes (i.e. cryptophyte cells with no ingested

15

prey); therefore the relationship between cryptophyte mixotrophy (fraction of active

mixotrophs) and predictor variables was nonlinear, and the distribution of data was skewed.

This analysis focused on summer and fall data because negligible mixotrophy was recorded in

spring. Like the cryptophyte biomass models, limitations on the number of 10 m observations

(n = 127) encouraged us to use all depths sampled (0 m – 30 m) and confined our analysis to a

maximum of 6 predictive variables. Variables hypothesized to influence cryptophyte

mixotrophy included S*ynechococcus* spp. prey concentration (cells/nL), phosphate (μM),

nitrogen (μM), ammonium (μM), and PAR (mol photon/m^2). For each VIF test, phosphate and

nitrogen were collinear. The analysis proceeded with phosphate only because prior research

found phosphate to be a significant predictor of phytoflagellate mixotrophy in the NGA (Busse

2021). Once nitrogen was removed the VIF for each mixotrophy model was <2. Poisson

regression models were run for total cryptophyte mixotrophy and mixotrophy by individual size

classes (3-5 μm, 5-10 μm, 10-15 μm, 15-20 μm, 20-25 μm). Ultimately, a quasipoisson

regression was performed on all models because regression diagnostics showed that the data

were clumped. This correction was made by confirming that the ratio of residual deviance to

degrees of freedom (df) was $\neq$ 1 for each model. Since various time intervals of PAR were

inherently collinear, hourly PAR, 6 h PAR, 12 h PAR, 24 h PAR, and 48 h PAR were analyzed

separately; all proved to be nonsignificant predictors of cryptophyte mixotrophy in the NGA.

Results

The NGA is a highly seasonal ecosystem with spatial and temporal variability that influences primary productivity and phytoplankton community composition at multiple scales. During spring 2021 some of the highest total chlorophyll-a values in this multi-decade time series were recorded (Figure 5c). Spring had a low fraction of chlorophyll-a in small cells (<20 μm) and microscopy revealed a diatom-dominated phytoplankton community with few cryptophytes. During summer and fall the average 10 m total chlorophyll-a decreased to < 1/3 of the chlorophyll-a in spring; in contrast, the average 10 m chlorophyll-a in small cells increased from an average of 22 % in spring to ~82 % in summer and fall (Figure 5d, Table 1). The large proportion of chlorophyll-a in small cells was associated with high biomass and high carbon to chlorophyll values for a small cell-dominated phytoplankton community in the NGA.

Cryptophyte Distribution in the NGA

Seasonality

Cryptophyte communities in the NGA exhibited strong seasonality. Marine cryptophytes were least abundant in spring, the summer season was composed of high abundances of small cells, and the fall season exhibited a transition to fewer and larger cryptophyte cells (Figure 6a). The maximum cryptophyte 10 m abundance and biomass were recorded in summer on the GAK transect at 7.88×10^3 cells/mL and at 1.2×10^5 ngC/L, respectively. In contrast, the fewest cryptophytes were recorded in spring (maximum abundance was 7.20×10^2 cells/mL, maximum biomass was 2.65×10^4 ngC/L). Summer cryptophyte biomass maximum was 4.5x the spring maximum. The largest size class (20-25 μm) of cryptophytes recorded in 2021 appeared in summer samples and was also present in fall but was not observed in spring samples (Figure

6b). In general, larger size classes (cells ≥ 10 μm) contributed a greater proportion to the total cryptophyte biomass, despite the higher abundance of smaller cells in all seasons (Figure 6b).

NMDS analysis of cryptophyte community composition by biomass showed separation of all seasons, with a tight cluster of spring samples (Figure 7). The overlap of summer and fall samples on axis 1 but modest separation along axis 2 is likely explained by the presence of large cells (20-25 μm) in summer and fall. There were obvious groupings of cryptophyte size classes: the smallest cells clustered closely together (3-10 μm), as did the medium-sized cells (10-20 μm), while the largest cells (20-25 μm) appeared in a unique ordination space high on axis 2 (Figure 7). Like the biomass biplot, the spring cryptophyte community separated distinctly from summer and fall based on cell abundance (Appendix Figure 25).

Cryptophyte biomass at 10 m was positively correlated with the proportion of chlorophyll-a in small cells (<20 μm) in all seasons and positively correlated with total chlorophyll-a in summer and fall 2021 (Table 2). Spring cryptophyte biomass at 10 m was also negatively correlated with ammonium concentration (Table 2). In contrast, summer biomass at 10 m was negatively correlated with water temperature, 24 h PAR, and 48 h PAR (Table 2). Fall cryptophyte biomass at 10 m was strongly negatively correlated with salinity, distance offshore, and all time-intervals of PAR, except 48 h PAR (Table 2). Additionally, ammonium concentration and 10 m cryptophyte biomass had a positive correlative relationship in the fall (Table 2).

Multiple linear regression models assessed relationships between cryptophyte biomass at all depths (0-30 m) and numerous environmental variables. This analysis focused on summer and fall data because few cryptophytes were recorded in spring and environmental variables are often dramatically different in spring in the NGA (Table 1). There was a significant increase

in log (biomass) as phosphate concentration decreased for all size classes in summer and fall (Table 3). When all cryptophyte size classes were combined, phosphate concentration had a strong negative relationship, ammonium concentration had a moderate positive relationship, and salinity had a weak positive relationship with log (total biomass) (Table 3).

Individual size classes were also analyzed using multiple linear regression models to expose potential taxon-specific variability in relationships between environmental variables and cryptophyte biomass. All size classes showed negative relationships with phosphate concentration. In addition, for the smallest two size classes of cryptophytes (3-10 µm), log (biomass) increased when the 48 h PAR term was negative (Table 3). While the linear model results were similar for the smallest cryptophytes (3-10 µm), a decrease in nitrogen had a positive effect on log (biomass) only for 5-10 µm cryptophytes (Table 3). Log (biomass) of the medium (10-15 µm) cryptophytes was the only size class that positively increased when ammonium concentrations increased (Table 3). Finally, log (biomass) of the largest 2 groups (15-25 µm) of cryptophytes exhibited a positive relationship with salinity (Table 3).

Cross-Shelf Gradients

In addition to seasonal variability, cryptophyte community composition in the NGA exhibited fine-scale spatial and temporal variability when each transect and season was examined individually (Figures 8-10). Summer on the GAK transect had the highest 10 m cryptophyte biomass in 2021 (Figure 9b). Cryptophyte biomass was higher on the shelf and lower offshore on the GAK and MID lines in summer and fall (Figures 9, 10). Despite lower total biomass, large cryptophyte cells were more abundant in offshore waters on the GAK line in summer and fall 2021 (Figures 9, 10). Both the GAK and MID lines had low total chlorophyll-a in

the fall (Table 1), but the largest size class (20-25 μm) of marine cryptophytes were valuable

contributors to total biomass (Figure 10). The smallest cryptophyte cells (3-5 μm) had minimal

biomass, or were nonexistent, in spring and fall in the NGA (Figures 8, 10).

Spring communities were primarily composed of medium sized (5-20 μm) cryptophytes

(Figure 8). The GAK line had substantially lower 10 m biomass than the KOD and MID transects

in spring (Figure 8b). The KOD line exhibited low offshore biomass while the GAK and MID

transects did not have cross-shelf trends (Figure 8).

In the summer, the smallest size class (3-5 μm) was important nearshore on the GAK

and MID lines, while the largest size class of cryptophytes (20-25 μm) was a significant

component of the nearshore KOD transect (Figure 9). This contrast in cryptophyte community

composition and ~5x higher total chlorophyll-a, predominately in large cells, at some stations

on the KOD line (Fig. 11) suggests a different summer ecosystem than the GAK and MID

transects. There was an obvious cross-shelf gradient in cryptophyte cell size on the KOD line in

summer, with average cell size decreasing with increasing distance offshore (Figure 9a).

In fall, high biomass of large cryptophyte cells (20-25 μm) marked a transition from a

small cell-dominated ecosystem (Figure 10). Large cells played an important role offshore on

both the GAK and MID transects in the fall (Figure 10). The GAK transect line in fall 2021 had

considerably higher 10 m cryptophyte biomass than the MID transect (Figure 10) The KOD

transect was not sampled in fall due to bad weather in the NGA.

NMDS analysis of spring, summer, and fall cryptophyte community composition by

biomass (ngC/L) showed all transect lines overlapped on both axis 1 and axis 2 (data not

shown).

Interannual Variability

Marine cryptophyte community composition and total biomass at 10 m on the GAK transect in summer showed significant variability in our four-year time series. Relative to other years, 2021 had intermediate cryptophyte cell size and total concentration at most stations sampled, except total concentration (cells/mL) was higher at offshore stations in 2021 (Figures 12a, 12c). Total cryptophyte biomass in 2021, both on the shelf and offshore, was lower than in 2018 and 2020 (Figure 12b). Cryptophyte cell size was typically smaller in 2021, explaining the lower total biomass when compared to 2018 and 2020 (Figure 8c). During 2019 a marine heat wave afflicted the NGA. The ecosystem implications of this disturbance were reflected in lower-than-average cryptophyte cell size, concentration, and biomass in 2019 (Figure 12). It is important to note that 2021 had largest sample size and 2018 the smallest, potentially leading to challenges in interpreting this time series.

Small Cell Phytoplankton Community Composition: How Important were Cryptophytes?

Flow cytometry data provided valuable insight into the community composition along with the biomass contribution of different groups comprising the summer and fall phytoplankton communities in the NGA. Small cells (<20 μm) comprised on average 91 % of the total chlorophyll-a measured at 10 m on the GAK and MID transects in summer and 79 % in fall (Table 1). Despite only 2x higher mean 10 m chlorophyll-a in summer (1.51 μg/L) over fall (0.75 μg/L), the maximum summer 10 m carbon biomass was 5x that of fall on the GAK transect (Figure 13a). There were spatial differences as well. Maximum 10 m carbon biomass on the GAK transect was 4.2x that on the MID transect in summer and 1.4x in fall (Figures 13a, 13b). Total small cell phytoplankton biomass (μgC/L) was lowest offshore on both GAK and MID transects

in summer (Figures 13a, 13b). In contrast, neither transect showed a cross-shelf trend in fall (Figures 13a, 13b).

On average, nanoeukaryotes and cryptophytes contributed ~75 % of the total biomass on the GAK and MID transects (Figures 13bc, 13d). Cryptophytes were more important nearshore on the MID line in summer and nearshore on both transects in fall (Figures 13c, 13d). Smaller cells, including picoeukaryotes and *Synechococcus* spp., increased in relative importance with increasing distance offshore on the GAK transect in summer (Figure 13c). Picoeukaryotes and *Synechococcus* spp. consistently contributed ~30 % of total biomass across the GAK transect in fall (Figure 13c). The total small cell phytoplankton biomass reached a maximum of 605 µgC/L at 25 km offshore on the GAK line in summer 2021 (Figure 13a). At this station, 98 % of total chlorophyll-a was in small cells (<20 µm).

NMDS analysis of the 10 m summer and fall phytoplankton community composition by biomass on the GAK and MID transects showed obvious distinction of small cell phytoplankton groups (Figure 14). *Synechococcus* spp. and picoeukaryotes, the smallest cells, grouped closely together (Figure 14). The considerable overlap of all samples along axis 1 and axis 2 suggests that NGA small cell-dominated phytoplankton communities were similar in summer and fall 2021 (Figure 14). However, the fall phytoplankton community clustered more tightly together than summer indicating less variability in community composition among fall samples (Figure 14).

Spearman correlation analysis revealed relationships among these small cell phytoplankton groups at 10 m and between environmental variables and each taxonomic group. *Synechococcus* spp , picoeukaryotes, nanoeukaryotes, and cryptophytes were strongly

22

positively correlated with each other, except *Synechococcus* spp. were not correlated with

cryptophytes (Table 4). *Synechococcus* spp. were positively correlated with chlorophyll-a in

small cells, but not with any abiotic variable. Picoeukaryotes, nanoeukaryotes, and

cryptophytes were all strongly positively correlated with both chlorophyll-a in small cells and

total chlorophyll-a (Table 4). Although nanoeukaryotes and cryptophytes were strongly

negatively correlated with water temperature, mean temperature was 1 °C lower in summer

than fall and total small-cell community biomass was higher in summer (Table 4).

Carbon to chlorophyll ratios (C:chl) for small cell-dominated phytoplankton communities

in the NGA were generally high and decreased from summer to fall (Figure 15). The mean 10 m

C:chl on the GAK line was 160 (SD = 33.2) in summer and 144 (SD = 24.5) in fall. The MID

transect had similar 10 m C:chl of 199 (SD = 68.2) in summer and 145 (SD = 23.2) in fall. In

summer, the highest C:chl corresponded to samples with high total biomass (Figures 13, 15). In

contrast, high C:chl in fall were associated with increased biomass contribution by the smallest

sized taxonomic groups, including picoeukaryotes and *Synechococcus* spp. (Figures 13, 15).

Cryptophyte Mixotrophy

This study presents strong evidence that cryptophytes in the NGA are mixotrophic. Up to 20

% of the total cryptophyte community contained ingested S*ynechococcus* spp. prey during the

summer and fall of 2021. Cryptophyte mixotrophy at 10 m in the NGA was highest in cells ≥10

μm, but cells <10 μm also demonstrated a capacity for mixotrophic feeding on S*ynechococcus*

spp. prey (Figures 16-20). The GAK transect had the highest fraction of active cryptophyte

mixotrophs of all size classes in both summer and fall while the MID had the lowest (Figures 16-

20). It is worth noting that almost no mixotrophy was observed on the KOD transect in summer

until 125 km offshore, where a shift in cryptophyte community composition occurred (Figures 9a, 16).

Quaisipoisson regression generalized linear models produced coefficients that were interpreted as incident rate ratios (% change in y with one unit change in x) for significant predictors of 0 – 30 m cryptophyte mixotrophy (Figure 21). For every 1 cell/nL increase in S*ynechococcus* spp. concentration, there was a 10.99x increase in cryptophyte mixotrophy; likewise, for every 1 μM increase in phosphate concentration, there was a 1.16x increase (Table 5). In contrast, with every 1μM increase in ammonium concentration there was a 0.71x decrease in cryptophyte mixotrophy (Table 5).

When cryptophyte size classes were analyzed independently, higher S*ynechococcus* spp. concentrations predicted higher cryptophyte mixotrophy for all but the smallest two size classes (3-10 μm) (Figure 22). Although results for the 5-10 μm size class were excluded by our model criteria, S*ynechococcus* spp. concentration likely had a weak positive predictive relationship and ammonium a weak negative relationship for mixotrophy in the 5-10 μm size class, with p-values of 0.12 and 0.17, respectively. In contrast, the 3-5 μm size class had no significant predictors of cryptophyte mixotrophy. The largest 3 size classes of cryptophytes (10-25 μm) demonstrated a strong capacity for mixotrophy (Figures 16-20). For every 1 cell/nL increase in S*ynechococcus* spp. concentration, cryptophyte mixotrophy increased 6.55x, 8.07x, and 14.52x for size classes 10-15 μm, 15-20 μm, and 20-25 μm, respectively (Table 5). Therefore, the positive effect of prey concentration on cryptophyte mixotrophy was stronger on larger cells. S*ynechococcus* spp. concentration was the only significant predictor for the size classes 10-15 μm and 15-20 μm (Table 5). In contrast, phosphate concentration also predicted

cryptophyte mixotrophy for the largest (20-25 μm) size class. For every 1 μM increase in

phosphate concentration, there was a 1.83x increase in cryptophyte mixotrophy for 20-25 μm

cryptophytes (Table 5). It is worth noting that ammonium and phosphate consistently had a p-

values ~ 0.1 before dropping out of individual size class mixotrophy models.

Discussion

Cryptophytes in the NGA

Cryptophytes were a significant component of the carbon biomass of small cell-dominated phytoplankton communities in the NGA in summer and fall 2021. Our results uncovered distinct cryptophyte size class groupings that are each related to a different set of environmental factors, suggesting niche partitioning and/or prevalence of numerous cryptophyte species in the NGA. Their versatility is likely associated with cryptophyte taxonomic variability and nutritional plasticity via mixotrophy (Clay and Kugrens 1999; Hoef-Emden et al. 2002).

Seasonality

Spring cryptophyte biomass was low when micro- and macronutrients that are essential to phytoplankton growth, including nitrogen and phosphate, were high; diatoms dominated the NGA in spring 2021. The spring bloom and increased water column stratification drew down essential micro- and macronutrients as the ecosystem transitioned from spring to summer. When all seasons were compared, cryptophyte biomass peaked in summer on the shelf at 1.2 x 10^5 ngC/L. Salinity gradually decreased from spring to fall due to increased freshwater runoff from mountains and glaciers surrounding the NGA (Beamer et al. 2017). Increased prevalence of water column mixing due to storms caused micro- and macronutrient concentrations to again rise in fall. Higher micro- and macronutrient concentrations and/or the employment of mixotrophy in the fall may have facilitated the survival of larger cryptophyte cells (20-25 µm) that require more micro- and macronutrients due to their low surface area to volume ratios.

Zooplankton predation on marine cryptophytes certainly impacted their seasonal biomass trends. Cryptophytes are nutritious prey attributed to a soft outer body wall, high concentrations of essential fatty acids, and lack of toxicity (Brett and Müller-Navarra 1997; Galloway and Winder 2015). A significant positive correlation between freshwater lake copepod predator abundance and cryptophytes was found by measuring the presence of precipitated alloxanthin, a cryptophyte-specific carotenoid pigment, in sediment traps (Barkhatov 2021). Furthermore, Barkhatov (2021) found evidence that freshwater copepods selectively consume cryptophytes, likely due to their high nutritional value. The strong seasonality of the NGA abiotic environment significantly influences zooplankton abundance (Coyle and Pinchuk 2005). The low spring 2021 cryptophyte biomass could be attributed to a typical NGA springtime peak of neocalanus copepod zooplankton abundance when water temperatures are low (Coyle and Pinchuk 2005). Likewise, NGA zooplankton populations often decline in summer, at least in part due to zooplankton phenology and increased abundance of nektonic predators (Coyle and Pinchuk 2005), coincident with the 2021 peak in cryptophyte abundance and biomass. Seasonal variability in the size structure of zooplankton predators also likely influenced cryptophyte biomass. In Antarctica cryptophytes are not grazed efficiently by large zooplankton predators due to their small size (Moline et al. 2004). Further research into the effect of zooplankton predators on the community composition structure and biomass of cryptophytes in the NGA is needed.

Cryptophyte Distribution and Biomass

While accurate phytoplankton community biomass estimates have been recognized for over 100 years as essential to understanding marine ecosystems, challenges in comparing data

persist due to differences in sampling methodologies and biomass conversion factors (Menden-Deuer and Lessard, 2000; Sutherland 1913). Here we present study comparisons on cryptophyte cell abundance, absolute biomass, and relative biomass estimates from temperate to arctic small cell-dominated communities worldwide. There is limited literature on cryptophyte abundance and biomass estimates in ecosystems like the NGA.

Cryptophyte abundance at 10 m in the NGA in summer and fall 2021 ranged from 3.21 x 10^1 – 7.88 x 10^3 cells/mL with a mean abundance of 1.01 x 10^3 cells/mL and a median of 6.15 x 10^2 cells/mL. A time series analysis of cryptophyte concentration at the Scripps Institution of Oceanography pier in La Jolla, California, USA (32 °N) from 2011-2016 found a mean abundance of 8.86 x 10^2 cells/mL (median 6.11 x 10^2 cells/mL); abundance ranged from 0 cells/mL in October 2012 to 1.31 x 10^4 cells/mL in July 2016 (Rammel 2021). In addition to high intra- and interannual variability in cryptophyte abundance, Rammel (2021) also found large differences over small spatial scales in San Diego Bay in summer 2019. This resembles the high spatial and temporal variability in cryptophyte abundance found in the NGA in 2021 (Rammel 2021).

A contrasting marine environment, the oligotrophic western Mediterranean Sea (40 °N), had average annual (March 2003- March 2004) cryptophyte abundances of 342 cells/mL which accounted for ~13 % of the small cell (3-20 μm) phytoplankton abundance (Unrein et al. 2014). Our estimate for the average NGA summer and fall 10 m cryptophyte abundance was ~3x that of the Mediterranean at 1.01 x 10^3 cells/mL. NGA cryptophytes only accounted for, on average, 1.35% of the 10 m total small cell (<20 μm) phytoplankton abundance but represented, on average, 18% of the total small cell phytoplankton biomass on the GAK and MID transects in summer and fall 2021. A greater contribution of larger cells to total community biomass in the

NGA likely explains the discrepancy in cryptophyte relative abundance when compared to an oligotrophic basin such as the Mediterranean (Unrein et al. 2014).

Cryptophyte communities in similar ecosystems were compared using biomass estimates. In the NGA in summer and fall 2021 cryptophyte biomass at 10 m ranged from 2.74 x 10^3 - 1.20 x 10^5 ngC/L with a mean of 2.98 x 10^4 ngC/L and a median of 2.40 x 10^4 ngC/L. These cryptophyte biomass estimates resemble other temperate and arctic marine ecosystems including Korea, the South Atlantic, and Antarctica (Garibotti et al. 2003; Jeong et al. 2013; Tarran et al. 2006). In Masan Bay, a semi-enclosed bay in Korea at 35 °N, annual cryptophyte biomass at the surface ranged from 0 - 6.68 x 10^6 ngC/L with a mean biomass of 1.99 x 10^5 ngC/L in 2004-2005 (Jeong et al. 2013). The higher mean biomass presented by Jeong et al. (2013) could be explained by the exclusively coastal nature of their study; this is supported by our findings that NGA cryptophyte biomass was typically higher nearshore in 2021. Estimates for the NGA closely aligned with cryptophyte biomass estimates for coastal Antarctica in austral summer (January-February 1996), which ranged from 6.90 x 10^3 – 3.61 x 10^4 ngC/L with a mean of 1.92 x 10^4 ngC/L (Garibotti et al. 2003). Cryptophyte biomass was lower in the oceanic South Atlantic basin at 35 °S in September-October 2003 and April-June 2004 where the mean surface value was only 6.7 x 10^3 ngC/L (Tarran et al. 2006).

NGA cryptophytes contributed 4-45 % of the total small cell (<20 μm) phytoplankton carbon biomass on the GAK and MID transects in summer and fall 2021. Similarly, Strom et al. (2010) found that cryptophytes were common on the NGA shelf in summer 2003. Studies from subarctic and temperate latitudes show similar cryptophyte contribution to summer biomass including 5-21% in the Baltic Sea (Griffiths et al. 2020) and 13-16% in the inland estuarine Salish

Sea off Washington State, USA and British Columbia, Canada (Del Bel Belluz et al. 2021). In the Salish Sea both cryptophytes and prasinophytes had high biomass during non-bloom conditions year-round (Del Bel Belluz et al. 2021). Similarly, at Ocean Station Papa in the subarctic oceanic Pacific, an environment comparable to NGA offshore stations, the 10-20 μm phytoplankton community was dominated by cryptophytes and dinoflagellates in August (Booth 1988).

Taken together these findings suggest that NGA 2021 cryptophyte biomass falls within the range of previous studies and that higher nearshore cryptophyte biomass might be a general feature of temperate, subarctic, and arctic oceans (Garibotti et al. 2003; Jeong et al. 2013; Tarran et al. 2006). Variability in cryptophyte abundance, biomass, and distribution both in the NGA and worldwide hints at an expansive ecological range and high diversity for this phytoplankton group.

Cryptophyte Niche Diversity

Our study recorded cryptophytes in a diverse array of conditions in the NGA including high nutrient environments in spring, low chlorophyll environments in summer and fall, micro- and macronutrient limited conditions in summer, and low salinity environments in fall. This niche diversity is associated with numerous cryptophyte evolutionary responses; these likely include but are not limited to clade and species diversity, a wide cellular size range, and mixotrophy (Del Bel Belluz et al. 2021; Rammel 2021).

Clustering of size classes in plots, linear modeling, and multivariate statistical analyses suggested that at least three different cryptophyte species or species groups with size ranges of 3-10 μm, 10-15 μm, and 15-25 μm play important roles in the NGA. While all cryptophytes demonstrated a strong negative relationship with phosphate concentration, individual size

classes varied in other aspects of their distribution and relationship to environmental

properties (Table 6).

The smallest size class (3-5 μm) of cryptophytes had the greatest relative contribution

nearshore and on the shelf in summer 2021. Cells 5-10 μm did not present any evident seasonal

or cross-shelf trends and were generally present in low or moderate relative abundances in

spring and moderate or high relative abundances in summer and fall 2021. Although abundance

and biomass trends were variable between cryptophytes 3-5 μm and 5-10 μm, models showed

both size classes were strongly associated with lower phosphate concentrations and modestly

associated with lower light conditions. This suggests that cryptophytes 3-10 μm accumulate

more biomass and/or are more competitive than other phytoplankton under lower light

conditions. Cryptophytes 5-10 μm were also moderately associated with lower nitrogen

concentrations (Table 6).

Medium sized (10-15 μm) cryptophytes occupied a unique niche. Increases in ammonium

concentration and decreases in phosphate concentration were associated with increased

biomass of 10-15 μm cryptophytes (Table 6). This size class was the main component of spring

communities and persisted to contribute ~25% of total cryptophyte biomass across all transects

in summer and ~50% in fall.

The largest (15-25 μm) cryptophytes recorded in this study were associated with higher

salinities and lower phosphate concentrations (Table 6). Cryptophytes 20-25 μm in size were an

important component offshore in high salinity waters on the GAK and MID lines in fall. In

contrast, these large cells also had high biomass inshore on the KOD transect in summer where

total chlorophyll-a was ~5x higher than on the GAK and MID transects and the phytoplankton

31

community was large cell-dominated (Figure 11). This apparent niche variability of large

cryptophytes could be explained by species differences or eddy transport but requires further

research.

Our findings of a negative relationship between cryptophytes and phosphate were also

described for marine ecosystems in coastal southern California, USA (Rammel 2021), coastal

Korea (Jeong et al. 2013), and Denmark (Altenburger et al. 2020). This relationship hints that

photosynthetic cryptophytes in the NGA and elsewhere are not limited by phosphate

concentrations or that they selectively acquire phosphate via alternate routes such as

mixotrophy.

Results demonstrating that cryptophytes can thrive in various environmental niches in

the NGA suggest high diversity and adaptability of this phytoplankton group. These conclusions

are supported by studies in the Salish Sea suggesting that weak correlations between

cryptophytes and specific environmental conditions are due to versatility, high diversity, and

competitive advantages of cryptophytes when compared to other phytoplankton groups (Del

Bel Belluz et al. 2021).

The likelihood that NGA cryptophyte environmental niches are associated with high

species diversity is supported by metagenomic research showing high genetic and

environmental diversity of clade 4 marine cryptophytes in temperate waters (Rammel 2021).

These recent findings provide further support that clade 4 cryptophytes, which include the

genera *Teleaulax, Geminigera*, and *Plagioselmis*, dominate in temperate marine environments

(Medlin and Orozco 2017; Marie et al. 2010; Needham et al. 2018; Supraha et al. 2014). This

information suggests that NGA cryptophytes of the same clade can inhabit disparate

environments. Likewise, metagenomic studies in the Mediterranean Sea found high diversity,

including 6 cryptophyte genera and 11 species, associated with variability in cryptophyte cell

volume throughout the year (Unrein et al. 2014). Cryptophyte genus was also connected to

spatial and temporal trends in biomass in the Baltic Sea and Coastal Korea (Griffiths et al. 2020;

Kang et al. 2021).

Cryptophyte Time Series

Predicted global sea surface temperature warming of 2-4 °C by 2100 (Cooley et al. 2022)

will increase water column stratification and likely affect nutrient supply to favor smaller

phytoplankton taxa that are adapted to low micro- and macronutrient concentrations (Bindoff

et al. 2019; Henson et al. 2021). Our results showed lower cryptophyte abundance, biomass,

and smaller cell size during a 2019 NGA marine heat wave (Figure 23) (Suryan et al. 2021).

Research in the Baltic Sea also found decreasing cryptophyte biomass under rapid warming

conditions since the 1980's (Griffiths et al. 2020; Suikkanen et al. 2013).

Climate models predict increased prevalence of marine heat waves and other extreme

ecosystem anomalies in the future (Walsh et al. 2018). Warmer water temperatures will likely

increase phytoplankton growth rates and a longer growing season is predicted to result in

increased biomass production in the NGA (Duffy et al. 2017; Henson et al. 2021; Pennekamp et

al. 2018; Worm et al. 2006). However, larger phytoplankton are expected to decrease in

relative abundance due to limiting micro- and macronutrient supplies associated with increased

water column stratification (Dutkiewicz et al. 2020; Henson et al. 2021). Although climate

change is expected to decrease the variety of available phytoplankton niches, taxa that can

survive in a wide range of environmental niches, like cryptophyte mixotrophs, might be less

vulnerable to extinction (Henson et al. 2021; Hillebrand et al. 2018). It is plausible that both small cryptophytes that require minimal micro- and macronutrients and large cryptophytes that are mixotrophs will thrive in future climate-changed marine ecosystems due to their advantage over more specialized phytoplankton groups.

Small Cell-Dominated Phytoplankton Communities

NGA Biomass and Carbon to Chlorophyll Ratios

Our study found NGA carbon biomass up to 600 µgC/L in summer and fall, when total chlorophyll-a was less than 2 µg/L. Chlorophyll-a in small cells (<20 µm) at 10 m on the GAK and MID transects was on average 91 % of total chlorophyll-a in summer and 79 % in fall. Since our flow cytometric analysis was restricted to small cells (<20 µm), we have confidence that our data represent most of the phytoplankton community at these times.

Carbon biomass estimates for the NGA 10 m small cell (<20 µm) phytoplankton community ranged from 37-605 µgC/L for summer and fall 2021. Similarly, previous research by Burt et al. (2018) using optical measurements from an underway system found carbon biomass estimates for the subarctic Pacific in the summer to vary from 20 – 400 µgC/L. The study region in Burt et al. (2018) encompassed the NGA but also contained a wider range of marine environmental conditions, including Barkley Canyon off Vancouver Island, British Columbia, Canada where the maximum carbon biomass and highest variability were recorded.

High carbon biomass of these NGA small cell-dominated communities resulted in high C:chl. We found C:chl between 82-293 for summer and fall 2021 in the NGA, higher than previously expected. High NGA ratios were likely due to very high total biomass at nearshore stations in summer and lower ratios the result of low total biomass and low chlorophyll at some

shelf stations in fall. Similarly, high C:chl at NGA offshore stations in summer and fall 2021 were associated with moderate biomass of small phytoplankton cells in a low chlorophyll iron-limited environment.

Small Cell-Dominated Phytoplankton Community Composition

Results from our study demonstrated that photosynthetic nanoeukaryotes, including cryptophytes, are critical components of the NGA ecosystem. Summer and fall communities were dominated by these phytoplankton groups, contributing ~75 % of the total biomass across the GAK and MID transects. Cryptophytes had higher relative abundance nearshore and on the shelf than in oceanic waters in both summer and fall 2021. Low salinity waters nearshore on the MID transect in summer had high relative abundance of *Synechococcus* spp. Picoeukaryotes and *Synechococcus* spp. generally increased in relative abundance with increasing distance offshore on the GAK transect in summer 2021; contrasting trends were present for larger cells. Likewise, other studies in the NGA found *Synechococcus* spp. and small phytoflagellates dominant in offshore iron-limited waters (Strom et al. 2006; Strom et al. 2010).

Community composition results from our study were supported by other research in Arctic, subarctic, and temperate ecosystems indicating that phytoflagellates <15 μm in size, including cryptophytes, dominate small cell phytoplankton communities (Bolaños et al. 2020; Garibotti et al. 2003; Tarran et al. 2006). In common with the NGA in 2021, Tarran et al. (2006) found nanoeukaryotes, including cryptophytes, contributed 65-85% of total phytoplankton carbon biomass in North Atlantic temperate waters. Although a lower latitude ecosystem, flow cytometry analysis of a small cell-dominated phytoplankton community in the Northern

Adriatic Sea found estimates for relative contribution of cryptophytes and nanoeukaryotes to be 10% and 43%, respectively (Radi 2009).

Our results provide additional evidence that small cell-dominated phytoplankton communities can have carbon biomass levels comparable to, or higher than, diatom-dominated spring blooms in both the North Atlantic and the North Pacific (Strom et al. 2016; Westberry et al. 2016). This consistent underestimation of small cell-dominated community carbon biomass demonstrates that chlorophyll concentrations are not always an accurate predictor of carbon biomass (Behrenfeld et al. 2016; Veldhuis & Kraay 2004; Westberry et al. 2016). Employment of ecosystem-specific biomass conversion factors for both in situ and remote-sensed chlorophyll-a observations for diverse phytoplankton assemblages will improve our understanding of this important measure of ecosystem resilience (Menden-Deuer and Lessard 2000; Garibotti et al. 2003; Verity et al. 1992). Understanding the dynamics of small cell-dominated phytoplankton communities is crucial since small phytoflagellates (<20 μm) are often major components of phytoplankton communities and are key drivers of marine carbon and nutrient cycling (Bolaños et al. 2020; Worden et al. 2015). Results from this study demonstrated that small cell-dominated phytoplankton communities are vital to the present-day functioning of subarctic marine ecosystems. Climate models predict that smaller and more versatile phytoplankton communities, like those found in summer and fall in the NGA, will increase in importance in future climate-changed oceans as temperature and water column stratification increase (Henson et al. 2021).

Cryptophyte Mixotrophy

Despite widespread acknowledgement of small-celled phytoplankton mixotrophy as an important influence on ocean biogeochemical cycling and food web models, in situ evidence is scarce (Flynn et al. 2013). It is now generally accepted that mixotrophy is the norm rather than the exception for phytoflagellates such as marine cryptophytes (Flynn et al. 2013; Jeong et al. 2010; Stoecker et al. 2009). Not only are mixotrophic protists ubiquitous, they also frequently dominate the lower trophic levels of marine ecosystems (Jeong et al. 2010; Sanders 1991; Stoeker et al. 2009; Zubkow and Tarran 2008). Phytoplankton mixotrophy is employed to obtain fixed carbon, micro- and macronutrients, trace elements, and/or energy (Stoecker et al. 2017).

Cryptophytes are constitutive mixotrophs, protists that contain photosynthetic machinery and the associated regulatory genes, and only feed in response to certain conditions in their environment (Leeuwe et al. 2020; Stoecker and Lavrentyev 2018). Experiments using fluorescently labeled beads demonstrated that cryptophyte mixotrophy is influenced by dissolved organic carbon concentration, light intensity, and prey concentration (Porter 1988; Sanders et al. 1990). Studies on phytoflagellate mixotrophy in a mesocosm experiment using water from the oligotrophic NW Mediterranean showed that cryptophytes were the second most important mixotrophic group, responsible for 8% of total grazing by mixotrophs, surpassed only by haptophytes that contributed 40% of total mixotrophic grazing (Unrein et al. 2014). One of the few in situ studies on cryptophyte mixotrophy suggests that mixotrophy enables freshwater cryptophytes to survive Antarctic polar winters under ice in a low-light environment (Marshall and Laybourn-Parry 2002).

Our hypothesis that cryptophytes in high micro- and macronutrient nutrient environments would be purely autotrophic was supported by low, or nonexistent, mixotrophy during spring 2021 when nutrient concentrations were highest. However, we were unable to find support for our hypothesis that PAR will have a negative relationship with mixotrophy. Our study presented strong evidence that NGA cryptophyte mixotrophy is primarily by prey availability and that higher phosphate and lower ammonium concentrations are important mixotrophy predictors for some size classes of cryptophytes. Since feeding increased with prey (*Synechococcus* spp.) concentration, NGA cryptophytes are constitutive mixotrophs that feed (at least in part) in response to prey availability. It is probable that an interaction of prey concentration and micro- and/or macronutrient concentrations explains spatial and temporal variability in cryptophyte mixotrophy in the NGA.

Results from our study revealed ecotype variability for each size class of mixotrophic cryptophytes. When assessed as independent size classes there was little evidence for mixotrophy in the smallest cryptophyte (3-5 μm) size class. Although statistically nonsignificant (p ~ 0.13), the 5-10 μm cryptophytes demonstrated a positive relationship with prey concentration and a negative relationship with ammonium. It is possible that the 5-10 μm size class was nitrate limited and opportunistically fed on *Synechococcus* spp as a nitrogen source. This idea is supported by higher 5-10 μm cryptophyte mixotrophy nearshore and on the shelf where nitrogen and ammonium concentrations were lower. Furthermore, the significance of ammonium as a mixotrophy predictor in the model including all cryptophyte size classes is likely driven predominately by the 5 -10 μm size class.

Larger cryptophyte cells (>10 µm) were more likely to be mixotrophs than smaller cells

in both summer and fall in the NGA. Mixotrophy in cryptophytes 10-20 µm was controlled only

by prey concentration in the NGA. This suggests that 10-20 µm cryptophytes opportunistically

feed on *Synechococcus* spp. either as a micronutrient, macronutrient, or carbon subsidy for

energy and cellular growth (Li et al. 2022; Stoecker et al. 2017). Our results of prey

concentration-dependent mixotrophy are supported by evidence from a laboratory study using

natural populations of *Synechococcus* spp. from Korean waters, which demonstrated a positive

correlation between cryptophyte ingestion rates and prey concentration; up to 40% of the

population of *Synechococcus* spp. was consumed by cryptophytes in one hour (Yoo et al. 2017).

Similar support for co-occurrence of *Synechococcus* spp. and cryptophyte blooms was found by

Rammel (2021), who showed a high positive correlation between the cryptophyte *T.*

amphioxeia and *Synechococcus* spp. abundance. Antarctic studies also show that mixotrophic

cryptophytes in freshwater lakes have a greater grazing impact on bacterial biomass than do

heterotrophic nanoflagellates (Roberts and Laybourn-Parry 1999).

It is probable that NGA 10-20 µm mixotrophic cryptophytes were not light limited and

were simultaneously feeding and photosynthesizing in summer and fall 2021. The lack of

correlation with PAR and cryptophyte mixotrophy suggests that high macronutrient

concentrations and high prey availability had a compounding effect to promote higher 10-20

µm cryptophyte growth rates than those possible with photosynthesis alone. Many

phytoflagellate species reach faster growth rates as mixotrophs than when employing

photosynthesis or feeding alone (Adolf et al. 2006; Burkholder et al. 2008; Jeong et al. 2010).

Light-dependent mixotrophy for this size class of cryptophytes is supported by studies on

mixotrophic dinoflagellates (Li et al. 1999). Similarly, in chrysophytes (*Ochromonas* species) feeding enhanced photosynthesis (Livanou et al. 2020), and both feeding and photosynthesis rates covaried with light availability (Wilken et al. 2020); Lie et al. (2018) even found a transcriptomic response to support this relationship.

Our results conflict with a recent study showing higher rates of cryptophyte feeding in low light conditions in fall 2019 in the NGA (Busse 2021). Results from Busse (2021) suggested that cryptophytes consumed prey for fixed carbon rather than macronutrient acquisition. This discrepancy could be explained by high interannual variability in both phytoplankton community composition and environmental conditions in the NGA or by a limited sample size in the Busse (2021) study (n = 7) compared to our sample size (n = 127).

Higher prevalence of cryptophyte mixotrophy, especially by cells ≥ 15 μm, in offshore waters on the KOD and GAK transects in summer and the GAK transect in fall suggests that large cryptophytes consumed *Synechococcus* spp. to subsidize micronutrients. The positive relationship between phosphate concentration and cryptophyte mixotrophy could be driven primarily by large (20-25 μm) cells and indicate that cryptophytes offshore are in HNLC waters (where macronutrients occur at relatively high concentrations) and need to feed on *Synechococcus* spp. to obtain iron. This finding is further supported by an absence of mixotrophy in a nutrient replete summer nearshore environment on the KOD line despite high biomass of large (> 15 μm) cryptophyte cells (Figure 9a, Figure 16). The higher incidence of mixotrophy in large cryptophytes can be explained by the increased challenge for larger cells to meet their energetic needs from photosynthesis and ambient dissolved micro- and macronutrients alone due to lower cellular surface area to volume ratios (Anderson et al. 2017).

Our hypothesis of micronutrient limitation-driven mixotrophy in large cryptophyte cells was supported by a study in oligotrophic Mediterranean waters demonstrating a clear positive relationship between cryptophyte cell size and grazing rates (Unrein et al. 2014). Similarly, a mesocosm experiment in a freshwater lake in Japan determined that cryptophytes can successfully utilize nitrogen and phosphorous from bacteria in a nutrient depleted environment (Urabe et al. 2000). Studies from temperate waters show that bacterivory provides mixotrophic predators with concentrated nutrients and offers a competitive advantage over pure autotrophs even in nutrient replete environments (Zubkov and Tarran 2008).

Our findings contrast with results found by other studies showing increased cryptophyte mixotrophy with decreased phosphate concentration in mesocosm experiments from oligotrophic Mediterranean waters (Unrein et al. 2014) and a freshwater lake in Japan (Urabe et al. 2000). Similarly, a laboratory study using Mediterranean source water found an immediate response of decreased phytoflagellate feeding when phosphate limitation was relieved (Oikonomou et al. 2020). A plausible explanation for this difference is that the above experiments contained phosphate-limited phytoplankton communities while our NGA in situ communities were instead iron-limited. Iron limitation in oceanic waters is often associated with high concentrations of macronutrients, like phosphate (Wu et al. 2009).

Variability in cryptophyte feeding strategy and detection of mixotrophy in diverse environmental conditions in the NGA suggests that numerous cryptophyte mixotrophy strategies exist both in subarctic ecosystems and worldwide (Unrein et al. 2014). Since our study was constrained to assessing mixotrophy on *Synechococcus* spp., the fraction of active mixotrophs would likely be higher if other heterotrophic bacteria prey were included in our

analysis. While there is a metabolic cost to maintaining both photosynthetic and phagotrophic

machinery, cryptophyte mixotrophy in the NGA likely increases primary production, improves

inorganic nutrient cycling within the water column, and enhances the transfer of carbon

biomass to higher trophic levels (Li et al. 2022; Marshall and Laybourn-Parry 2002; Ward and

Follows 2016).

Outlook

The versatility and high biomass contribution of marine cryptophytes make them a vital component of the NGA ecosystem in summer and fall. Climate models project global declines in phytoplankton biomass, euphotic zone nutrient concentrations, and carbon export flux to the deep ocean by 2100 (Cooley et. al 2022). In Arctic and subarctic ecosystems, advancements in the annual timing of the optimal phytoplankton growth period are predicted by 2100 (Cooley et. al 2022). Lending support for the 'Paradox of the Plankton' theory, both intra-and interannual reorganization in the size structure, taxa composition, and plasticity in nutritional strategy of NGA small cell-dominated phytoplankton communities suggests that high diversity and competition promote high ecosystem productivity (Hutchinson 1961). Phytoplankton that are resilient to changes in micro- and macronutrient availability, like small size classes of cryptophytes or mixotrophs, will help mitigate the negative ecosystem responses to climate-changed oceans (Martiny et al. 2022). Results from this study presented novel findings of high phytoplankton community carbon biomass and high carbon to chlorophyll ratios for the NGA in summer and fall 2021. We suggest that small cell-dominated phytoplankton communities, including mixotrophic phytoflagellates, are critical components of stratified subarctic marine environments and might be key to maintaining long-term resilience of these highly productive ecosystems. Projected decreases in subarctic ecosystem services due to anthropogenic climate change (Cooley et. al 2022) may be ameliorated if climate projections could factor in both the influence of higher-than-expected carbon biomass of small cell-dominated phytoplankton communities and the effects of mixotrophic phytoplankton on carbon and nutrient cycling.

Recommendations for future research include in situ measurements of phytoflagellate mixotrophy using a flow cytometry-detected acidic vacuole probe (lysotracker) to detect food vacuoles in mixotrophs (Beisner et al. 2019; Costa et al. 2022). Further efforts to include phytoflagellate mixotrophy into food web models in the NGA will increase our understanding of the resilience of subarctic marine ecosystems. Finally, assessment of the small cell phytoplankton community during the spring bloom could reveal a mixed-assemblage and alter currently accepted carbon biomass and flux estimates for a diatom-dominated bloom (Bolaños et al. 2020).
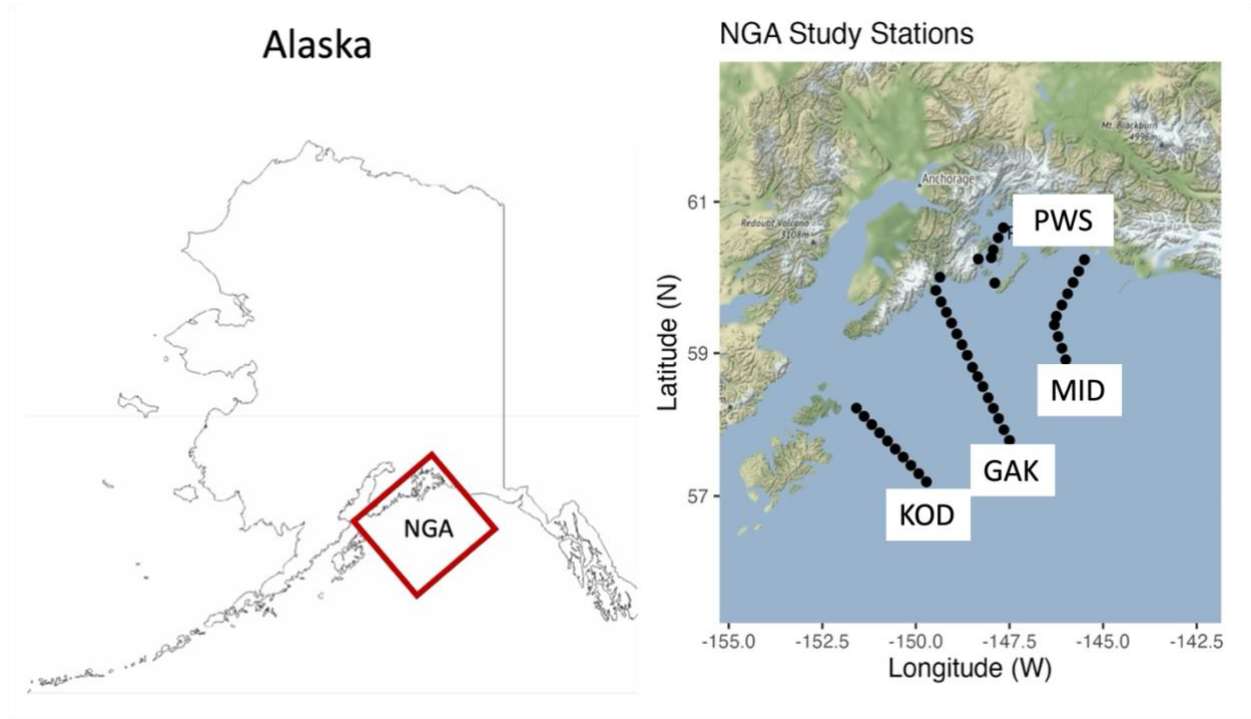
Figure 1: The Northern Gulf of Alaska (NGA) study site. Transects sampled included Kodiak (KOD), Seward Line (GAK), Middleton Island Line (MID), and Prince William Sound (PWS).
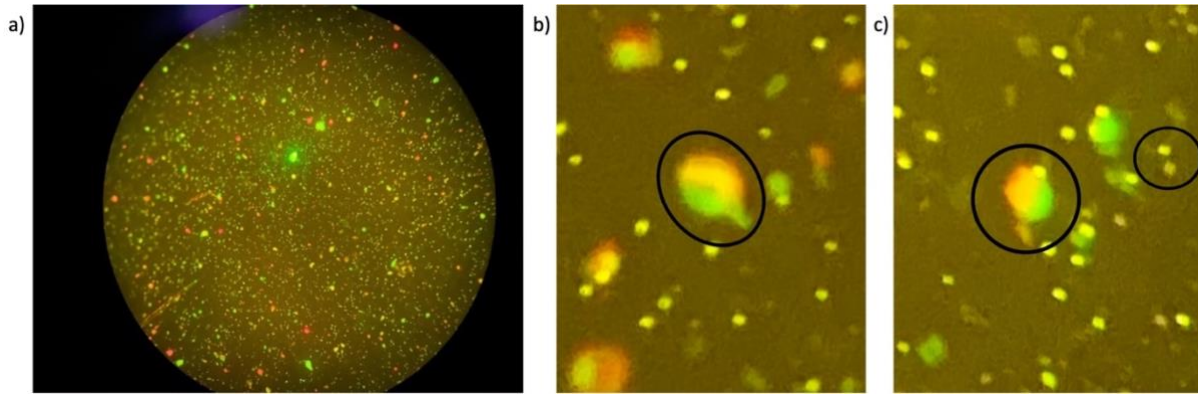
Figure 2: Epifluorescence microscopy examples of a) eyepiece view at 400x, b) tear-shaped cryptophyte cell at 1000x, and c) sphere-shaped cryptophyte cell and two *Synechococcus* spp. cells at 1000x.
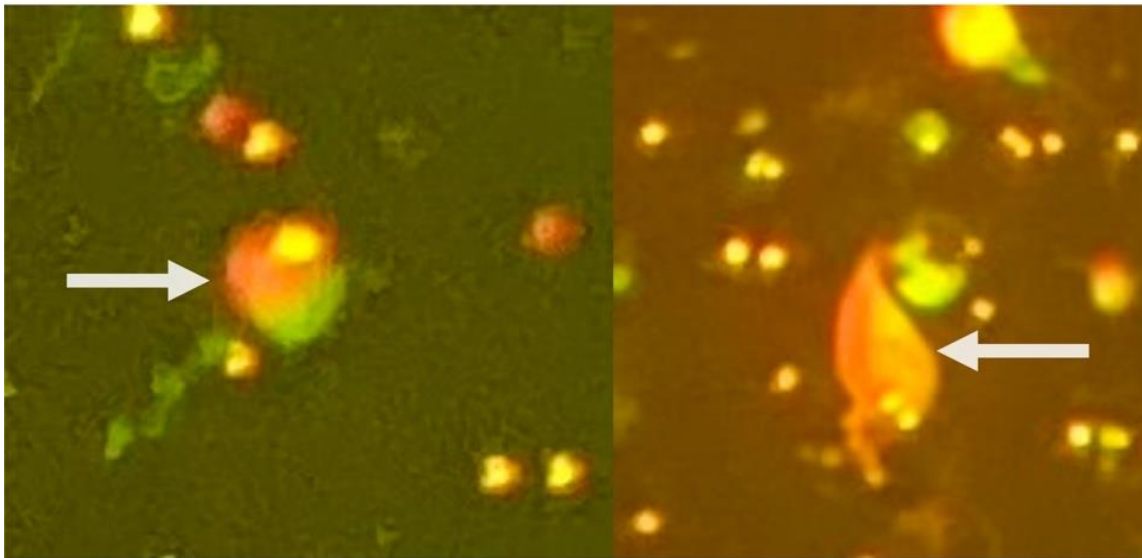
Figure 3: Cryptophyte cells (indicated by white arrows) with ingested *Synechococcus* spp. prey.
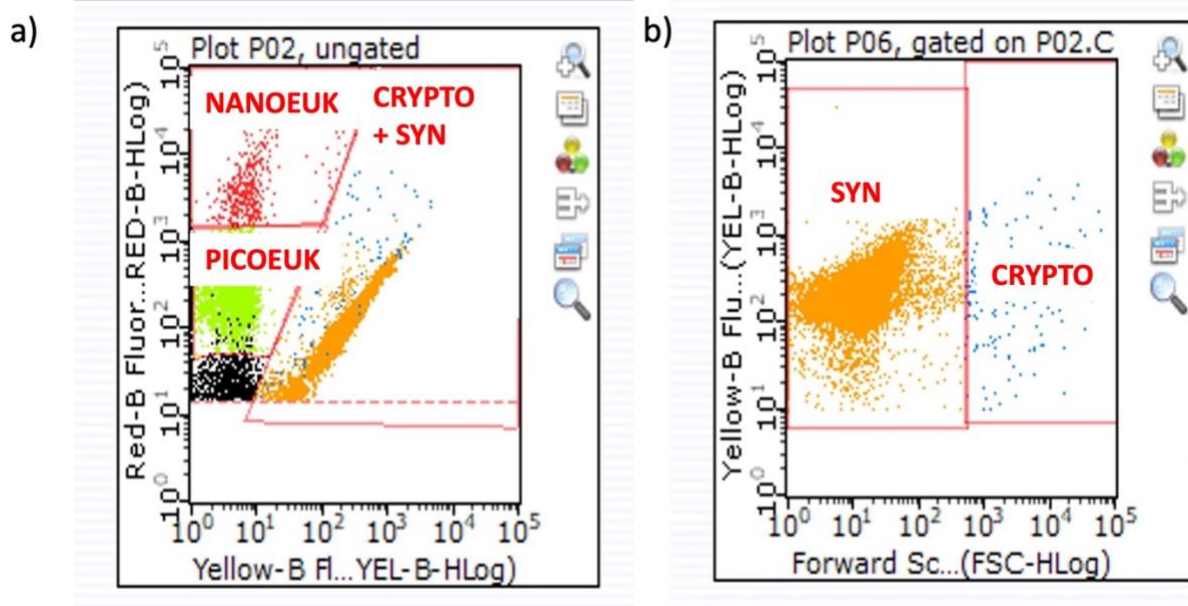
Figure 4: Cytograms on Guava InCyte software showing how statistical gates differentiated a) Photosynthetic nanoeukaryotes (NANOEUK), picoeukaryotes (PICOEUK), cryptophytes (CRYPTO), and *Synechococcus* (SYN) from each other and b) *Synechococcus* spp. from cryptophytes.
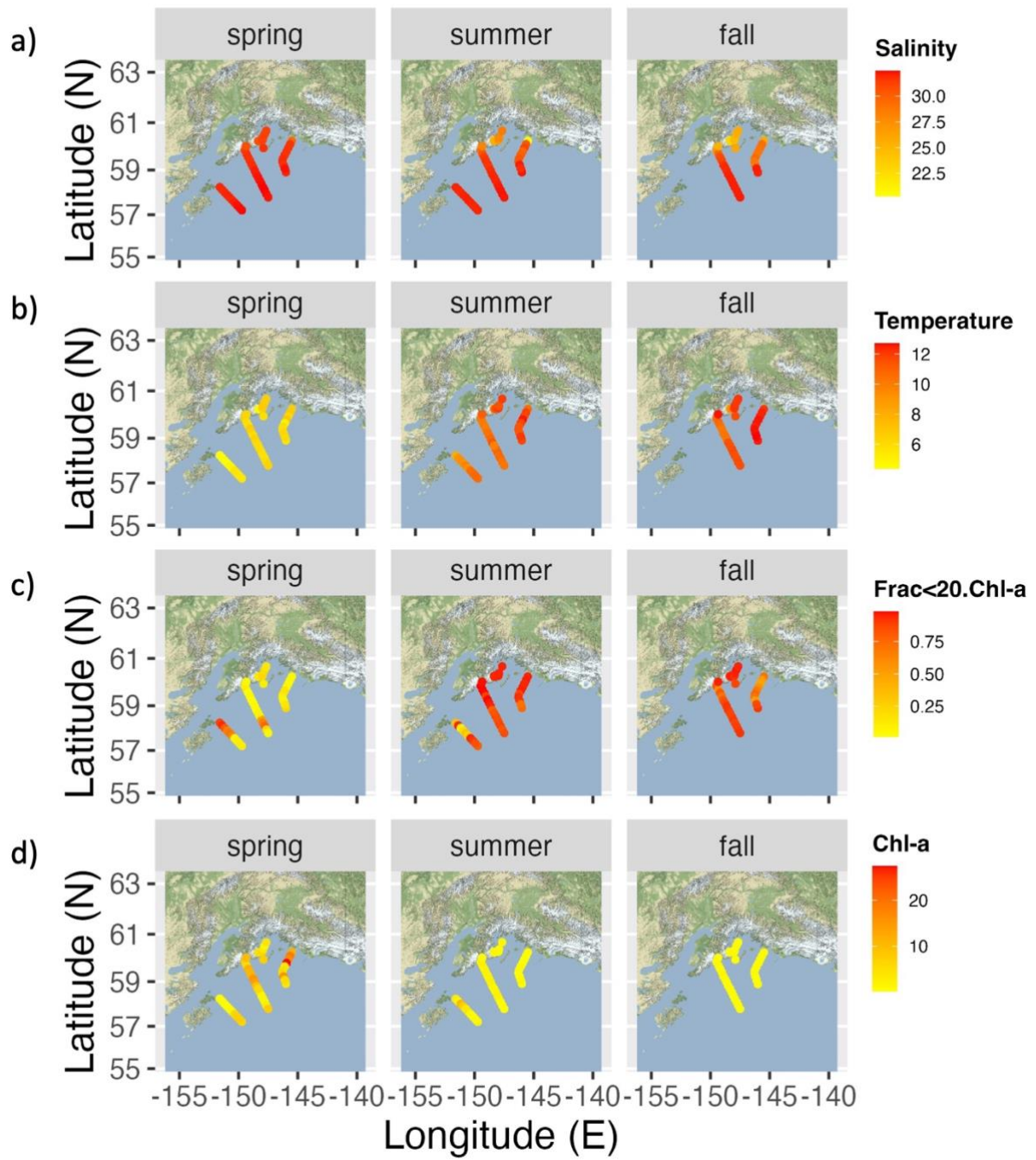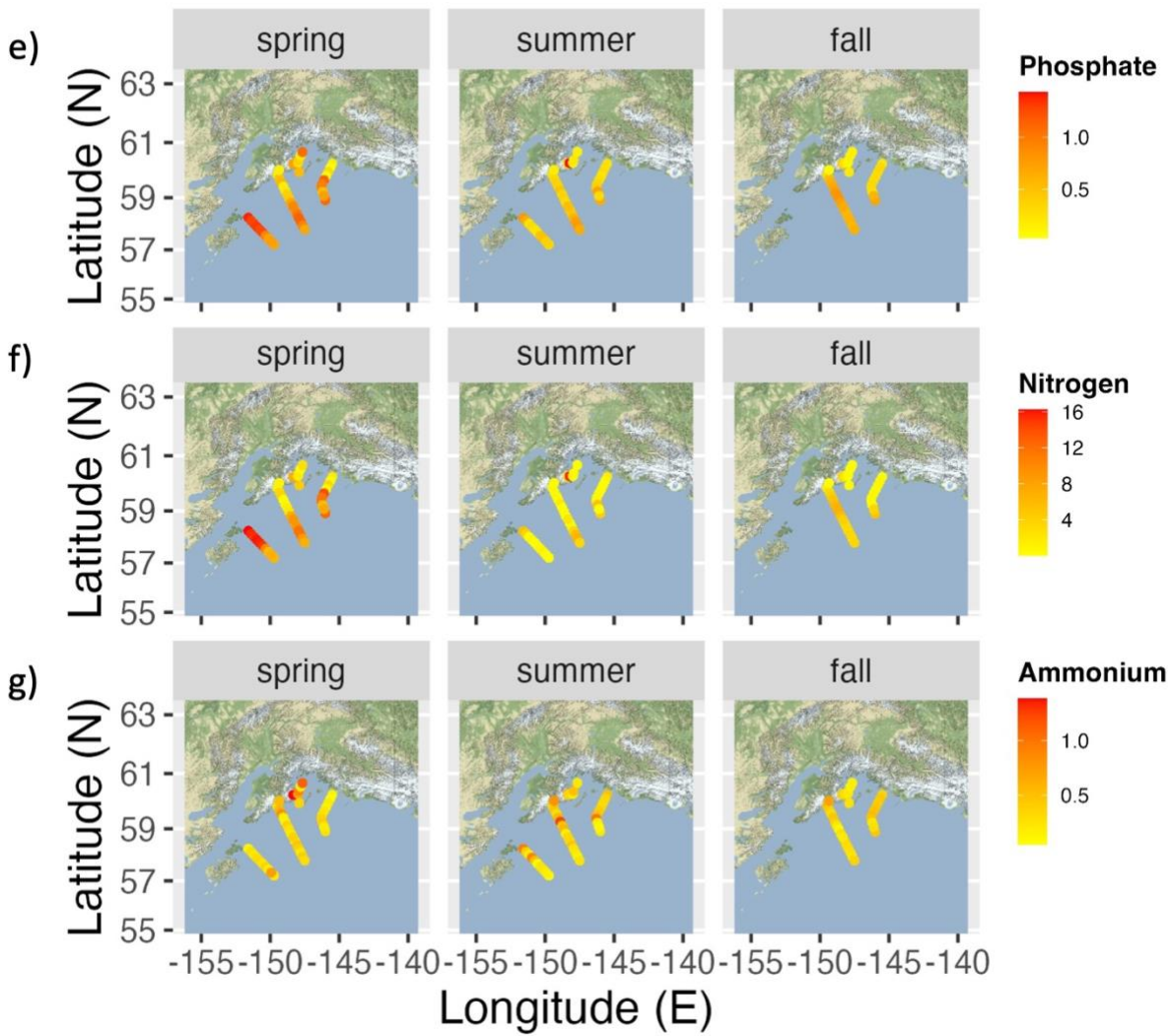
Figure 5: Seasonal changes in environmental variables in the NGA in 2021. The Kodiak transect (KOD) is furthest west, the Seward transect (GAK) in the middle, and the Middleton Island transect (MID) furthest east. Mean 0-10 m a) salinity (psu), b) temperature (°C), c) fraction of chlorophyll-a in cells <20 μm, d) total chlorophyll-a (μg/L), e) phosphate (μM), f) nitrogen (nitrite + nitrate, μM), g) ammonium (μM).

Table 1: Environmental conditions at 10 m by season (mean +/- SE): temperature (°C), salinity (psu), nitrogen (nitrite + nitrate, μM), ammonium (μM), phosphate (μM), silicate (μM), fraction of chlorophyll-a in cells <20 μm, total chlorophyll-a (μg/L), and PAR received at 10 m during the 24 h period prior to sample collection (mol photon/m^2).

	Spring	Summer	Fall
Temperature	5.68 +/- 0.10	10.42 +/- 0.15	11.44 +/- 0.19
Salinity	31.84 +/- 0.07	30.77 +/- 0.28	29.28 +/- 0.50
Nitrogen	7.33 +/- 0.78	1.79 +/- 0.40	2.86 +/- 0.37
Ammonium	0.45 +/- 0.06	0.51 +/- 0.06	0.36 +/- 0.03
Phosphate	0.74 +/- 0.06	0.43 +/- 0.03	0.47 +/- 0.04
Silicate	10.87 +/- 1.34	9.38 +/- 0.63	11.89 +/- 0.31
Frac. <20 Chl-a	0.22 +/- 0.04	0.83 +/- 0.03	0.82 +/- 0.02
Chl-a	6.60 +/- 0.84	2.01 +/- 0.28	0.69 +/- 0.05
24 h PAR	11.52 +/- 2.14	9.15 +/- 1.58	8.63 +/- 1.85
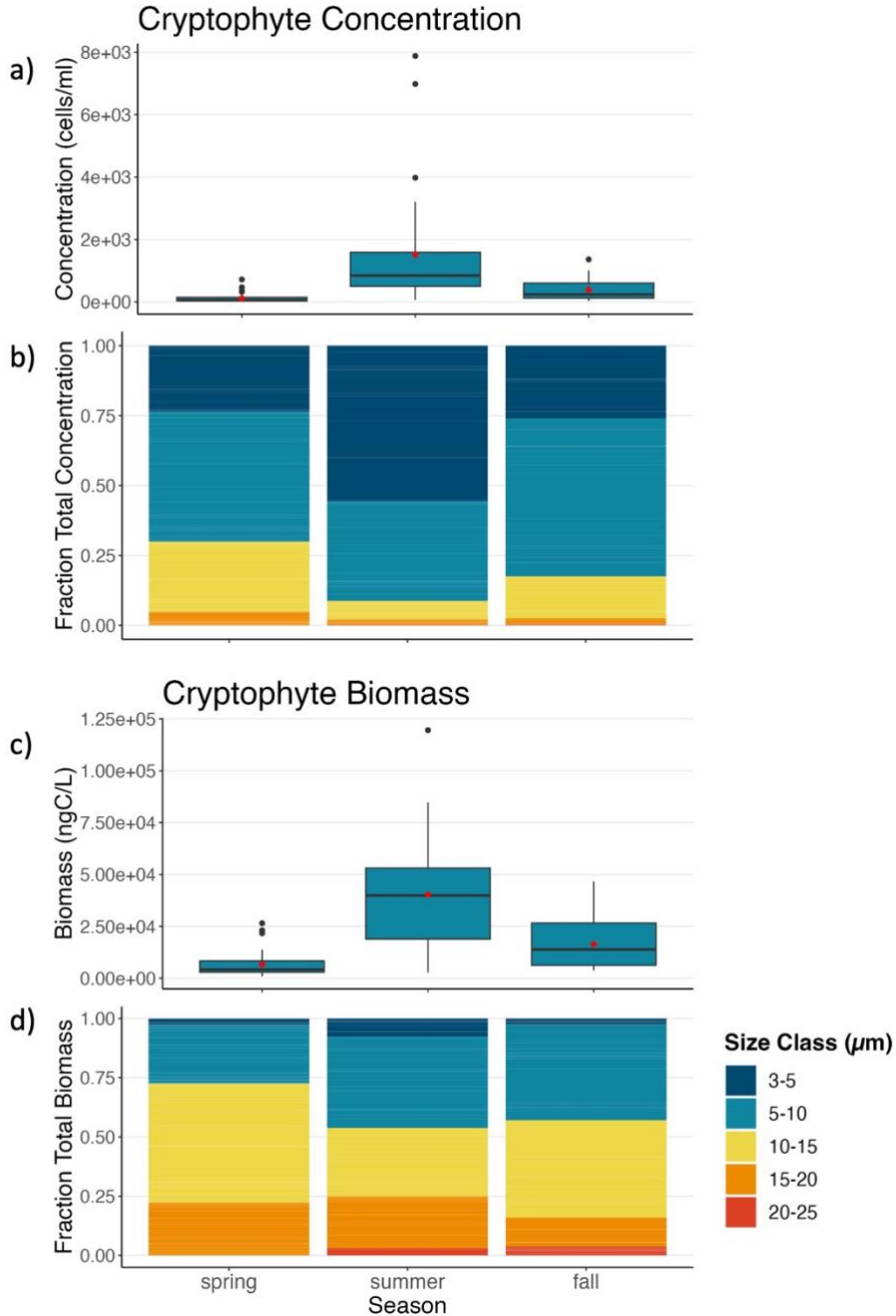
Figure 6: Box and whisker plots depicting the distribution of (a) cryptophyte concentration (cells/mL) and (c) biomass (ngC/L) at 10 m including all stations sampled separated by season. The median is represented by the heavy black line, the upper and lower hinges correspond to the 25th and 75th percentiles, the upper and lower whiskers extend from the hinge to 1.5x the inter-quartile range, and the data points beyond the end of the whiskers are outliers. The red dot shows the mean 10 m value for each season. Bar plots showing cryptophyte size classes as a fraction of total concentration (b) and biomass (d) at 10 m. Size classes included cells between 3-5 μm, 5-10 μm, 15-20 μm, and 20-25 μm. The size class 20-25 μm was not recorded in any spring samples.
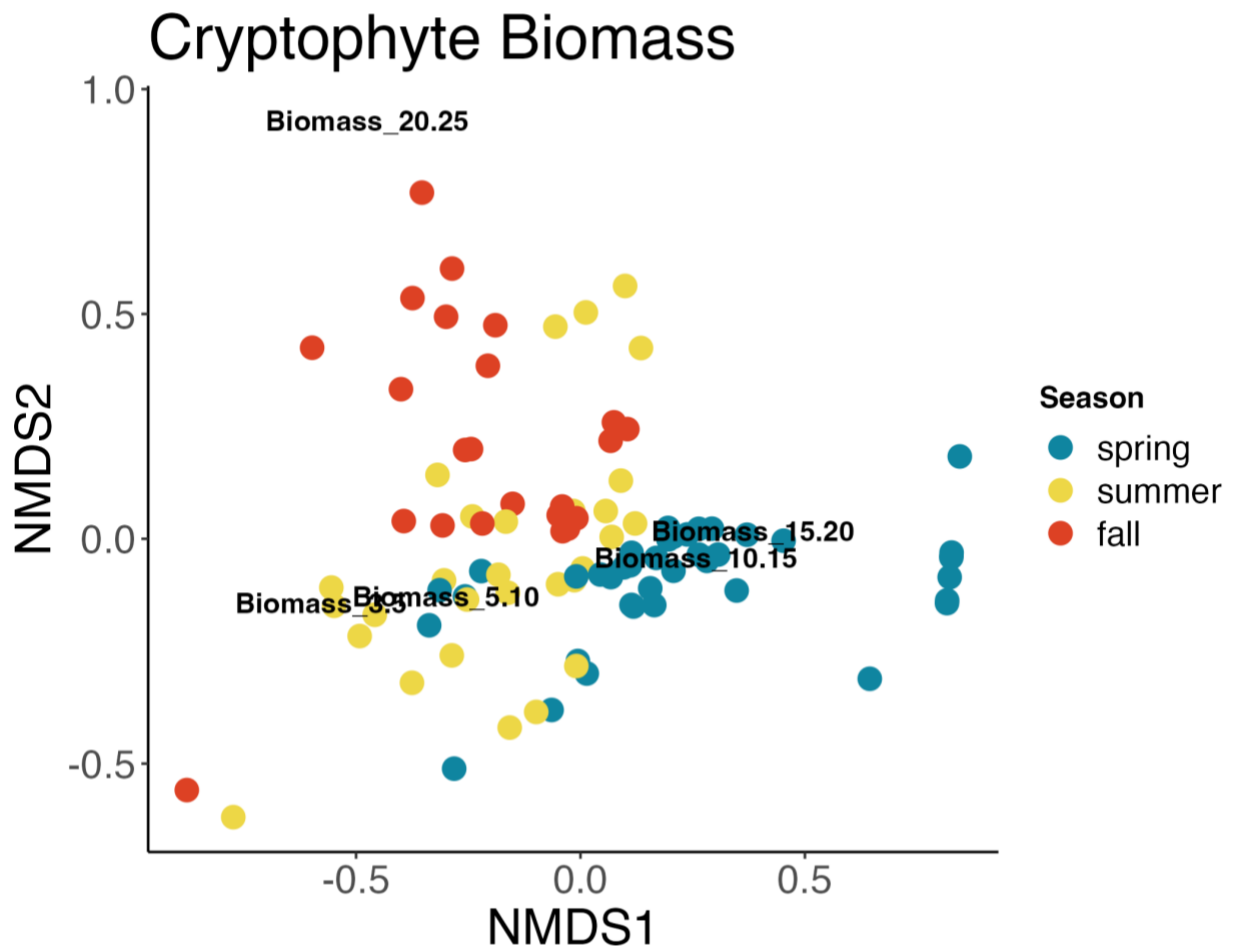
Figure 7: NMDS ordinations of 10 m cryptophyte biomass. Colors represent season and cryptophyte size classes are mapped in their ordination space. Bray-Curtis dissimilarity measure was used. Low stress (0.1) and convergent solutions were found with 2 NMDS dimensions.

Table 2: Spearman correlation coefficients for relationships between total cryptophyte biomass at 10 m and environmental variables, separated by season. Correlation coefficients for temperature (°C), salinity (psu), nitrogen (nitrite + nitrate, μM), ammonium (μM), phosphate (μM), chlorophyll-a in cells <20 μm (μg/L), total chlorophyll-a (μg/L), PAR received at 10 m during the 1, 24, and 48 h prior to sample collection (mol photon/m^2), and distance offshore (km) are presented. p-values are bolded if ≤ 0.1, bolded and * if ≤ 0.05, bolded and ** if ≤ 0.01.

	Spring	Summer	Fall
Temperature	-0.17	**-0.42**	-0.32
Salinity	-0.19	-0.25	**-0.73****
Nitrogen	0.19	-0.36	-0.20
Ammonium	**-0.32**	0.12	**0.42**
Phosphate	0.13	-0.30	-0.21
<20 Chl-a	**0.43***	**0.74****	**0.52***
Total Chl-a	-0.08	**0.83****	**0.66****
Hourly PAR	0.10	-0.23	**-0.51***
6 h PAR	0.02	-0.32	**-0.57***
12 h PAR	0.04	-0.27	**-0.57***
24 h PAR	-0.02	**-0.54****	**-0.51***
48 h PAR	-0.01	**-0.55****	-0.39
Dist. Offshore	-0.19	-0.29	**-0.71****

Table 3: Linear model result*s* for relationships between distinct size classes of cryptophyte biomass at 0 - 30 m in summer and fall 2021 and environmental variables including salinity (Sal), phosphate (P), nitrogen (nitrite + nitrate) (N), ammonium (NH_4), and cumulative PAR received 48 hours prior to sample collection (PAR.48.h). All cryptophyte biomass data were log transformed for best residuals fit. p-values are bolded if ≤ 0.1, bolded and * if ≤ 0.05, bolded and ** if ≤ 0.01. Adjusted R^2 represents the percentage of variance explained by that model. The F statistic (F stat) is the variance between sample means divided by the variance within the sample means. DF = n-1.

Cryptophyte size class	Linear Model	Adjusted R^2	F stat / DF
Total biomass	Log(Total_Biomass) = 2.47 − 1.35(**P****) + 0.19(**NH_4***) + 0.08(**Sal****)	0.35	23.37 / 120
3-5 μm	Log(Biomass_3-5) = 3.63 − 1.45(**P****) − 0.005(**PAR.48.h**)	0.27	19.38 / 98
5-10 μm	Log(Biomass_5-10) = 4.25 − 0.46(**P***) − 0.05(**N****) - 0.003(**PAR.48.h**)	0.33	20.15 / 116
10-15 μm	Log(Biomass_10-15) = 4.10 − 1.00(**P****) + 0.25(**NH_4***)	0.20	16.49 / 120
15-20 μm	Log(Biomass_15-20) = 0.87 - 1.24(**P****) + 0.10(**Sal***)	0.13	10.2 / 116
20-25 μm	Log(Biomass_20-25) = -2.16 − 1.28(**P****) + 0.18(**Sal****)	0.27	14.24 / 71

Figure 8: Cryptophyte biomass (ngC/L) at 10 m in spring on the (a) KOD, (b) GAK, and (c) MID transects (left). Cryptophyte size classes as a fraction of total biomass at 10 m (right). Size classes recorded included cells between 3-5 μm, 5-10 μm, 10-15 μm, and 15-20 μm. The size class 20-25 μm was observed only in summer and fall samples.

55
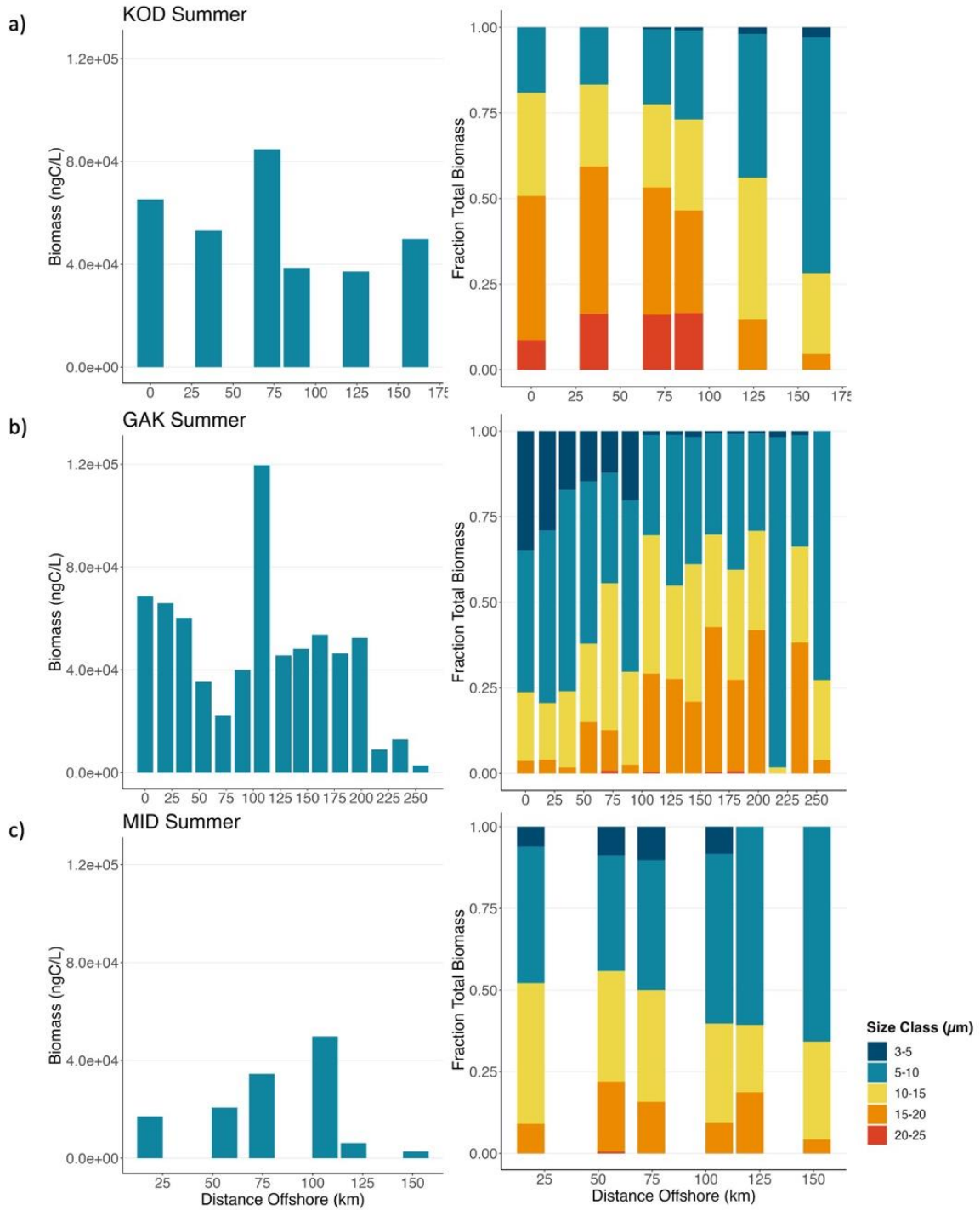
Figure 9: Cryptophyte biomass (ngC/L) at 10 m in summer on the (a) KOD, (b) GAK, and (c) MID transects (left). Cryptophyte size classes as a fraction of total biomass at 10 m (right). Size classes recorded included cells between 3-5 μm, 5-10 μm, 10-15 μm, and 15-20 μm. The size class 20-25 μm was observed only in summer and fall samples. Blank spaces indicate no sample taken.
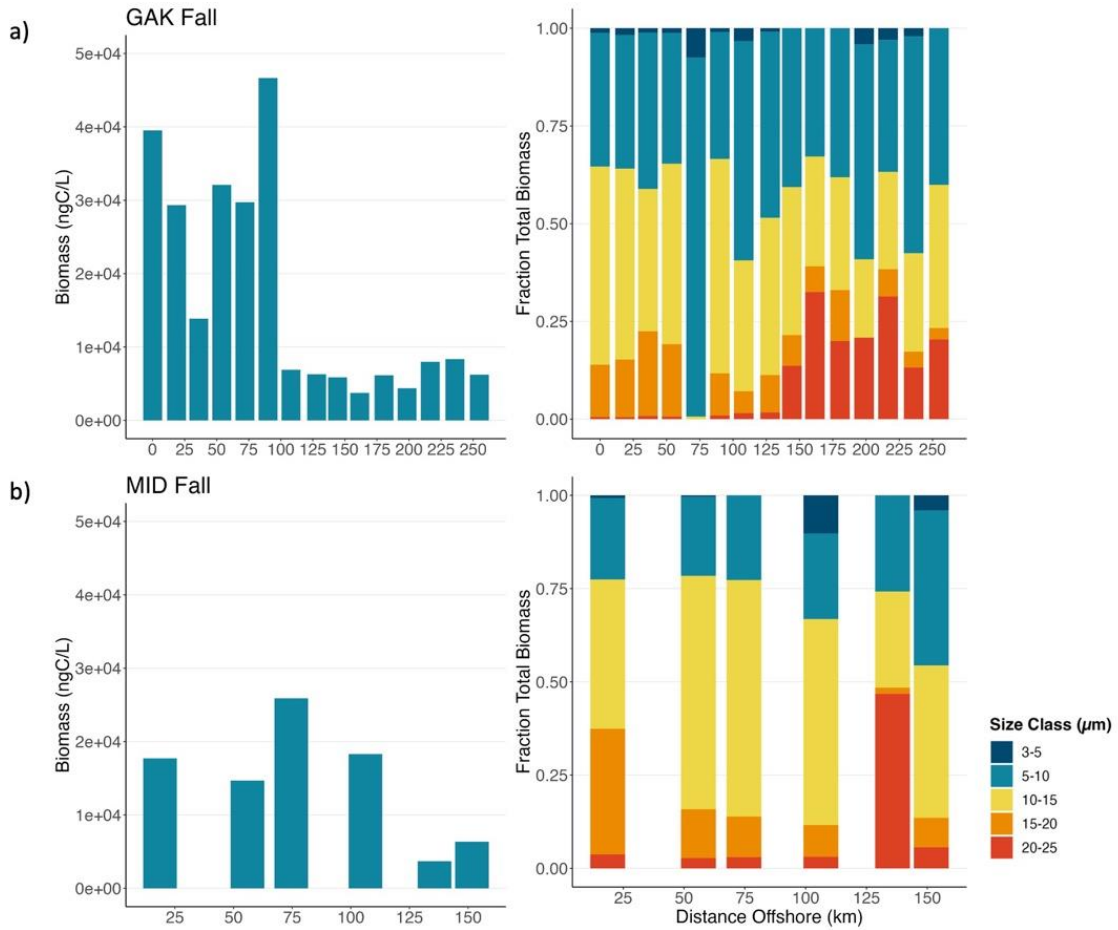
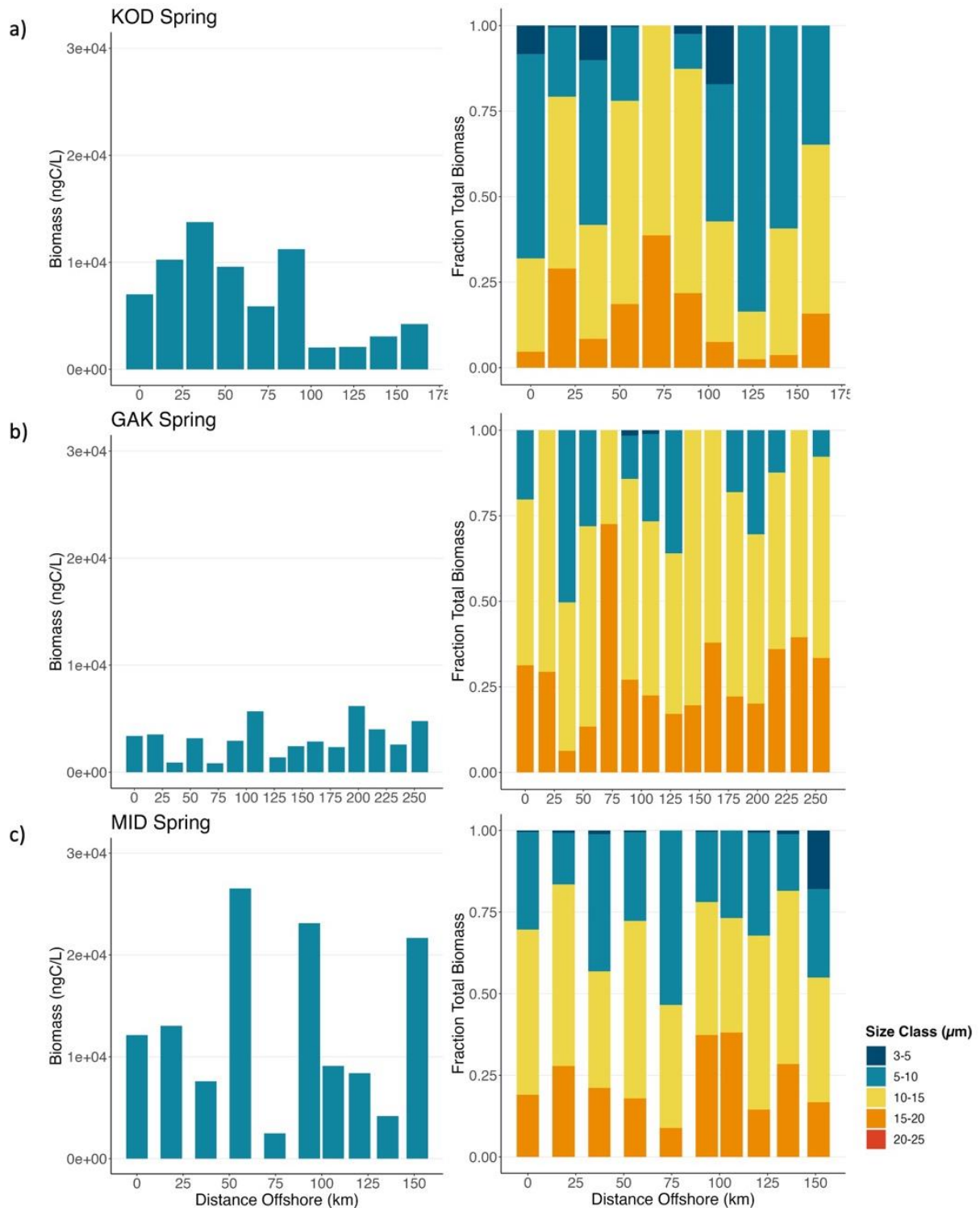Figure 10: Cryptophyte biomass (ngC/L) at 10 m in fall on the (a) GAK and (b) MID transects (left). Cryptophyte size classes as a fraction of total biomass at 10 m (right). Size classes recorded included cells between 3-5 µm, 5-10 µm, 10-15 µm, and 15-20 µm. The size class 20-25 µm was observed only in summer and fall samples. Blank spaces indicate no sample taken. The KOD transect was not sampled in fall 2021.
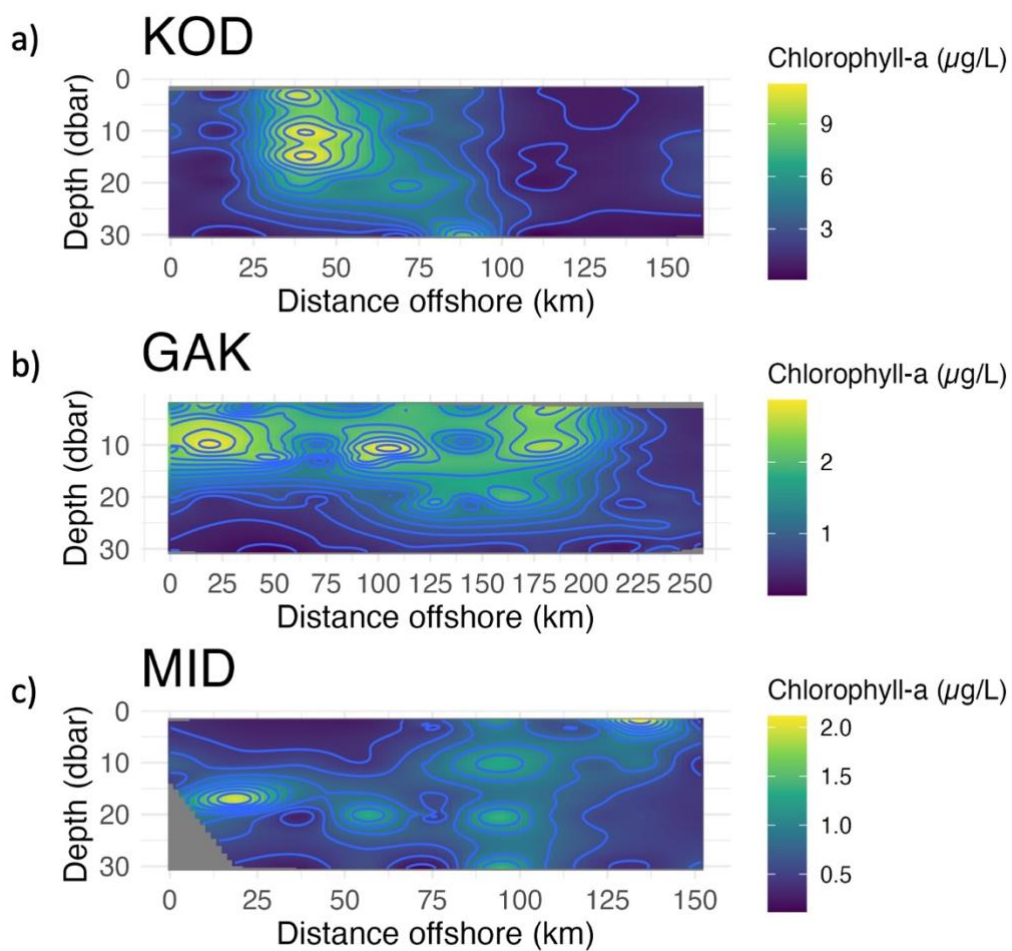
Figure 11: Section plots of 0-30 dbar chlorophyll-a concentration (μg/L) on the (a) KOD, (b) GAK, and (c) MID transects in summer 2021. Note different chl-a scales.
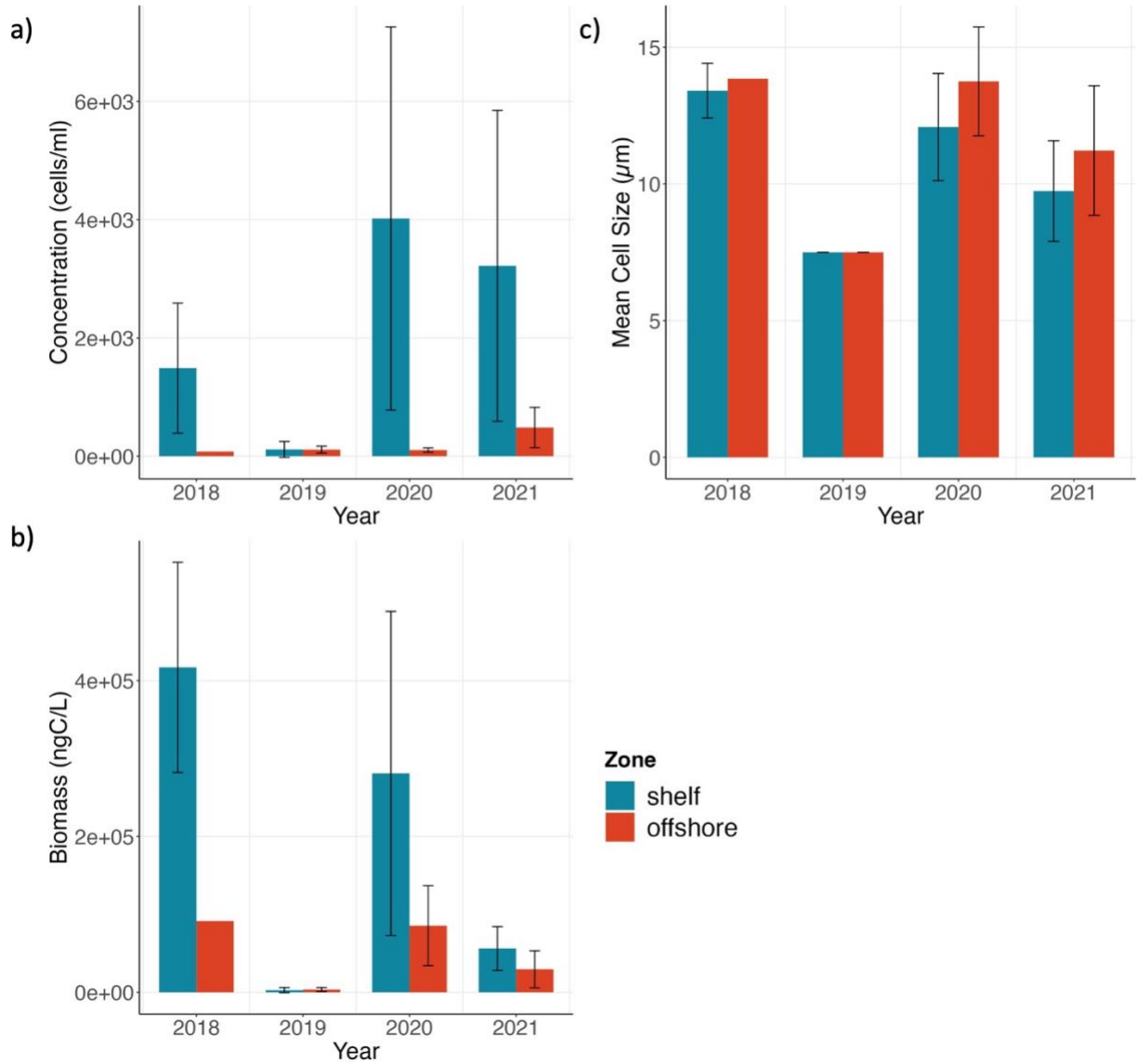
Figure 12: Four-year time series of cryptophyte mean (a) concentration (cells/mL), (b) biomass (ngC/L), and (c) cell size (μm) at 10 m on shelf versus offshore GAK stations in summer. 'Shelf' includes data from 0-144 km offshore, and 'offshore' includes data from 144-250 km. Error bars show standard deviation of mean (2018 shelf n = 3, offshore n = 1; 2019 shelf n = 4, offshore n = 2; 2020 shelf n = 5, offshore n = 3; 2021 shelf n = 9, offshore n = 6).
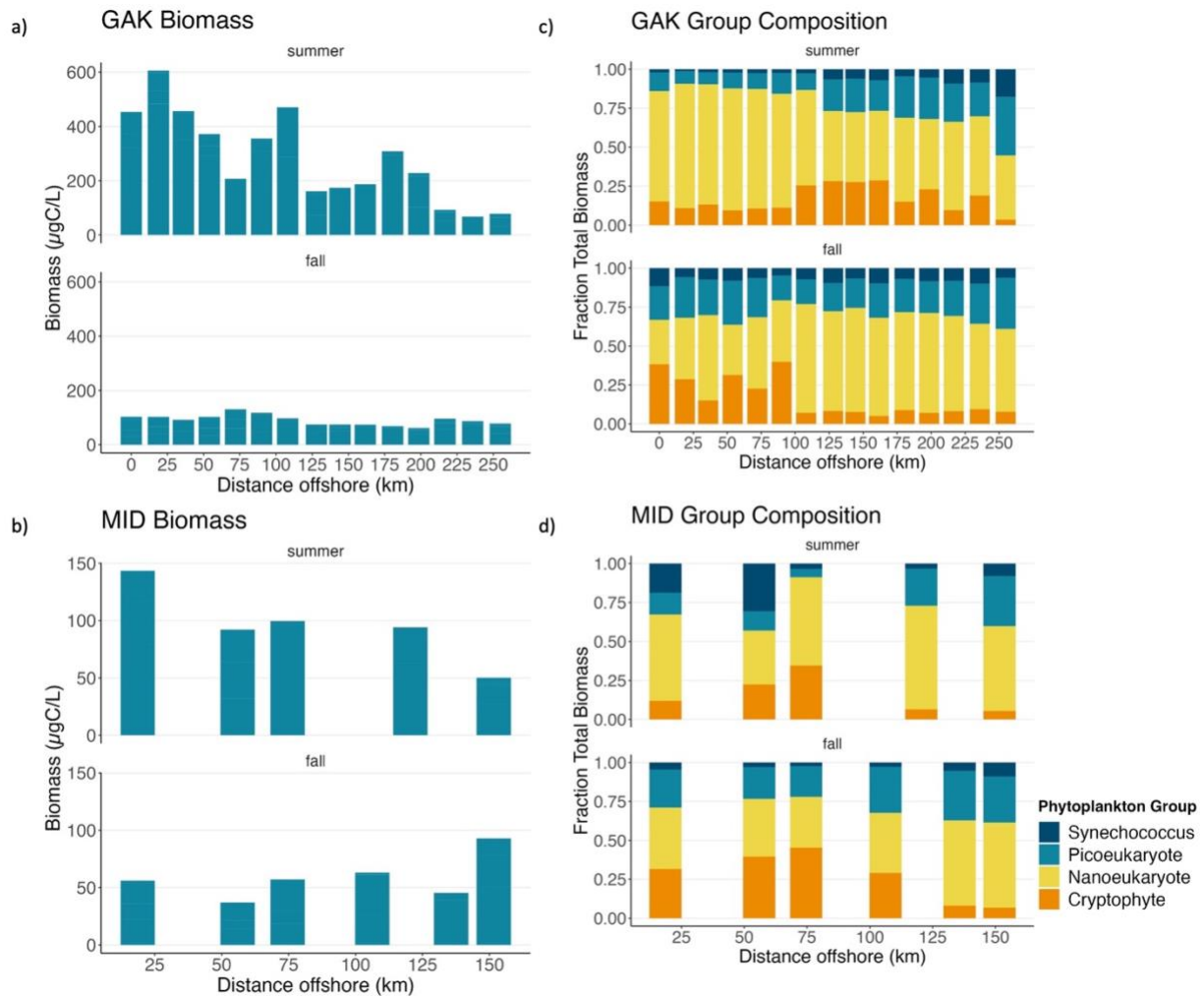
Figure 13: Small-cell community phytoplankton biomass (μgC/L) at 10 m in summer and fall on the (a) GAK and (b) MID transects. Phytoplankton taxonomic group as a fraction of total biomass at 10 m on the (c) GAK and (d) MID transects. Phytoplankton groups recorded included *Synechococcus* spp, picoeukaryotes, nanoeukaryotes, and cryptophytes. Blank spaces indicate no sample taken. Note different biomass scales.
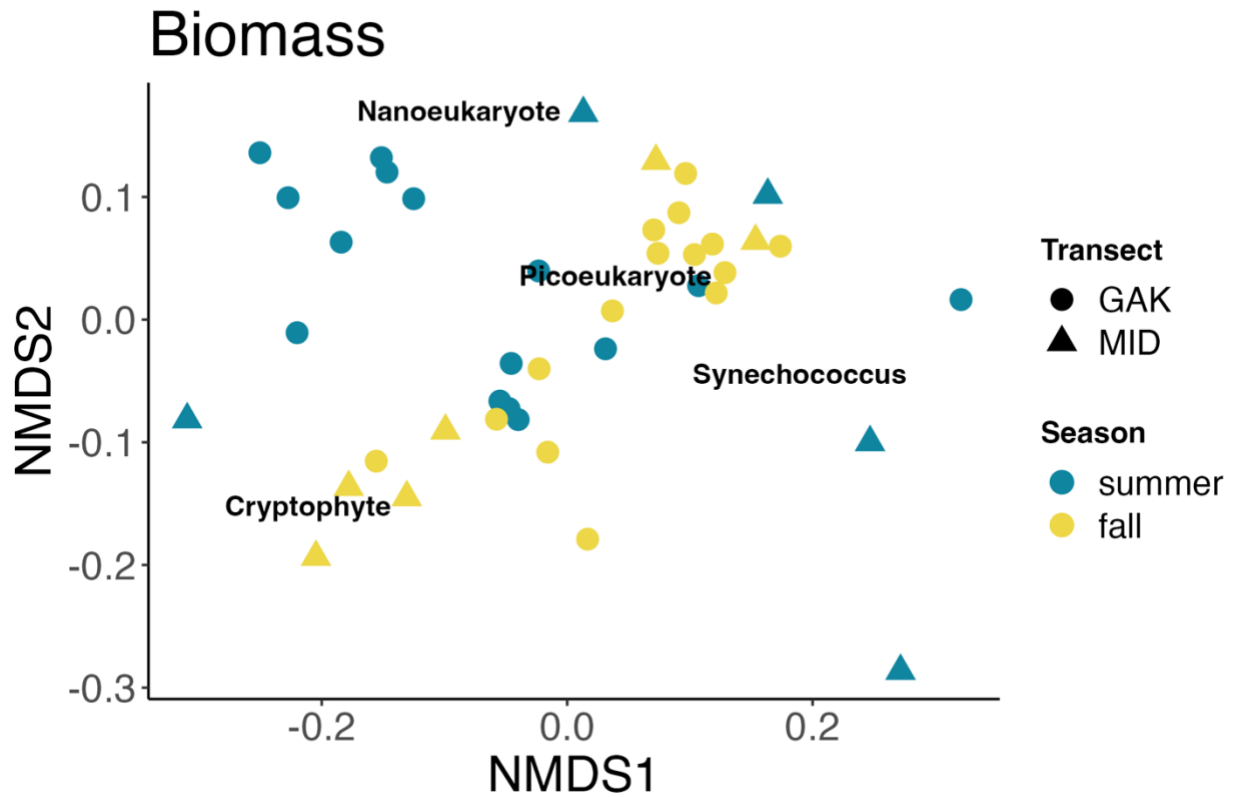
Figure 14: NMDS ordinations of small-cell phytoplankton biomass composition at 10 m on the GAK and MID transects in summer and fall. Colors represent the NMDS separation of season and phytoplankton taxonomic groups are mapped in their ordination space on top. Bray-Curtis dissimilarity measure was used. Low stress (stress = 0.12) and convergent solutions were found with 2 NMDS dimensions.

Table 4: Spearman correlation coefficients for relationships between summer and fall 10 m biomass of small-cell phytoplankton taxonomic groups and environmental variables. Correlation coefficients for picoeukaryotes, nanoeukaryotes, cryptophytes, *Synechococcus* spp. (all μgC/L), temperature (°C), salinity (psu), nitrogen (nitrite + nitrate, μM), ammonium (μM), phosphate (μM), silicate (μM), chlorophyll-a in cells <20 μm (μg/L), total chlorophyll-a (μg/L), PAR received at 10 m during the 1, 24, and 48 h prior to sample collection (mol photon/m^2), and distance offshore (km) are presented. p-values are bolded if ≤ 0.1, bolded and * if ≤ 0.05, bolded and ** if ≤ 0.01.

|	*Syn* spp.	Picoeuk	Nanoeuk	Crypto
Picoeukaryote	**0.62****	1.0	**0.60****	**0.46****
Nanoeukaryote	**0.54****	**0.60****	1.0	**0.33***
Cryptophyte	0.21	**0.46****	**0.33***	1.0
Temperature	0.02	-0.27	**-0.34***	**-0.55****
Salinity	-0.12	-0.03	-0.04	**-0.37***
Nitrogen	-0.25	-0.22	-0.12	**-0.47****
Ammonium	-0.04	0.00	-0.05	0.15
Phosphate	-0.17	-0.14	0.03	**-0.42****
Silicate	0.08	0.13	0.12	-0.26
<20 Chl-a	**0.31**	**0.65****	**0.71****	**0.78****
Total Chlorophyll-a	0.02	**0.49****	**0.40****	**0.85****
Hourly PAR	0.09	-0.08	0.15	**-0.34***
6 h PAR	0.10	-0.10	0.09	**-0.34***
12 h PAR	0.05	-0.12	0.05	-0.28
24 h PAR	-0.01	-0.12	-0.03	**-0.46****
48 h PAR	0.08	-0.03	0.02	**-0.36***
Distance offshore	0.07	0.03	-0.01	**-0.40****
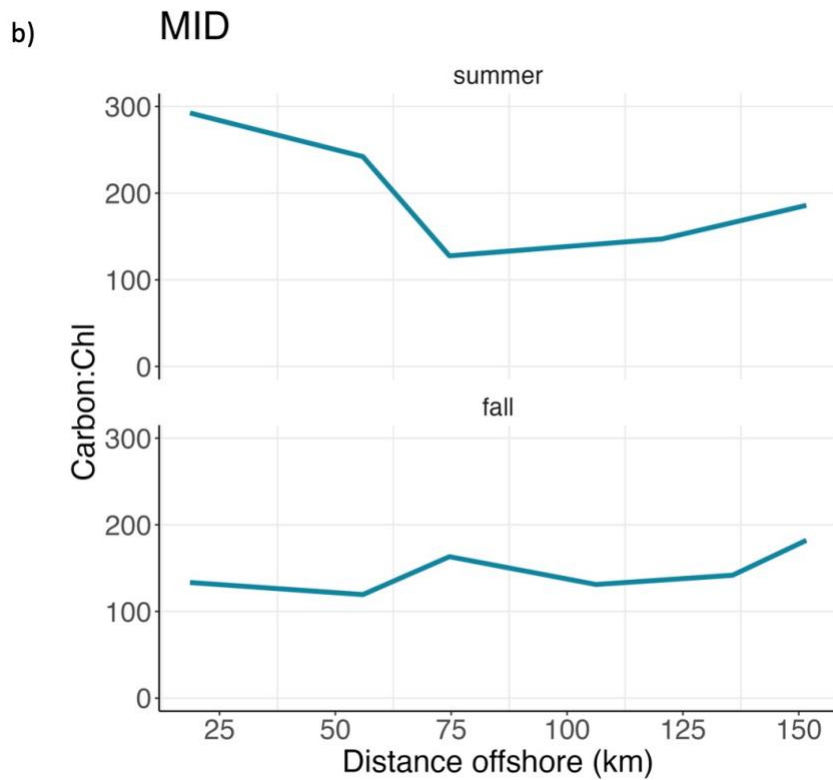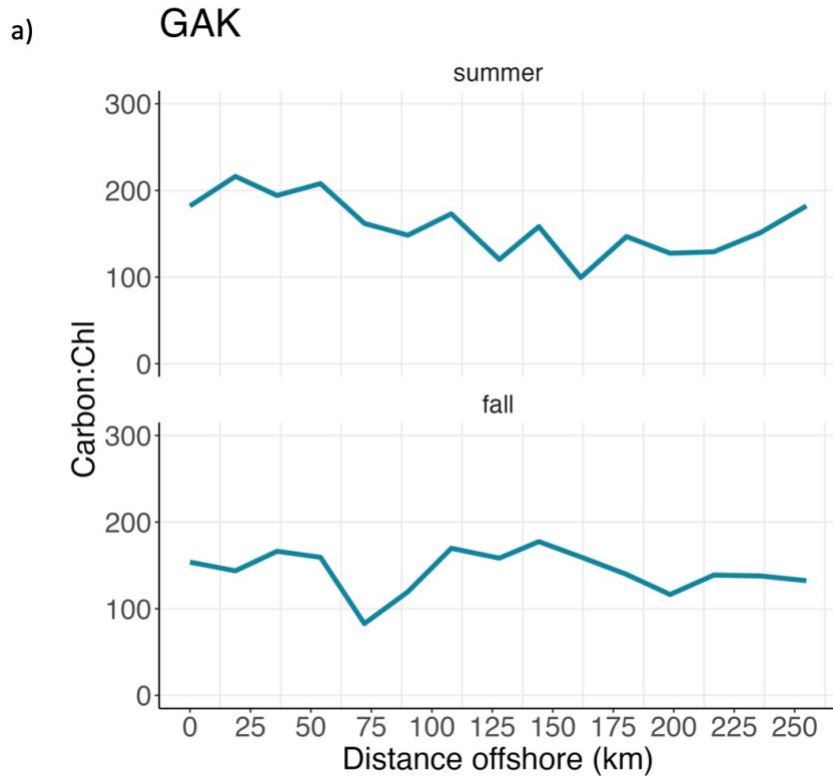
Figure 15: Ratio of total small-cell community phytoplankton carbon biomass to small-cell (< 20 μm) chlorophyll-a (μg:μg) at 10 m on the (a) GAK and (b) MID transects in summer and fall.
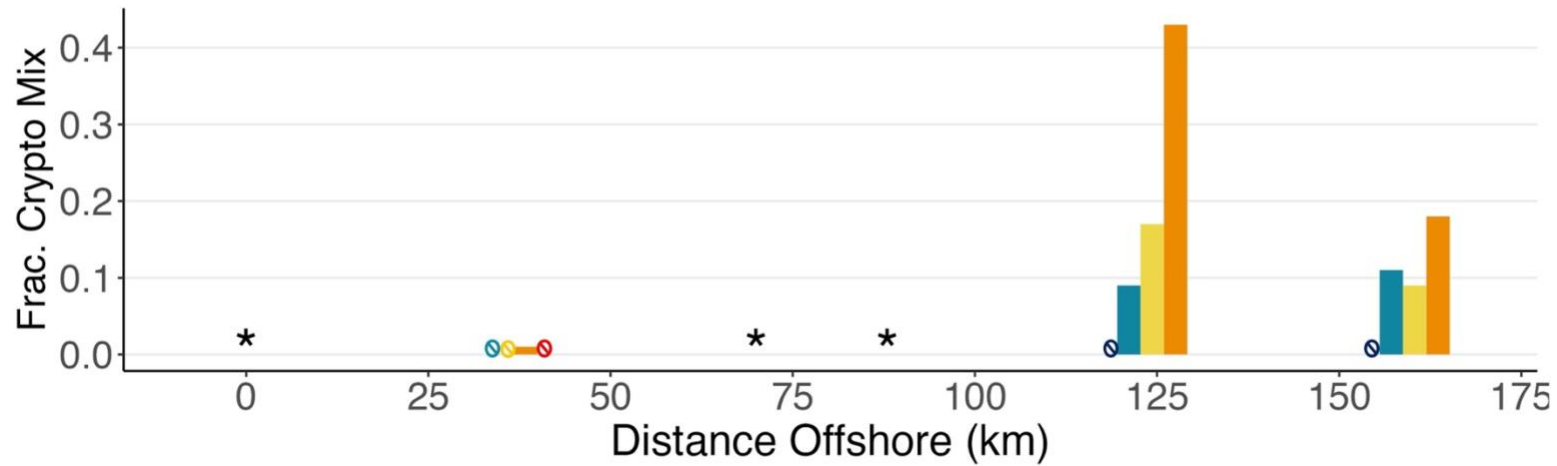
Figure 16: KOD transect in summer, including a) cryptophyte mixotrophy at 10 m (fraction of cryptophyte cells feeding on *Synechococcus* spp. prey for each size class), (b) total cryptophyte concentration (cells/mL) at each station sampled, and (c) cryptophyte size classes as a fraction of total concentration 10 m. Note: * is for samples processed but no active mixotrophs were detected and ⊘, corresponding to the legend color, indicates the presence of a size class but no active mixotrophs of that size class were recorded.
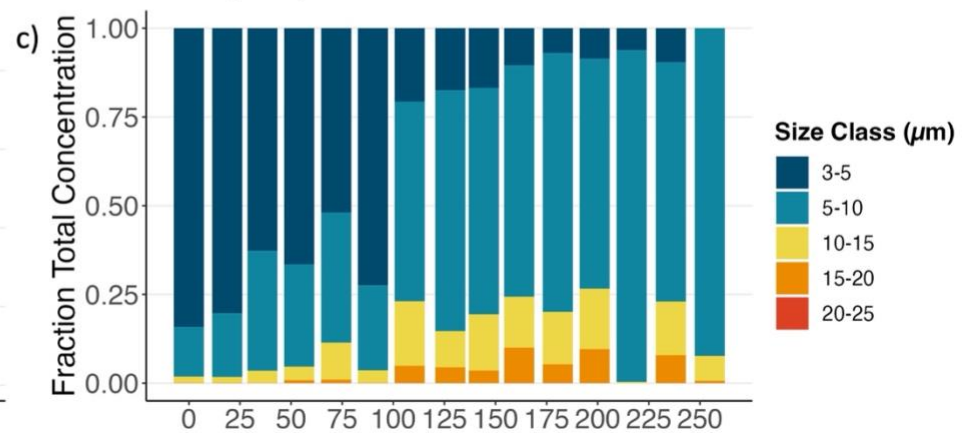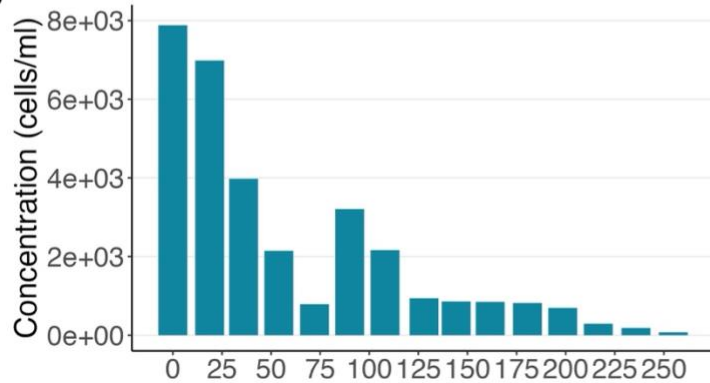
Figure 17: GAK transect in summer, including a) cryptophyte mixotrophy at 10 m (fraction of cryptophyte cells feeding on *Synechococcus* spp. prey for each size class), (b) total cryptophyte concentration (cells/mL) at each station sampled, and (c) cryptophyte size classes as a fraction of total concentration 10 m. Note: * is for samples processed but no active mixotrophs were detected and ⊘, corresponding to the legend color, indicates the presence of a size class but no active mixotrophs of that size class were recorded.
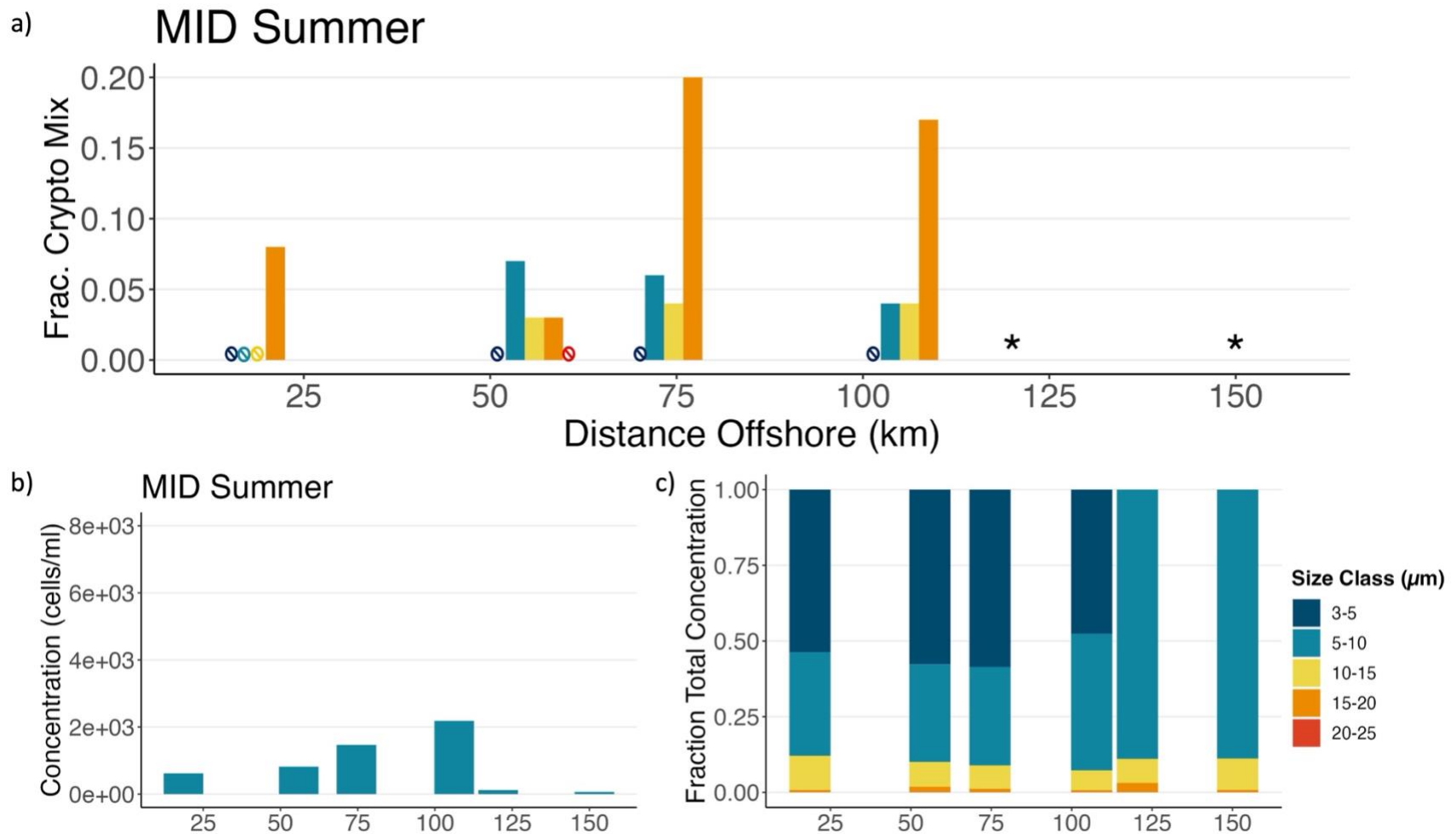
Figure 18: MID transect in summer, including a) cryptophyte mixotrophy at 10 m (fraction of cryptophyte cells feeding on *Synechococcus* spp. prey for each size class), (b) total cryptophyte concentration (cells/mL) at each station sampled, and (c) cryptophyte size classes as a fraction of total concentration 10 m. Note: * is for samples processed but no active mixotrophs were detected and ⊘, corresponding to the legend color, indicates the presence of a size class but no active mixotrophs of that size class were recorded.
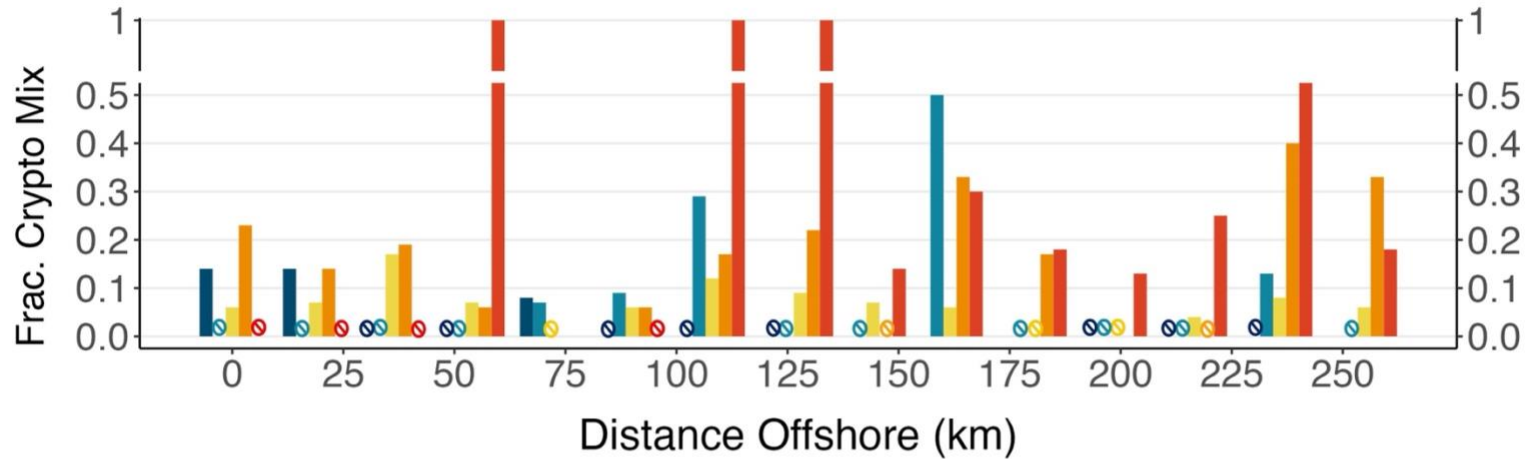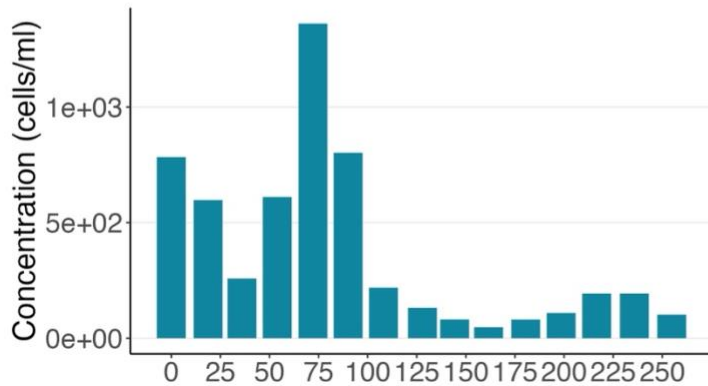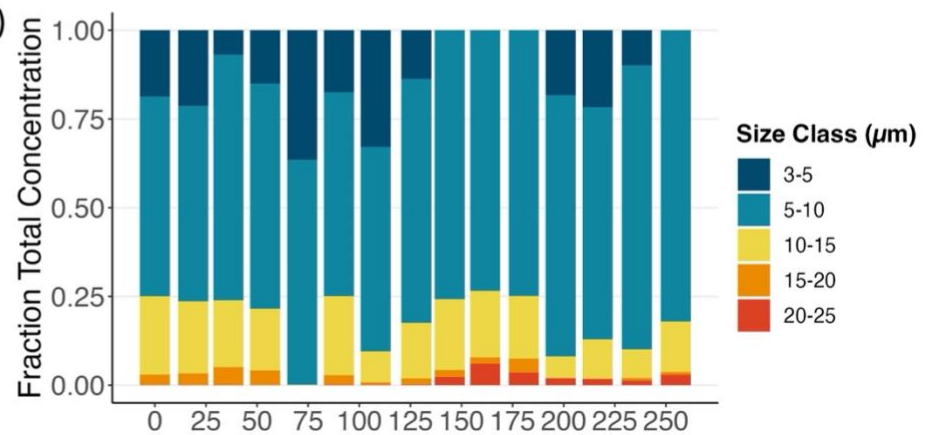
Figure 19: GAK transect in fall, including a) cryptophyte mixotrophy at 10 m (fraction of cryptophyte cells feeding on *Synechococcus* spp. prey for each size class), (b) total cryptophyte concentration (cells/mL) at each station sampled, and (c) cryptophyte size classes as a fraction of total concentration 10 m. Note: * is for samples processed but no active mixotrophs were detected and ⊘, corresponding to the legend color, indicates the presence of a size class but no active mixotrophs of that size class were recorded.
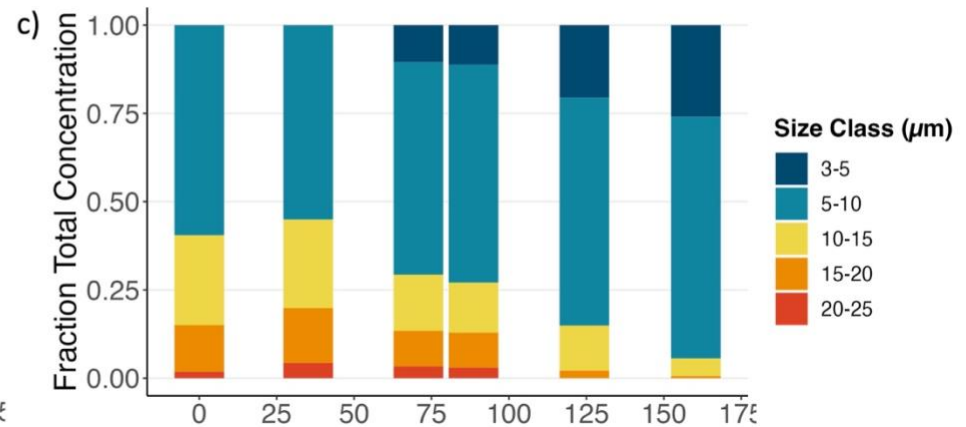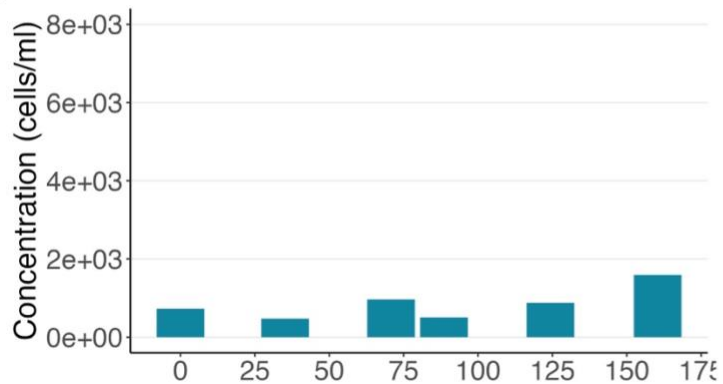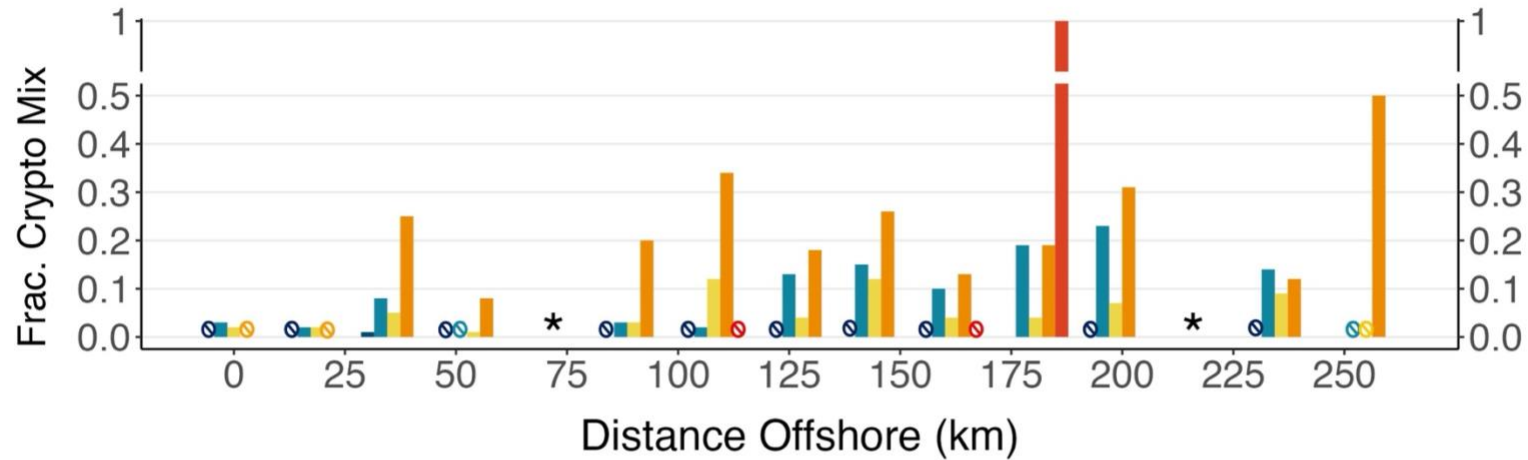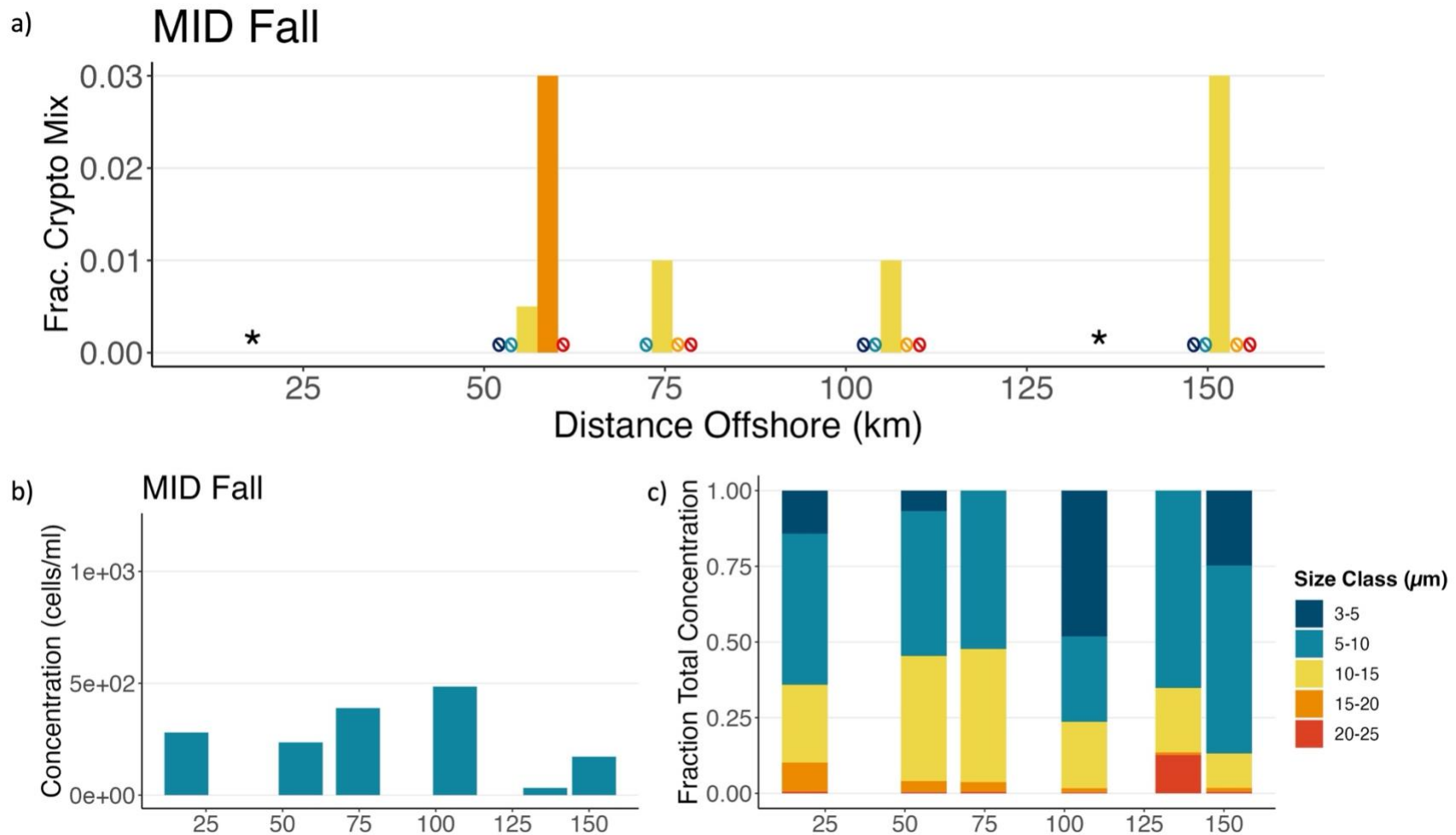
Figure 20: MID transect in fall, including a) cryptophyte mixotrophy at 10 m (fraction of cryptophyte cells feeding on *Synechococcus* spp. prey for each size class), (b) total cryptophyte concentration (cells/mL) at each station sampled, and (c) cryptophyte size classes as a fraction of total concentration 10 m. Note: * is for samples processed but no active mixotrophs were detected and ⊘, corresponding to the legend color, indicates the presence of a size class but no active mixotrophs of that size class were recorded.
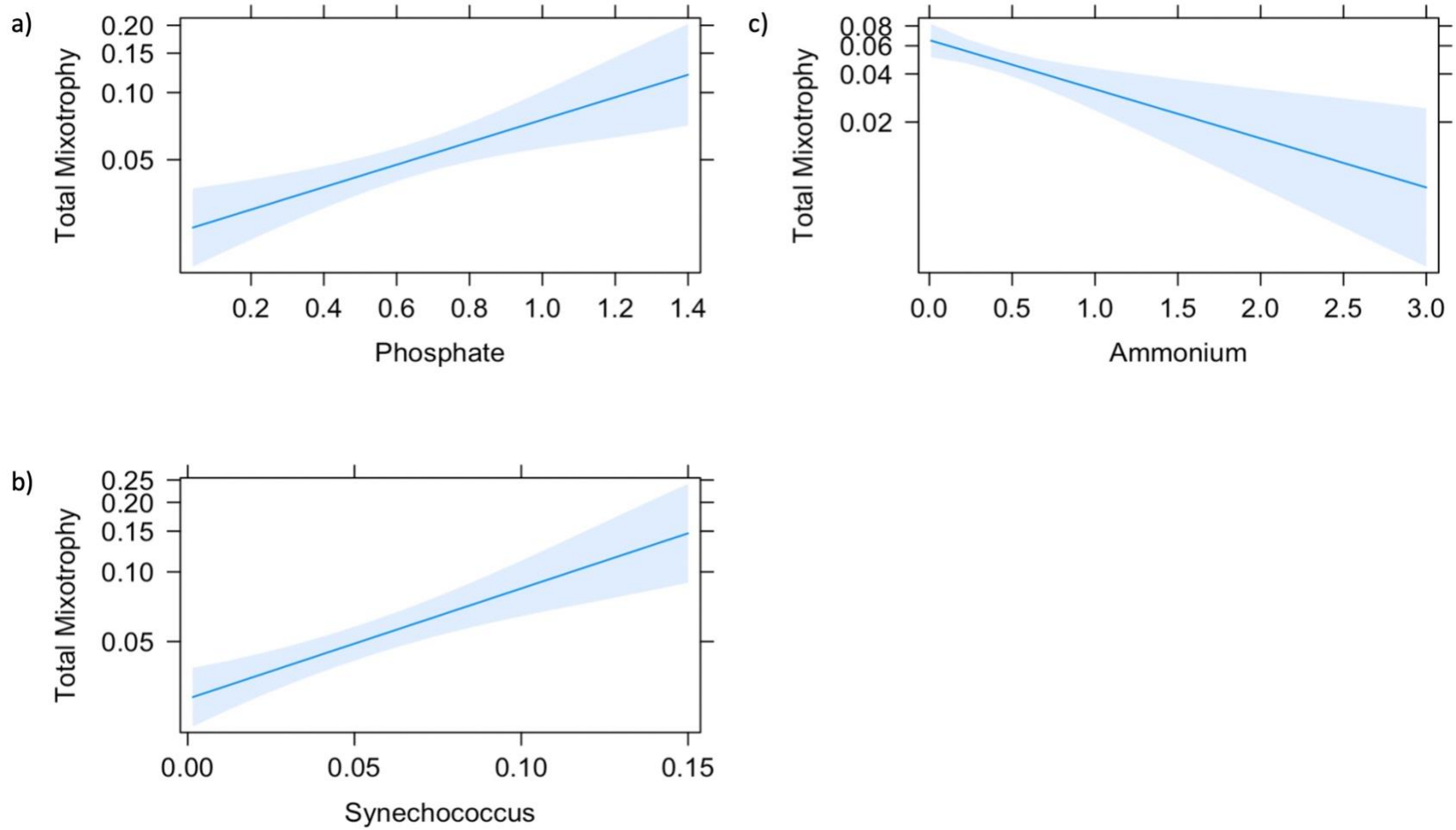
Figure 21: Quasipoisson regression effect plots for significant predictors of total cryptophyte mixotrophy a) phosphate (μM), b) *Synechococcus* spp. (cells/nL), and c) ammonium (μM).
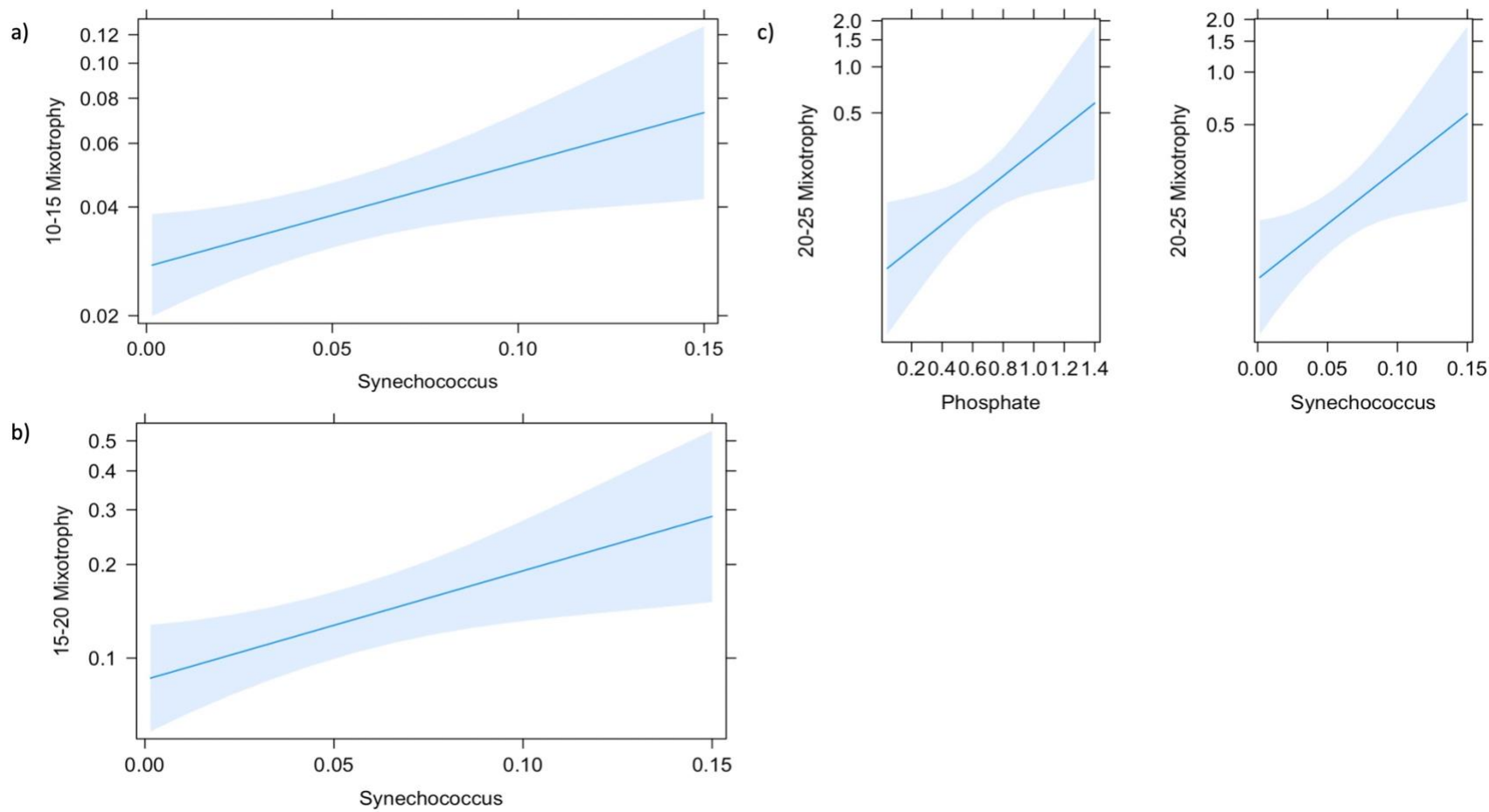
Figure 22: Quasipoisson regression effect plots for significant predictors [phosphate (μM) and *Synechococcus* spp. (cells/nL)] of cryptophyte mixotrophy by size class a) 10-15 μm, b) 15-20 μm, and c) 20-25 μm.

Table 5: Quasipoisson generalized linear model results for relationships between distinct size classes of cryptophyte mixotrophy at 0 -30 m in summer and fall 2021 and environmental variables including phosphate (P), ammonium (NH$_4$), and *Synechococcus* spp. (Syn). p-values are bolded if ≤ 0.1, bolded and * if ≤ 0.05, bolded and ** if ≤ 0.01. The dispersion parameter demonstrates the spread of the data around the mean. The residual deviance is a measure of goodness of fit and shows how well the response (mixotrophy) is predicted by all the model variables, with a lower value indicating a better model fit. DF = n (sample size) - # of predictors in model.

Cryptophyte size class	Quasipoisson model	Dispersion parameter	Residual deviance / DF
Total mixotrophy	Log(Total Mixotrophy) = -3.82 + 1.16(**P****) − 0.71(**NH$_4$****) + 10.99(**Syn****)	0.037	4.89 / 121
10-15 μm	Log(10-15 Mixotrophy) = -3.60 + 6.55(**Syn***)	0.05	5.89 / 125
15-20 μm	Log(15-20 Mixotrophy) = -2.46 + 8.07(**Syn****)	0.24	23.1 / 124
20-25 μm	Log(20-25 Mixotrophy) = -3.72 + 1.83(**P***) + 14.52(**Syn***)	0.59	49.75 / 122

Table 6: Ecological niches of all cryptophytes and individual size classes of marine cryptophytes in the NGA in spring, summer, and fall 2021. Variables associated with cryptophyte niche partitioning included: season (spring, summer, or fall), habitat location on a transect line (nearshore, shelf, or offshore), temperature (°C), salinity (psu), chlorophyll-a (total (μg/L) and fraction in cells <20 μm), PAR (received between 1-48 h prior to sample collection, depth corrected for 10 m (mol photon/m^2)), NH_4 (ammonium (μM)), N (nitrite + nitrate (μM)), and mixotrophy (fraction of cryptophyte cells that consumed *Synechococcus* spp. prey). + indicates a positive relationship between cryptophytes of a particular size class and a niche variable and ++ shows strong positive relationship. Likewise – indicates a negative relationship with a niche variable and - - shows a strong negative relationship.

Cryptophyte Size Class	Spring	Summer	Fall	Nearshore	Shelf	Offshore	Temp.	Sal.	Chl-a	PAR	P	NH₄	N	Mixotrophy
All Cryptophytes	+	++	++	++	++	+	- (summer)	+	++	- (summer & fall)	--	- (spring) + (summer & fall)		++ prey concentration + phosphate – ammonium
3-5 µm	+	++	+	++	+	+				-	--			
5-10 µm	+	++	++	+	+	+				-	--		-	
10-15 µm	++	+	++	+	+	+					--	+		++ prey concentration
15-20 µm	+	+	+	+	+	+		+			--			++ prey concentration
20-25 µm		+	++	+		++		+			--			++ prey concentration + phosphate

72
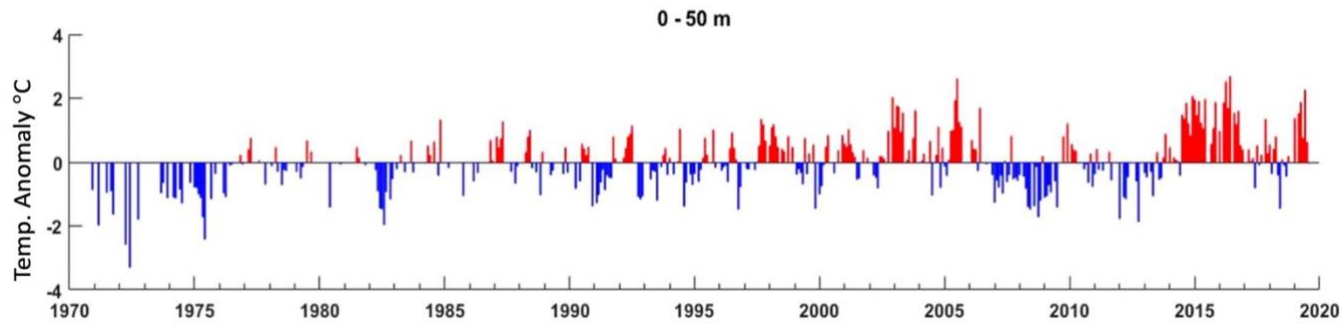
Figure 23: Temperature anomalies (°C) of the upper (0-50 m) water column at the GAK1 station in the Northern Gulf of Alaska (NGA) from 1973 to 2019 (Suryan et al. 2021). A multi-year heatwave afflicted the (NGA) in starting in 2014.
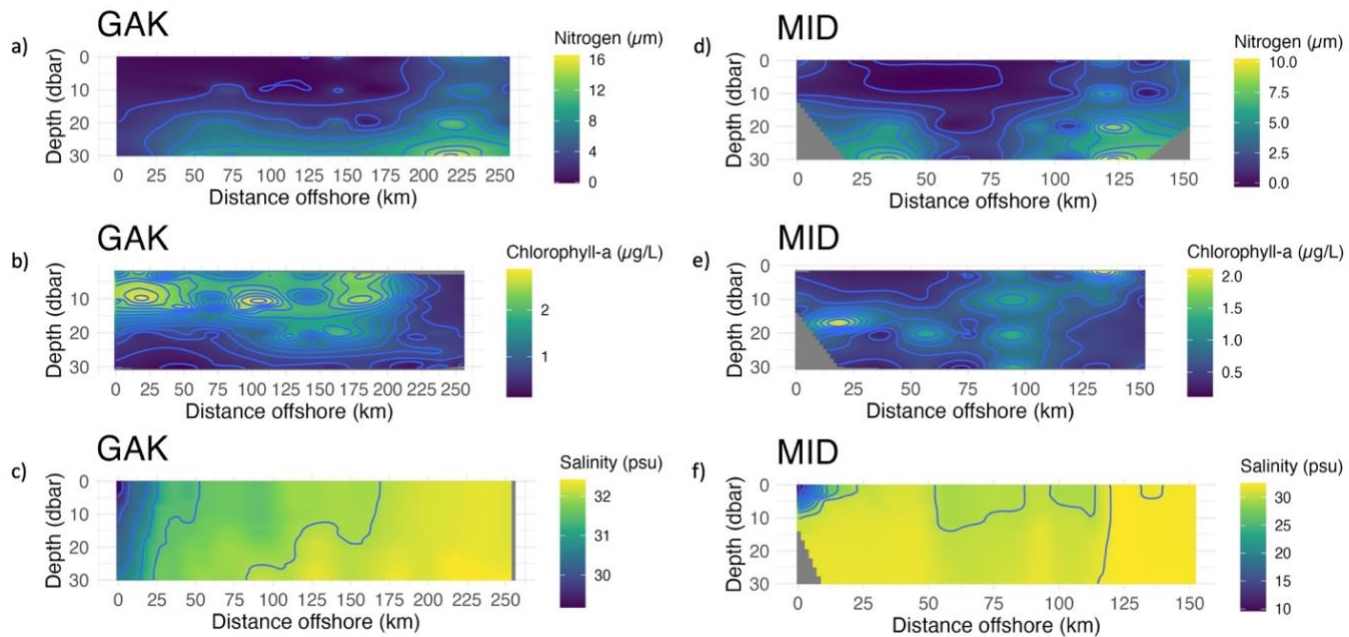
Figure 24: Section plots of 0-30 dbar nitrogen (nitrite + nitrate, µM), chlorophyll-a concentration (µg/L), and salinity (psu) on the GAK (a-c) and MID (d-f) transects in summer 2021. Note variable scales.

Literature Cited

Adolf, J. E., D. K. Stoecker, and L. W. Harding. 2006. The balance of autotrophy and heterotrophy during mixotrophic growth of Karlodinium micrum (Dinophyceae). Journal of Plankton Research 28:737–751. https://doi.org/10.1093/plankt/fbl007.

Anderson, R., K. Jürgens, and P. J. Hansen. 2017. Mixotrophic Phytoflagellate Bacterivory Field Measurements Strongly Biased by Standard Approaches: A Case Study. Frontiers in Microbiology 8:1398. https://doi.org/10.3389/fmicb.2017.

Altenburger, A., H. E. Blossom, L. Garcia-Cuetos, H. H. Jakobsen, J. Carstensen, N. Lundholm, P. J. Hansen, Ø. Moestrup, and L. Haraguchi. 2020. Dimorphism in cryptophytes—The case of *Teleaulax amphioxeia / Plagioselmis prolonga* and its ecological implications. Science Advances 6:eabb1611. DOI: 10.1126/sciadv.abb161.

Barkhatov, Y. V. 2021. Measuring Alloxanthin as a Proxy Approach in a Study of Trophic Relationships between Zooplankton and Cryptophyte Algae in Lake Shira. Journal of Siberian Federal University. Biology:154–167. http://journal.sfu-kras.ru/en/article/141373.

Beamer, J. P., D. F. Hill, D. McGrath, A. Arendt, and C. Kienholz. 2017. Hydrologic impacts of changes in climate and glacier extent in the Gulf of Alaska watershed. Water Resources Research 53:7502–7520. https://doi.org/10.1002/2016WR020033.

Behrenfeld, M. J., R. T. O'Malley, E. S. Boss, T. K. Westberry, J. R. Graff, K. H. Halsey, A. J. Milligan, D. A. Siegel, and M. B. Brown. 2016. Revaluating ocean warming impacts on global phytoplankton. Nature Climate Change 6:323–330. DOI: 10.1038/nclimate2838.

Beisner, B. E., H.-P. Grossart, and J. M. Gasol. 2019. A guide to methods for estimating phago-

mixotrophy in nanophytoplankton. Journal of Plankton Research 41:77–89.

https://doi.org/10.1093/plankt/fbz008.

Bindoff, N. L. et al. 2019. In IPCC Special Report on the Ocean and Cryosphere in a Changing Climate

(eds H.-O. Pörtner, D. C. Roberts, V. Masson-Delmotte, P. Zhai, M. Tignor, E. Poloczanska, K.

Mintenbeck, A. Alegrı̌a, M. Nicolai, A. Okem, J. Petzold, B. Rama, N. M. W) Cambridge

University Press (2019).

Bolaños, L. M., L. Karp-Boss, C. J. Choi, A. Z. Worden, J. R. Graff, N. Haëntjens, A. P. Chase, A. Della

Penna, P. Gaube, F. Morison, S. Menden-Deuer, T. K. Westberry, R. T. O'Malley, E. Boss, M. J.

Behrenfeld, and S. J. Giovannoni. 2020. Small phytoplankton dominate western North Atlantic

biomass. The ISME Journal 14:1663–1674. DOI: 10.1038/s41396-020-0636-0.

Booth, B. C. 1988. Size classes and major taxonomic groups of phytoplankton at two locations in the

subarctic pacific ocean in May and August, 1984. Marine Biology 97:275–286.

https://doi.org/10.1007/BF00391313.

Brett, M., and D. Müller-Navarra. 1997. The role of highly unsaturated fatty acids in aquatic food

web processes. Freshwater Biology 38:483–499. DOI: 10.1046/j.1365-2427.1997.00220.x.

Burkholder, J. M., P. M. Glibert, and H. M. Skelton. 2008. Mixotrophy, a major mode of nutrition for

harmful algal species in eutrophic waters. Harmful Algae 8:77–93.

https://doi.org/10.1016/j.hal.2008.08.010.

Burt, W. J., T. K. Westberry, M. J. Behrenfeld, C. Zeng, R. W. Izett, and P. D. Tortell. 2018. Carbon:

Chlorophyll Ratios and Net Primary Productivity of Subarctic Pacific Surface Waters Derived

From Autonomous Shipboard Sensors. Global Biogeochemical Cycles 32:267–288.

https://doi.org/10.1002/2017GB005783.

Busse, H. (2021). Mixotrophy by Phytoflagellates in the Northern Gulf of Alaska: Impacts of Physico-

Chemical Characteristics and Prey Concentration on Feeding by Photosynthetic Nano- and

Dinoflagellates:71.

Clay, B. L., and P. Kugrens. 1999. Characterization of Hemiselmis amylosa sp. nov. and Phylogenetic

Placement of the Blue-Green Cryptomonads H. amylosa and Falcomonas daucoides. Protist

150:297–310. DOI: 10.1016/S1434-4610(99)70031-3.

Clay, B. L., P. Kugrens, and R. E. Lee. 1999. A revised classification of Cryptophyta. Botanical Journal

of the Linnean Society 131:131–151. https://doi.org/10.1111/j.1095-8339.1999.tb01845.x.

Cooley, S., D. Schoeman, L. Bopp, P. Boyd, S. Donner, D.Y. Ghebrehiwet, S.-I. Ito, W. Kiessling, P.

Martinetto, E. Ojea, M.-F. Racault, B. Rost, and M. Skern-Mauritzen. 2022: Oceans and Coastal

Ecosystems and Their Services. In: Climate Change 2022: Impacts, Adaptation and Vulnerability.

Contribution of Working Group II to the Sixth Assessment Report of the Intergovernmental

Panel on Climate Change [H.-O. Pörtner, D.C. Roberts, M. Tignor, E.S. Poloczanska, K.

Mintenbeck, A. Alegría, M. Craig, S. Langsdorf, S. Löschke, V. Möller, A. Okem, B. Rama (eds.)].

Cambridge University Press, Cambridge, UK and New York, NY, USA, pp. 379–550.

Costa, M. R. A., H. Sarmento, V. Becker, I. L. Bagatini, and F. Unrein. 2022. Phytoplankton

phagotrophy across nutrients and light gradients using different measurement techniques.

Journal of Plankton Research 44:507–520. DOI: 10.1093/plankt/fbac035.

Coyle, K. O., and A. I. Pinchuk. 2005. Seasonal cross-shelf distribution of major zooplankton taxa on

the northern Gulf of Alaska shelf relative to water mass properties, species depth preferences

and vertical migration behavior. Deep Sea Research Part II: Topical Studies in Oceanography 52:217–245. https://linkinghub.elsevier.com/retrieve/pii/S0967064504002395.

Del Bel Belluz, J., M. A. Peña, J. M. Jackson, and N. Nemcek. 2021. Phytoplankton Composition and Environmental Drivers in the Northern Strait of Georgia (Salish Sea), British Columbia, Canada. Estuaries and Coasts 44:1419–1439. https://doi.org/10.1007/s12237-020-00858-2.

Duffy, J. E., C. M. Godwin, and B. J. Cardinale. 2017. Biodiversity effects in the wild are common and as strong as key drivers of productivity. Nature 549:261–264. https://doi.org/10.1038/nature23886.

Dutkiewicz, S., P. Cermeno, O. Jahn, M. J. Follows, A. E. Hickman, D. A. A. Taniguchi, and B. A. Ward. 2020. Dimensions of marine phytoplankton diversity. Biogeosciences 17:609–634. https://doi.org/10.5194/bg-17-609-2020.

Flynn, K. J., and A. Mitra. 2009. Building the "perfect beast": modelling mixotrophic plankton. Journal of Plankton Research 31:965–992. https://doi.org/10.1093/plankt/fbp044.

Flynn, K. J., D. K. Stoecker, A. Mitra, J. A. Raven, P. M. Glibert, P. J. Hansen, E. Granéli, and J. M. Burkholder. 2013. Misuse of the phytoplankton–zooplankton dichotomy: the need to assign organisms as mixotrophs within plankton functional types. Journal of Plankton Research 35:3–11. https://doi.org/10.1093/plankt/fbs062.

Galloway, A. W. E., and M. Winder. 2015. Partitioning the Relative Importance of Phylogeny and Environmental Conditions on Phytoplankton Fatty Acids. PLOS ONE 10:e0130053. https://doi.org/10.1371/journal.pone.0130053.

Garibotti, I., M. Vernet, W. Kozlowski, and M. Ferrario. 2003. Composition and biomass of phytoplankton assemblages in coastal Antarctic waters: a comparison of chemotaxonomic and microscopic analyses. Marine Ecology Progress Series 247:27–42. DOI:10.3354/meps247027.

Gerringa, L. J. A., H. J. W. de Baar, and K. R. Timmermans. 2000. A comparison of iron limitation of phytoplankton in natural oceanic waters and laboratory media conditioned with EDTA. Marine Chemistry 68:335–346. https://doi.org/10.1016/S0304-4203(99)00092-4.

Griffiths, J. R., S. Lehtinen, S. Suikkanen, and M. Winder. 2020. Limited evidence for common interannual trends in Baltic Sea summer phytoplankton biomass. PLOS ONE 15:e0231690. https://doi.org/10.1371/journal.pone.0231690.

Hansen, P. J., L. T. Nielsen, M. Johnson, T. Berge, and K. J. Flynn. 2013. Acquired phototrophy in Mesodinium and Dinophysis – A review of cellular organization, prey selectivity, nutrient uptake and bioenergetics. Harmful Algae 28:126–139. https://doi.org/10.1016/j.hal.2013.06.004.

Heidenreich, K. M., and T. L. Richardson. 2020. Photopigment, Absorption, and Growth Responses of Marine Cryptophytes to Varying Spectral Irradiance. Journal of Phycology 56:507–520. https://doi.org/10.1111/jpy.12962.

Henson, S. A., B. B. Cael, S. R. Allen, and S. Dutkiewicz. 2021. Future phytoplankton diversity in a changing climate. Nature Communications 12:5372. https://doi.org/10.1038/s41467-021-25699-w.

Hillebrand, H., B. Blasius, E. T. Borer, J. M. Chase, J. A. Downing, B. K. Eriksson, C. T. Filstrup, W. S. Harpole, D. Hodapp, S. Larsen, A. M. Lewandowska, E. W. Seabloom, D. B. Van de Waal, and A. B. Ryabov. 2018. Biodiversity change is uncoupled from species richness trends: Consequences

for conservation and monitoring. Journal of Applied Ecology 55:169–184.

https://doi.org/10.1111/1365-2664.12959.

Hoef-Emden, K., B. Marin, and M. Melkonian. 2002. Nuclear and Nucleomorph SSU rDNA Phylogeny

in the Cryptophyta and the Evolution of Cryptophyte Diversity. Journal of Molecular Evolution

55:161–179. https://doi.org/10.1007/s00239-002-2313-5.

Hutchinson, G. E. 1961. The Paradox of the Plankton. The American Naturalist, 95(882)137–145.

http://www.jstor.org/stable/2458386.

Jeong, H. J., Y. D. Yoo, J. S. Kim, K. A. Seong, N. S. Kang, and T. H. Kim. 2010. Growth, feeding and

ecological roles of the mixotrophic and heterotrophic dinoflagellates in marine planktonic food

webs. Ocean Science Journal 45:65–91. https://doi.org/10.1007/s12601-010-0007-2.

Jeong, H. J., Y. D. Yoo, K. H. Lee, T. H. Kim, K. A. Seong, N. S. Kang, S. Y. Lee, J. S. Kim, S. Kim, and W.

H. Yih. 2013. Red tides in Masan Bay, Korea in 2004–2005: I. Daily variations in the abundance

of red-tide organisms and environmental factors. Harmful Algae 30:S75–S88.

https://doi.org/10.1016/j.hal.2013.10.008.

Kang, Y., C.-H. Moon, H.-J. Kim, Y. H. Yoon, and C.-K. Kang. 2021. Water Quality Improvement Shifts

the Dominant Phytoplankton Group From Cryptophytes to Diatoms in a Coastal Ecosystem.

Frontiers in Marine Science 8:710891. https://doi.org/10.3389/fmars.2021.710891.

Kugrens, P. and Lee, R. E. 1987. An ultrastructural survey of cryptomonad periplasts using quick-

freezing freeze fracture techniques. Journal of Phycology, 23(s2), 365–376.

https://doi.org/10.1111/j.1529-8817.1987.tb04146.x.

Kugrens, P. and Lee, R.E. 1988. Ultrastructure of fertilization in a cryptomonad. J. Phycol. 24, 385–

393. https://doi.org/10.1111/j.1529-8817.1988.tb04481.x.

Leeuwe, M. A., A. L. Webb, H. J. Venables, R. J. W. Visser, M. P. Meredith, J. T. M. Elzenga, and J. Stefels. 2020. Annual patterns in phytoplankton phenology in Antarctic coastal waters explained by environmental drivers. Limnology and Oceanography 65:1651–1668. https://doi.org/10.1002/lno.11477.

Li, A., D. K. Stoecker, and J.E. Adolf. 1999. Feeding, pigmentation, photosynthesis and growth of the mixotrophic dinoflagellate Gyrodinium galatheanum. Aquatic Microbial Ecology 19:163–176.

Li, Q., K. F. Edwards, C. R. Schvarcz, and G. F. Steward. 2022. Broad phylogenetic and functional diversity among mixotrophic consumers of Prochlorococcus. The ISME Journal 16:1557–1569. https://doi.org/10.1038/s41396-022-01204-z.

Lie, A. A. Y., Z. Liu, R. Terrado, A. O. Tatters, K. B. Heidelberg, and D. A. Caron. 2018. A tale of two mixotrophic chrysophytes: Insights into the metabolisms of two Ochromonas species (Chrysophyceae) through a comparison of gene expression. PLOS ONE 13:e0192439. https://doi.org/10.1371/journal.pone.0192439.

Lindemann, C., Ø. Fiksen, K. H. Andersen, and D. L. Aksnes. 2016. Scaling Laws in Phytoplankton Nutrient Uptake Affinity. Frontiers in Marine Science 3. https://doi.org/10.3389/fmars.2016.00026.

Litzow, M., K. Bailey, F. Prahl, and R. Heintz. 2006. Climate regime shifts and reorganization of fish communities: the essential fatty acid limitation hypothesis. Marine Ecology Progress Series 315:1–11. DOI: 10.3354/meps315001.

Livanou, E., K. Barsakis, S. Psarra, and K. Lika. 2020. Modelling the nutritional strategies in mixotrophic nanoflagellates. Ecological Modelling 428:109053. DOI:10.1016/j.ecolmodel.2020.109053.

Marie, D., Shi, X. L., Rigaut-Jalabert, F., & Vaulot, D. 2010. Use of flow cytometric sorting to better

assess the diversity of small photosynthetic eukaryotes in the English Channel. FEMS

Microbiology Ecology, 72(2), 165–178. https://doi.org/10.1111/j.1574-6941.2010.00842.x.

Marshall, W., and J. Laybourn-Parry. 2002. The balance between photosynthesis and grazing in

Antarctic mixotrophic cryptophytes during summer: *Cryptophytes in Antarctic lakes*. Freshwater

Biology 47:2060–2070. https://doi.org/10.1046/j.1365-2427.2002.00950.x.

Martiny, A. C., G. I. Hagstrom, T. DeVries, R. T. Letscher, G. L. Britten, C. A. Garcia, E. Galbraith, D.

Karl, S. A. Levin, M. W. Lomas, A. R. Moreno, D. Talmy, W. Wang, and K. Matsumoto. 2022.

Marine phytoplankton resilience may moderate oligotrophic ecosystem responses and

biogeochemical feedbacks to climate change. Limnology and Oceanography 67.

https://doi.org/10.1002/lno.12029.

Medlin, L., and J. Orozco. 2017. Molecular Techniques for the Detection of Organisms in Aquatic

Environments, with Emphasis on Harmful Algal Bloom Species. Sensors 17:1184.

https://doi.org/10.3390/s17051184.

Menden-Deuer, S., and E. J. Lessard. 2000. Carbon to volume relationships for dinoflagellates,

diatoms, and other protist plankton. Limnology and Oceanography 45:569–579.

DOI:10.4319/lo.2000.45.3.0569.

Mendes, C. R. B., V. M. Tavano, M. C. Leal, M. S. de Souza, V. Brotas, and C. A. E. Garcia. 2013. Shifts

in the dominance between diatoms and cryptophytes during three late summers in the

Bransfield Strait (Antarctic Peninsula). Polar Biology 36:537–547. DOI:10.1007/s00300-012-

1282-4.

Mendes, C. R. B., V. M. Tavano, T. S. Dotto, R. Kerr, M. S. de Souza, C. A. E. Garcia, and E. R. Secchi. 2018. New insights on the dominance of cryptophytes in Antarctic coastal waters: A case study in Gerlache Strait. Deep Sea Research Part II: Topical Studies in Oceanography 149:161–170. doi:10.1016/j.dsr2.2017.02.010.

Mitra, A., K. J. Flynn, J. M. Burkholder, T. Berge, A. Calbet, J. A. Raven, E. Granéli, P. M. Glibert, P. J. Hansen, D. K. Stoecker, F. Thingstad, U. Tillmann, S. Våge, S. Wilken, and M. V. Zubkov. 2014. The role of mixotrophic protists in the biological carbon pump. Biogeosciences 11:995–1005. https://doi.org/10.5194/bg-11-995-2014.

Mitra, A., K. J. Flynn, U. Tillmann, J. A. Raven, D. Caron, D. K. Stoecker, F. Not, P. J. Hansen, G. Hallegraeff, R. Sanders, S. Wilken, G. McManus, M. Johnson, P. Pitta, S. Våge, T. Berge, A. Calbet, F. Thingstad, H. J. Jeong, J. Burkholder, P. M. Glibert, E. Granéli, and V. Lundgren. 2016. Defining Planktonic Protist Functional Groups on Mechanisms for Energy and Nutrient Acquisition: Incorporation of Diverse Mixotrophic Strategies. Protist 167:106–120. https://doi.org/10.1016/j.protis.2016.01.003.

Moline, M. A., H. Claustre, T. K. Frazer, O. Schofield, and M. Vernet. 2004. Alteration of the food web along the Antarctic Peninsula in response to a regional warming trend: ALTERATION OF THE ANTARCTIC FOOD WEB. Global Change Biology 10:1973–1980. DOI:10.1111/j.1365-2486.2004.00825.x.

Needham, D. M., E. B. Fichot, E. Wang, L. Berdjeb, J. A. Cram, C. G. Fichot, and J. A. Fuhrman. 2018. Dynamics and interactions of highly resolved marine plankton via automated high-frequency sampling. The ISME Journal 12:2417–2432. DOI: 10.1038/s41396-018-0169-y.

Novarino, G. 2012. Cryptomonad taxonomy in the 21st century: The first 200 years. In Phycological

Reports (pp. 19-52). Institute of Botany, Polish Academy of Sciences, Krakow. DOI:

https://www.researchgate.net/publication/265520014.

Novarino, G., and I. A. N. Lucas. 1993. Some proposals for a new classification system of the

Cryptophyceae. Botanical Journal of the Linnean Society 111:3–21.

https://doi.org/10.1111/j.1095-8339.1993.tb01886.x.

Oikonomou, A., E. Livanou, M. Mandalakis, A. Lagaria, and S. Psarra. 2020. Grazing effect of

flagellates on bacteria in response to phosphate addition in the oligotrophic Cretan Sea, NE

Mediterranean. FEMS Microbiology Ecology 96:fiaa086. DOI: 10.1093/femsec/fiaa086.

Olson, R. J., S. W. Chisholm, E. R. Zettler, and E. V. Armbrust. 1990. Pigments, size, and distributions

of Synechococcus in the North Atlantic and Pacific Oceans. Limnology and Oceanography

35:45–58. https://doi.org/10.4319/lo.1990.35.1.0045.

Olusoji, O. D., J. W. Spaak, M. Holmes, T. Neyens, M. Aerts, and F. De Laender. 2021. cyanoFilter: An

R package to identify phytoplankton populations from flow cytometry data using cell

pigmentation and granularity. Ecological Modelling 460:109743. DOI:

10.1016/j.ecolmodel.2021.109743.

O'Neill, K., N. Aghaeepour, J. Špidlen, and R. Brinkman. 2013. Flow Cytometry Bioinformatics. PLoS

Computational Biology 9:e1003365. https://doi.org/10.1371/journal.pcbi.1003365.

Pennekamp, F., M. Pontarp, A. Tabi, F. Altermatt, R. Alther, Y. Choffat, E. A. Fronhofer, P.

Ganesanandamoorthy, A. Garnier, J. I. Griffiths, S. Greene, K. Horgan, T. M. Massie, E. Mächler,

G. M. Palamara, M. Seymour, and O. L. Petchey. 2018. Biodiversity increases and decreases

ecosystem stability. Nature 563:109–112. https://doi.org/10.1038/s41586-018-0627-8.

Porter, K. G. 1988. Phagotrophic phytoflagellates in microbial food webs. Hydrobiologia 159:89–97.

https://doi.org/10.1007/BF00007370.

Radi, T. 2009. Preliminary flow cytometric analyses of phototrophic pico- and nanophytoplankton

communities in the Northern Adriatic. Fresenius Environmental Bulletin 18:11.

Rammel, T. D. 2021. Spatial and Temporal Diversity and Abundance of Cryptophytes in San Diego

Coastal Waters. *UC San Diego*. ProQuest ID: Rammel_ucsd_0033M_20673. Merritt ID:

ark:/13030/m52g42c3. Retrieved from https://escholarship.org/uc/item/3pm0r1sp

Raven, J. 1997. Inorganic Carbon Acquisition by Marine Autotrophs. Pages 85–209 Advances in

Botanical Research. Elsevier.

Roberts, E. C., and J. Laybourn-Parry. 1999. Mixotrophic cryptophytes and their predators in the Dry

Valley lakes of Antarctica: Antarctic mixotrophic cryptophytes. Freshwater Biology 41:737–746.

https://doi.org/10.1046/j.1365-2427.1999.00401.x.

Sanders, R. W. 1991. Mixotrophic Protists In Marine and Freshwater Ecosystems. The Journal of

Protozoology 38:76–81. https://doi.org/10.1111/j.1550-7408.1991.tb04805.x.

Sanders, R. W., K. G. Porter, and D. A. Caron. 1990. Relationship between phototrophy and

phagotrophy in the mixotrophic chrysophytePoterioochromonas malhamensis. Microbial

Ecology 19:97–109. https://doi.org/10.1007/BF02015056.

Schofield, O., G. Saba, K. Coleman, F. Carvalho, N. Couto, H. Ducklow, Z. Finkel, A. Irwin, A. Kahl, T.

Miles, M. Montes-Hugo, S. Stammerjohn, and N. Waite. 2017. Decadal variability in coastal

phytoplankton community composition in a changing West Antarctic Peninsula. Deep Sea

Research Part I: Oceanographic Research Papers 124:42–54.

https://doi.org/10.1016/j.dsr.2017.04.014.

Sosik, H. M., R. J. Olson, M. G. Neubert, A. Shalapyonok, and A. R. Solow. 2003. Growth rates of

coastal phytoplankton from time-series measurements with a submersible flow cytometer.

Limnology and Oceanography 48:1756–1765. https://doi.org/10.4319/lo.2003.48.5.1756.

Sterner, R. W., and K. L. Schulz. 1998. Zooplankton nutrition: recent progress and a reality check.

Aquatic Ecology 32, 261–279. DOI:10.1023/A:1009949400573.

Stoecker, D., M. Johnson, C. de Vargas, and F. Not. 2009. Acquired phototrophy in aquatic protists.

Aquatic Microbial Ecology 57:279–310. DOI:10.3354/ame01340.

Stoecker, D. K., P. J. Hansen, D. A. Caron, and A. Mitra. 2017. Mixotrophy in the Marine Plankton.

Annual Review of Marine Science 9:311–335. DOI: 10.1146/annurev-marine-010816-060617.

Stoecker, D. K., and P. J. Lavrentyev. 2018. Mixotrophic Plankton in the Polar Seas: A Pan-Arctic

Review. Frontiers in Marine Science 5:292. https://doi.org/10.3389/fmars.2018.00292.

Strom, S., M. Olson, E. Macri, and C. Mord. 2006. Cross-shelf gradients in phytoplankton community

structure, nutrient utilization, and growth rate in the coastal Gulf of Alaska. Marine Ecology

Progress Series 328:75–92. DOI:10.3354/meps328075.

Strom, S. L., E. L. Macri, and M. B. Olson. 2007. Microzooplankton grazing in the coastal Gulf of

Alaska: Variations in top-down control of phytoplankton. Limnology and Oceanography

52:1480–1494. DOI:10.4319/lo.2007.52.4.1480.

Strom, S., E. Macri, and K. Fredrickson. 2010. Light limitation of summer primary production in the

coastal Gulf of Alaska: physiological and environmental causes. Marine Ecology Progress Series

402:45–57. DOI:10.3354/meps08456.

Strom, S. L., K. A. Fredrickson, and K. J. Bright. 2016. Spring phytoplankton in the eastern coastal Gulf

of Alaska: Photosynthesis and production during high and low bloom years. Deep Sea Research

Part II: Topical Studies in Oceanography 132:107–121.

https://doi.org/10.1016/j.dsr2.2015.05.003.

Suikkanen, S., S. Pulina, J. Engström-Öst, M. Lehtiniemi, S. Lehtinen, and A. Brutemark. 2013. Climate

Change and Eutrophication Induced Shifts in Northern Summer Plankton Communities. PLoS

ONE 8:e66475. https://doi.org/10.1371/journal.pone.0066475.

Šupraha, L., Bosak, S., Ljubešić, Z., Mihanović, H., Olujić, G., Mikac, I., & Viličić, D. 2014. Cryptophyte

bloom in a Mediterranean estuary: High abundance of Plagioselmis cf. prolonga in the Krka

River estuary (eastern Adriatic Sea). Scientia Marina, 78(3), 329–338.

Suryan, R. M., M. L. Arimitsu, H. A. Coletti, R. R. Hopcroft, M. R. Lindeberg, S. J. Barbeaux, S. D.

Batten, W. J. Burt, M. A. Bishop, J. L. Bodkin, R. Brenner, R. W. Campbell, D. A. Cushing, S. L.

Danielson, M. W. Dorn, B. Drummond, D. Esler, T. Gelatt, D. H. Hanselman, S. A. Hatch, S.

Haught, K. Holderied, K. Iken, D. B. Irons, A. B. Kettle, D. G. Kimmel, B. Konar, K. J. Kuletz, B. J.

Laurel, J. M. Maniscalco, C. Matkin, C. A. E. McKinstry, D. H. Monson, J. R. Moran, D. Olsen, W.

A. Palsson, W. S. Pegau, J. F. Piatt, L. A. Rogers, N. A. Rojek, A. Schaefer, I. B. Spies, J. M. Straley,

S. L. Strom, K. L. Sweeney, M. Szymkowiak, B. P. Weitzman, E. M. Yasumiishi, and S. G. Zador.

2021. Ecosystem response persists after a prolonged marine heatwave. Scientific Reports

11:6235. https://doi.org/10.1038/s41598-021-83818-5.

Sutherland, G. K. 1913. Some Methods of Plankton Investigation. The Journal of Ecology 1:166.

Tarran, G. A., J. L. Heywood, and M. V. Zubkov. 2006. Latitudinal changes in the standing stocks of

nano- and picoeukaryotic phytoplankton in the Atlantic Ocean. Deep Sea Research Part II:

Topical Studies in Oceanography. 53:1516-1529. DOI:10.1016/j.dsr2.2006.05.004.

Unrein, F., J. M. Gasol, F. Not, I. Forn, and R. Massana. 2014. Mixotrophic haptophytes are key

bacterial grazers in oligotrophic coastal waters. The ISME Journal 8:164–176.

https://doi.org/10.1038/ismej.2013.132.

Urabe, J., T. B. Gurung, T. Yoshida, T. Sekino, M. Nakanishi, M. Maruo, and E. Nakayama. 2000. Diel

changes in phagotrophy by Cryptomonas in Lake Biwa. Limnology and Oceanography 45:1558–

1563. https://doi.org/10.4319/lo.2000.45.7.1558.

Veldhuis, M. J. W., and G. W. Kraay. 2004. Phytoplankton in the subtropical Atlantic Ocean: towards

a better assessment of biomass and composition. Deep Sea Research Part I: Oceanographic

Research Papers 51:507–530. DOI: 10.1016/j.dsr.2003.12.002.

Verity, P. G., C. Y. Robertson, C. R. Tronzo, M. G. Andrews, J. R. Nelson, and M. E. Sieracki. 1992.

Relationships between cell volume and the carbon and nitrogen content of marine

photosynthetic nanoplankton. Limnology and Oceanography 37:1434–1446.

https://doi.org/10.4319/lo.1992.37.7.1434.

Waite, J. N., and F. J. Mueter. 2013. Spatial and temporal variability of chlorophyll-a concentrations

in the coastal Gulf of Alaska, 1998–2011, using cloud-free reconstructions of SeaWiFS and

MODIS-Aqua data. Progress in Oceanography 116:179–192. DOI:10.1016/j.pocean.2013.07.006.

Walsh, J. E., R. L. Thoman, U. S. Bhatt, P. A. Bieniek, B. Brettschneider, M. Brubaker, S. Danielson, R.

Lader, F. Fetterer, K. Holderied, K. Iken, A. Mahoney, M. McCammon, and J. Partain. 2018. The

High Latitude Marine Heat Wave of 2016 and Its Impacts on Alaska. Bulletin of the American

Meteorological Society 99:S39–S43. https://doi.org/10.1175/BAMS-D-17-0105.1.

Ward, B. A., and M. J. Follows. 2016. Marine mixotrophy increases trophic transfer efficiency, mean organism size, and vertical carbon flux. Proceedings of the National Academy of Sciences 113:2958–2963. https://doi.org/10.1073/pnas.151711811.

Wassmann, P., and M. Reigstad. 2011. Future Arctic Ocean Seasonal Ice Zones and Implications for Pelagic-Benthic Coupling. Oceanography 24:220–231. DOI: https://www.jstor.org/stable/24861317.

Westberry, T. K., P. Schultz, M. J. Behrenfeld, J. P. Dunne, M. R. Hiscock, S. Maritorena, J. L. Sarmiento, and D. A. Siegel. 2016. Annual cycles of phytoplankton biomass in the subarctic Atlantic and Pacific Ocean. Global Biogeochemical Cycles 30:175–190. https://doi.org/10.1002/2015GB005276.

Whitney, F. A., D. W. Crawford, and T. Yoshimura. 2005. The uptake and export of silicon and nitrogen in HNLC waters of the NE Pacific Ocean. Deep Sea Research Part II: Topical Studies in Oceanography 52:1055–1067. https://doi.org/10.1016/j.dsr2.2005.02.006.

Wilken, S., C. J. Choi, and A. Z. Worden. 2020. Contrasting Mixotrophic Lifestyles Reveal Different Ecological Niches in Two Closely Related Marine Protists. Journal of Phycology 56:52–67. https://doi.org/10.1111/jpy.12920

Wilson JG, Overland JE. 1986. Meteorology. In: Hood DW, Zimmerman ST (eds) The Gulf of Alaska, physical environment and biological resources. US Department of Commerce, Washington, DC, p 31–54.

Worden, A. Z., M. J. Follows, S. J. Giovannoni, S. Wilken, A. E. Zimmerman, and P. J. Keeling. 2015. Rethinking the marine carbon cycle: Factoring in the multifarious lifestyles of microbes. Science 347:1257594. DOI: 10.1126/science.1257594.

Worm, B., E. B. Barbier, N. Beaumont, J. E. Duffy, C. Folke, B. S. Halpern, J. B. C. Jackson, H. K. Lotze,

   F. Micheli, S. R. Palumbi, E. Sala, K. A. Selkoe, J. J. Stachowicz, and R. Watson. 2006. Impacts of

   Biodiversity Loss on Ocean Ecosystem Services. Science 314:787–790.

   10.1126/science.1132294.

Wu, J., A. Aguilar-Islas, R. Rember, T. Weingartner, S. Danielson, and T. Whitledge. 2009. Size-

   fractionated iron distribution on the northern Gulf of Alaska. Geophysical Research Letters 36.

   https://doi.org/10.1029/2009GL038304.

Yang, E. C., J. H. Noh, S. Kim, and D. H. Choi. 2020. Plastid-encoded gene comparison reveals

   usefulness of *atp* B, *psa* A, and *rbc* L for identification and phylogeny of plastid-containing

   cryptophyte clades. Phycologia 59:154–164. https://doi.org/10.1080/00318884.2019.1709145.

Yoo, Y. D., K. A. Seong, H. J. Jeong, W. Yih, J.-R. Rho, S. W. Nam, and H. S. Kim. 2017. Mixotrophy in

   the marine red-tide cryptophyte Teleaulax amphioxeia and ingestion and grazing impact of

   cryptophytes on natural populations of bacteria in Korean coastal waters. Harmful Algae

   68:105–117. DOI: 10.1016/j.hal.2017.07.012.

Zubkov, M. V., and G. A. Tarran. 2008. High bacterivory by the smallest phytoplankton in the North

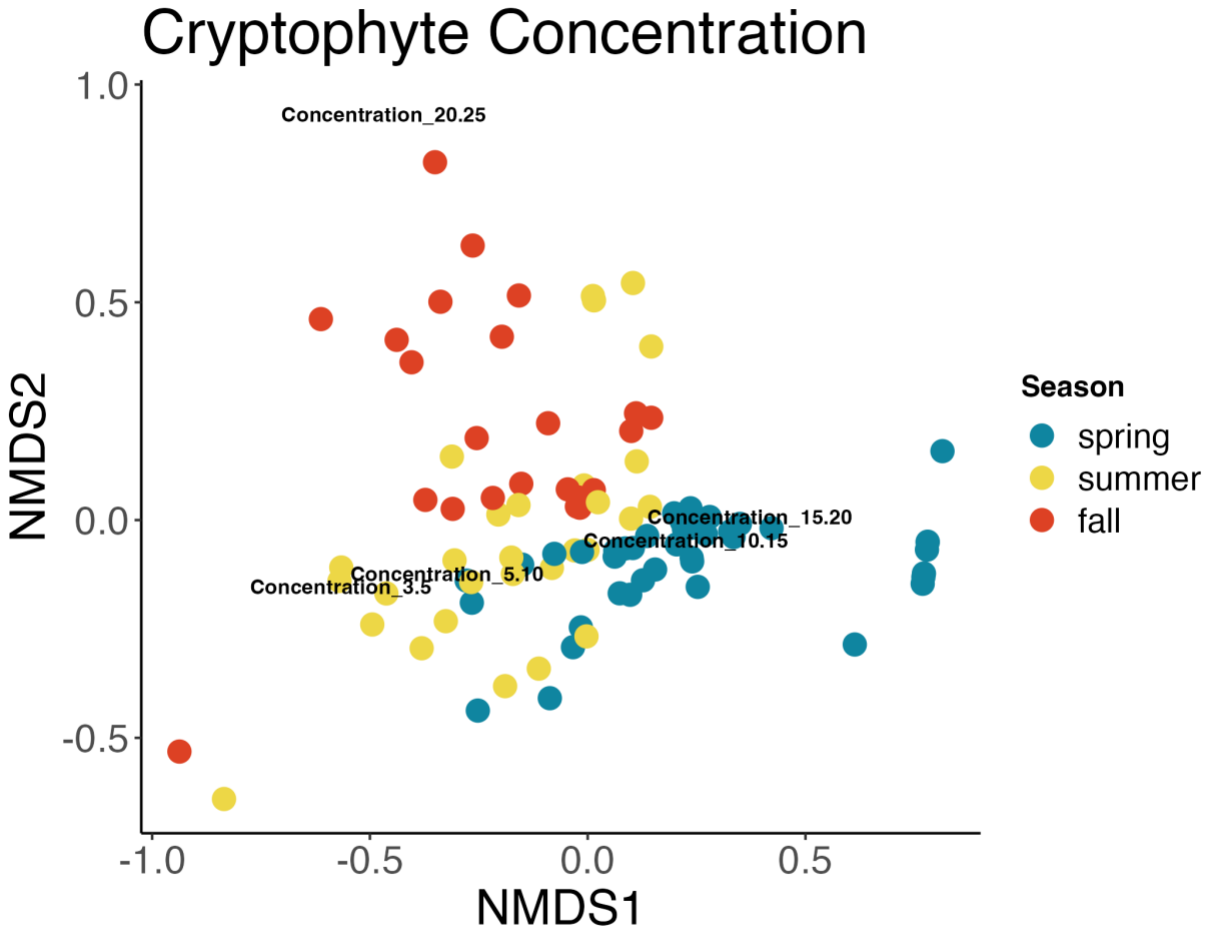   Atlantic Ocean. Nature 455:224–226. DOI: 10.1038/nature07236.

Figure 25: NMDS ordinations of 10 m cryptophyte concentration. Colors represent season and cryptophyte size classes are mapped in their ordination space on top. Bray-Curtis dissimilarity measure was used. Low stress (0.09) and convergent solutions were found with 2 NMDS dimensions.
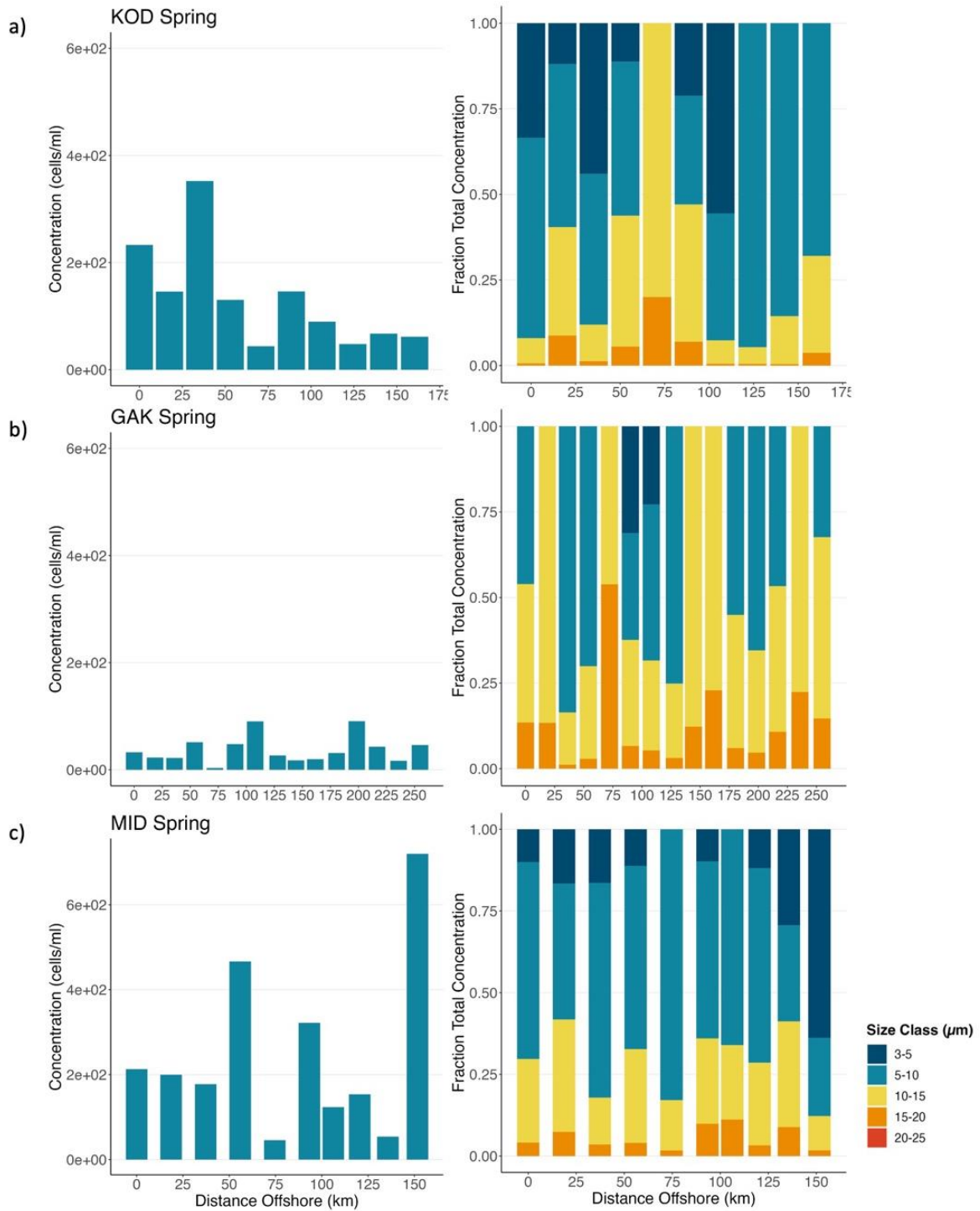
Figure 26: Cryptophyte concentration (cells/mL) at 10 m in spring on the (a) KOD, (b) GAK, and (c) MID transects (left). Cryptophyte size classes as a fraction of total concentration at 10 m (right). Size classes recorded included cells between 3-5 μm, 5-10 μm, 10-15 μm, and 15-20 μm. The size class 20-25 μm was observed only in summer and fall samples.
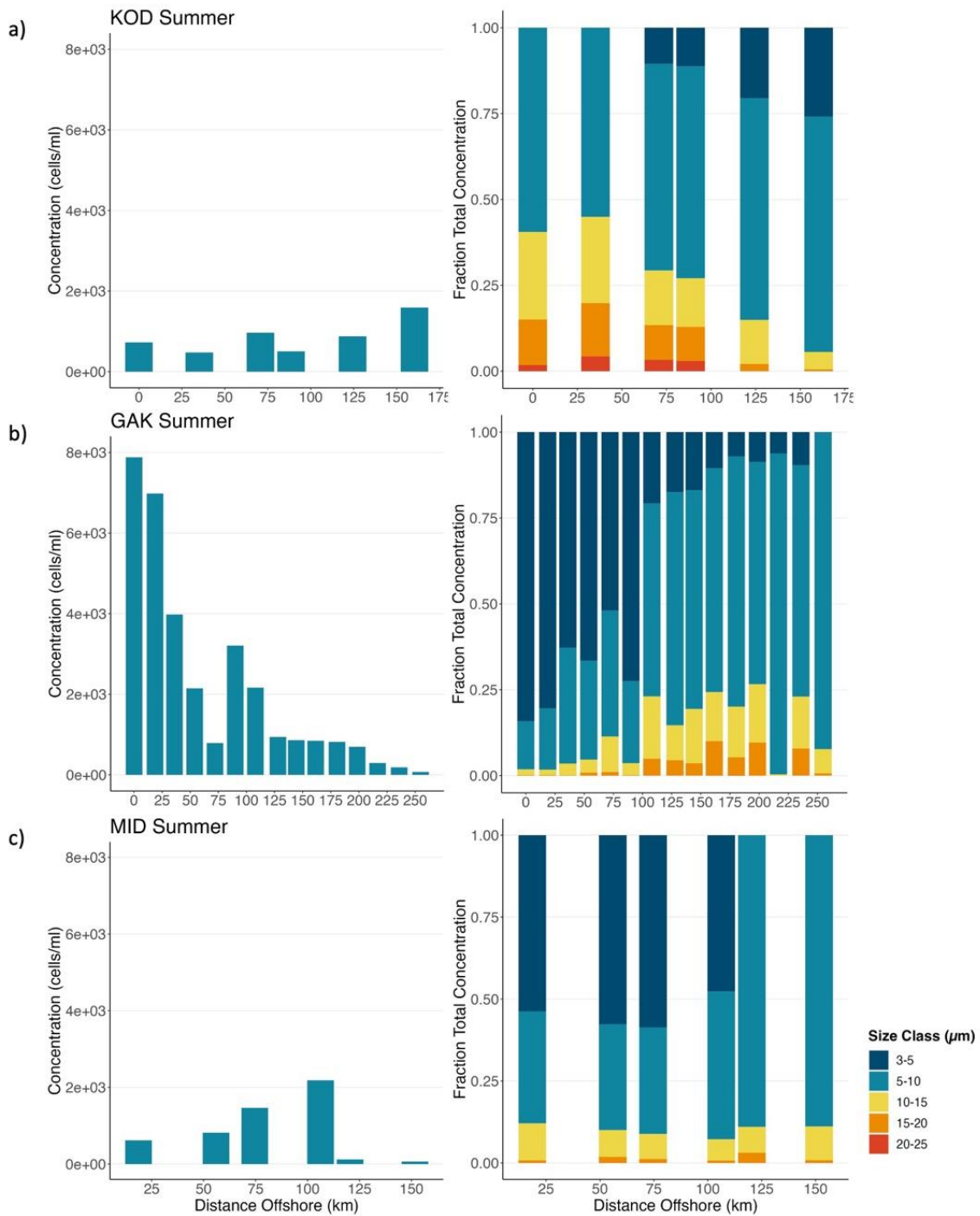
Figure 27: Cryptophyte concentration (cells/mL) at 10 m in summer on the (a) KOD, (b) GAK, and (c) MID transects (left). Cryptophyte size classes as a fraction of total concentration at 10 m (right). Size classes recorded included cells between 3-5 μm, 5-10 μm, 10-15 μm, and 15-20 μm. The size class 20-25 μm was observed only in summer and fall samples. Blank spaces indicate no sample taken.
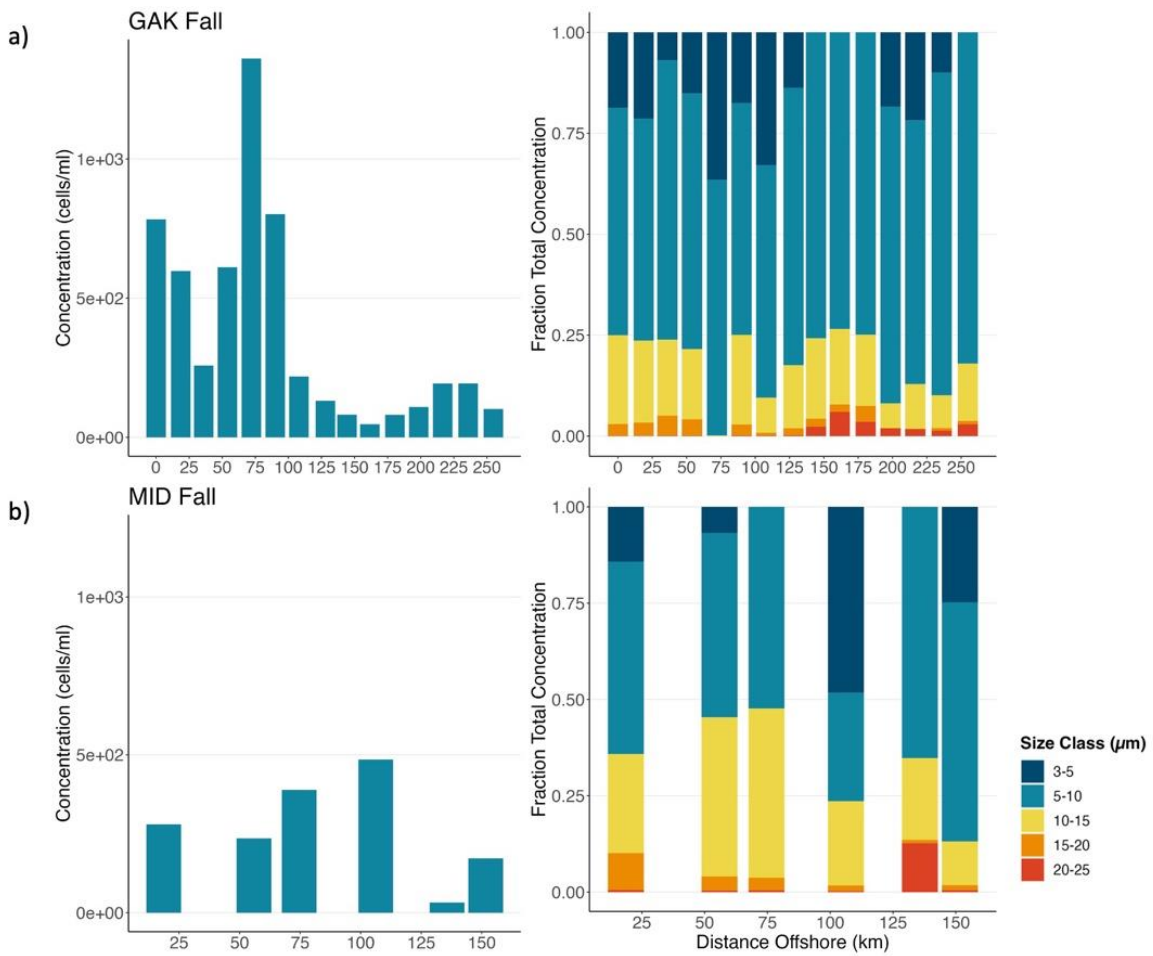
Figure 28: Cryptophyte concentration (cells/mL) at 10 m in fall on the (a) GAK and (b) MID transects (left). Cryptophyte size classes as a fraction of total concentration at 10 m (right). Size classes recorded included cells between 3-5 μm, 5-10 μm, 10-15 μm, and 15-20 μm. The size class 20-25 μm was observed only in summer and fall samples. Blank spaces indicate no sample taken. The KOD transect was not sampled in fall 2021.
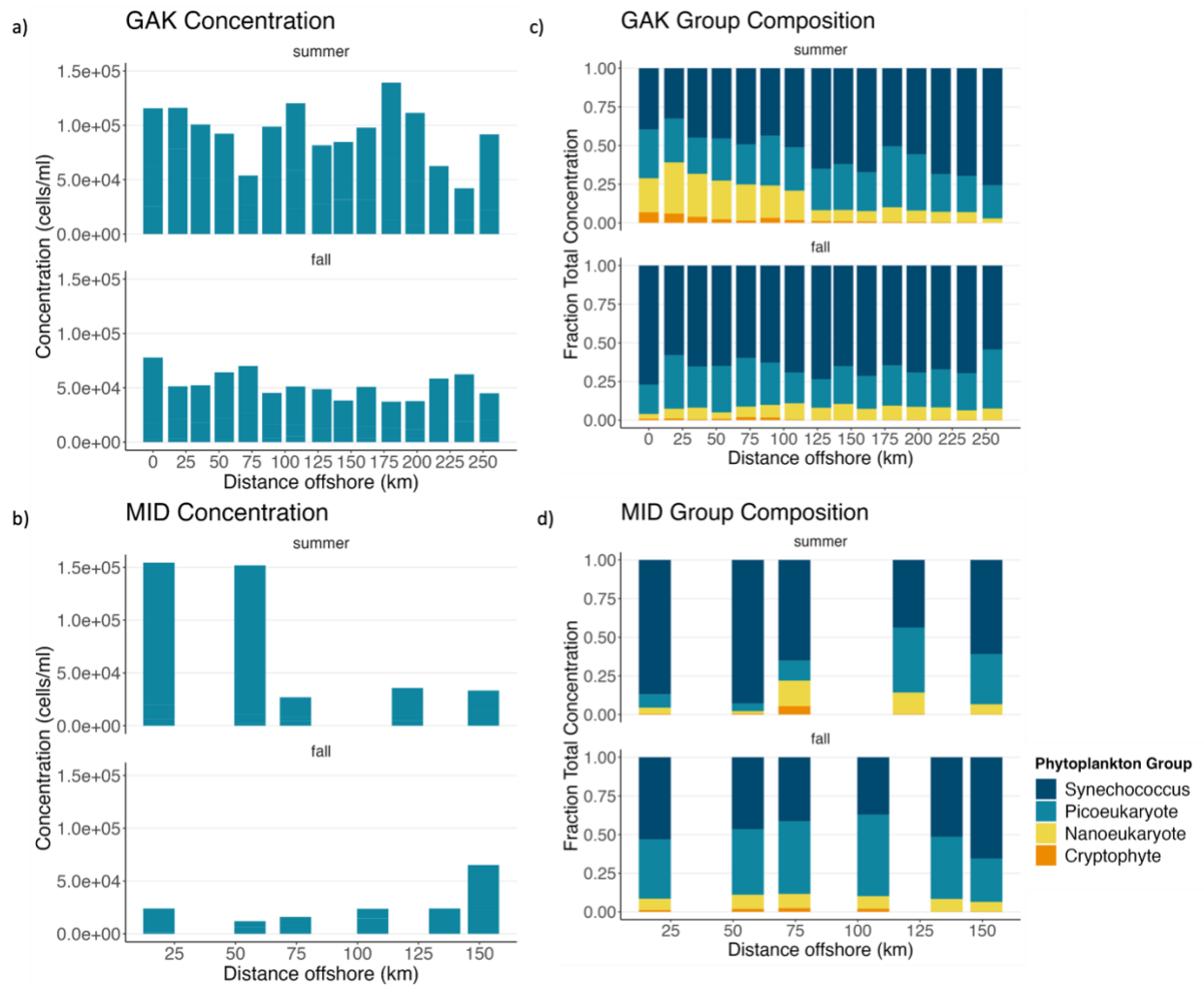
Figure 29: Small-cell community phytoplankton concentration (cells/mL) at 10 m in summer and fall on the (a) GAK and (b) MID transects. Phytoplankton taxonomic group as a fraction of total concentration at 10 m on the (c) GAK and (d) MID transects. Phytoplankton groups recorded included *Synechococcus* spp, picoeukaryotes, nanoeukaryotes, and cryptophytes. Blank spaces indicate no sample taken.
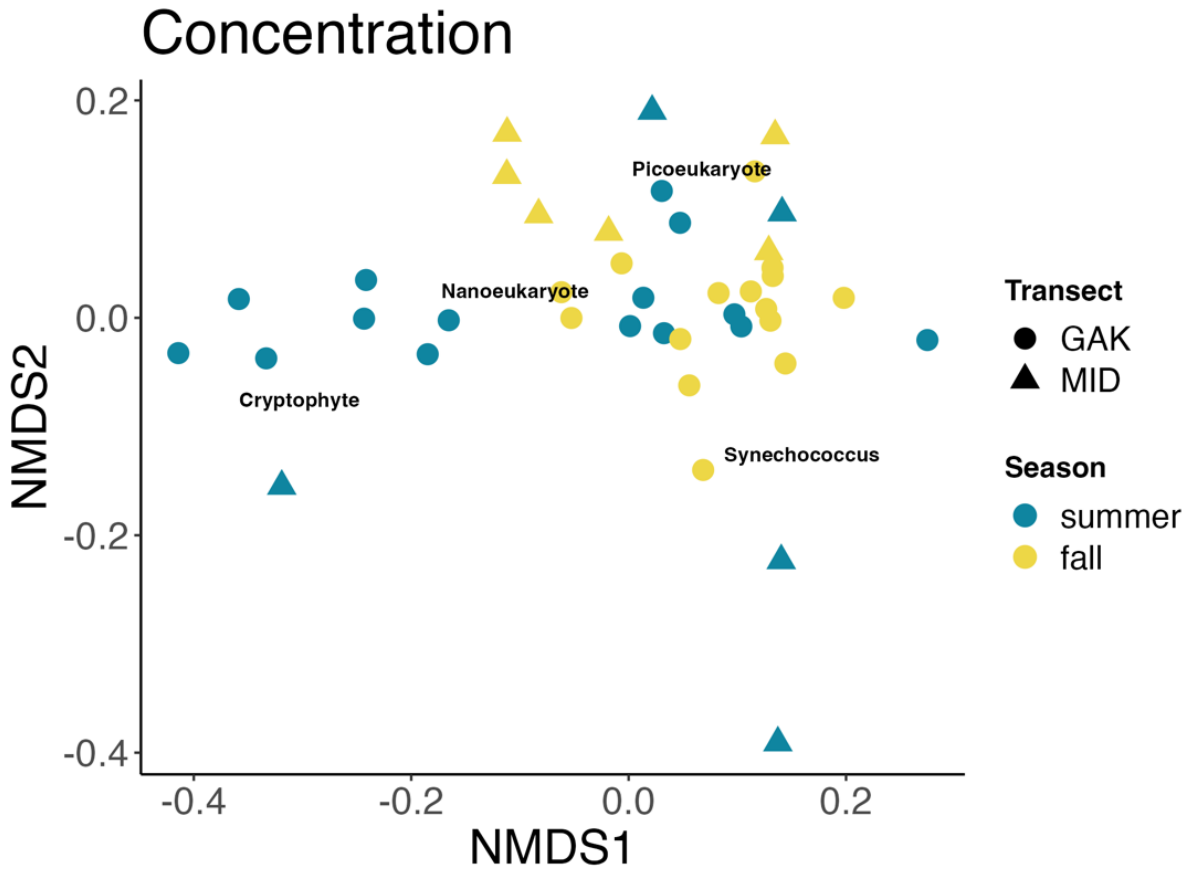
Figure 30: NMDS ordinations of small-cell community phytoplankton concentration at 10 m on the GAK and MID transects in summer and fall. Colors represent the NMDS separation of season and phytoplankton taxonomic groups are mapped in their ordination space on top. Bray-Curtis dissimilarity measure was used. Low stress (stress = 0.12) and convergent solutions were found with 2 NMDS dimensions.